GABA transmission in the suprachiasmatic nucleus

by Nathan J. Klett

a dissertation

Presented to the Neuroscience Graduate Program
and the Oregon Health & Science University School of Medicine
in partial fulfillment of the requirements for the degree of

Doctor of Philosophy

September 2015

TABLE OF CONTENTS

LIST OF FIGURES

CHAPTER 2: LOCAL GABA TRANSMISSION IS REQUIRED FOR SUPRACHIASMATIC NUCLEUS CIRCADIAN OUTPUT

CHAPTER 3: INTRACELLULAR CHLORIDE REGULATION IN NEURONS OF THE SUPRACHIASMATIC NUCLEUS

ABBREVIATIONS

aCSF	artificial cerebrospinal fluid
AP	action potential
AVP	arginine vasopressin
AVP+	arginine vasopressin positive
cAMP	cyclic adenosine monophosphate
CCC	cation chloride cotransporter
CCD	charge-coupled device
CCK	cholecystokinin
CFP	cyan fluorescent protein
$[Cl^-]_i$	intracellular chloride concentration
CNQX	6-cyano-7-nitroquinoxaline-2,3-dione
CREB	cAMP response element-binding protein
DD	dark-dark, or constant darkness
E_{Cl}	chloride reversal potential
E_{GABA}	GABAergic reversal potential
eGFP	enhanced green fluorescent protein
EGTA	ethylene glycol tetraacetic acid
ENK	enkephalin
GABA	gamma-Aminobutyric acid
GAD	glutamate decarboxylase
GFP	green fluorescent protein
GRP	gastrin releasing peptide
HEPES	4-(2-hydroxyethyl)-1-piperazineethanesulfonic acid
IGL	intergeniculate leaflet
KCC	potassium-chloride cotransporters
LD	light-dark
mGPSC	miniature GABA-mediated post-synaptic current
NA	numerical aperature
NKCC1	sodium-potassium-chloride cotransporters, subtype 1
NMDA	N-Methyl-D-aspartic acid

NPY	neuropeptide Y
NT	neurotensin
RHT	retinohypothalamic tract
R_s	series resistance
ROI	region of interest
R_{Cl}	chloride ratio
PACAP	pituitary adenylate cyclase-activating peptide
PER	period
VGAT	vesicular GABA transporter
VIP	vasoactive intestinal polypeptide
VIP+	vasoactive intestinal polypeptide positive
V_m	membrane potential
SCN	suprachiasmatic nucleus
SP	substance P
SS	somatostatin
T_b	body temperature
TTX	tetrodotoxin
YFP	yellow fluorescent protein
ZT	zeitgeber time

ACKNOWLEDGMENTS

First and foremost, I'd like to thank Dr. Charles Allen for the tremendous support over the last four years. I have learned immensely from his optimistic and unbiased approach to scientific investigation. Dr. Allen welcomed me into his research group before the projects presented in this dissertation had received funding. Working with Dr. Allen has given me the opportunity to add several new techniques to my repertoire, which will without doubt be useful skills to have in my future career. Further, I am grateful to Dr. Allen for introducing me to chronobiology—a field full of interesting and unique areas of research. I consider the suprachiasmatic nucleus to be an ideal model system for neuroscience research, as it offers tractability at all levels of neuroscience investigation: genetic, physiological, and behavioral.

I would like to thank the members of Dr. Allen's research group including Drs. Olga Cravetchi, Mykhalo Moldavan, and Robert Irwin. The consultation of Dr. Irwin was indispensible for the development my dissertation work. Dr. Cravetchi helped to keep me equipped with the mice and tissue necessary for my experiments. I thank Dr. Moldavan for offering insightful discussion of my dissertation research. I must also thank Mike Lasarev of the Oregon Institute for Occupational Health Sciences for his help with statistical analysis.

The hypotheses addressed in the second chapter of this dissertation were originally developed by my collaborators Heinrich Gompf and Patrick Fuller while under the direction of Cliff Saper. With the tools available to them, Drs. Gompf and Fuller recognized the potential to investigate the functional role of local GABA transmission within the suprachiasmatic nucleus. Therefore, I am grateful to have been given the

opportunity to work with the intersectional genetic models and adeno-associated vectors used in this study, tools which represent some of the most modern techniques in neuroscience research. Most of the mice in these experiments were prepared under their direction at Beth Israel Medical Center before being shipped to Oregon Health and Science University for experimentation. The telemetrical measurement and analysis of mouse core body temperature and whole-body locomotor activity were performed and contributed by Drs. Gompf, Fuller, and Saper.

I would also like to thank my thesis committee: Dr. Michael Andresen, Dr. Laurence Trussell, Dr. Craig Jahr, Dr. David Rossi, and Dr. Susan Ingram. The guidance I received from these scholars over the years directly improved the quality of the research presented in this dissertation. Lastly, I am indebted to the numerous people who have contributed to my scientific development over the years including Dr. Joel Karp, Aditya Bhattacharji, Dr. Manuel Covarrubias, Dr. Steve Cassady, Dr. Karl Kandler, Dr. German Barrionuevo, Dr. Emilio Galvan, Dr. Chris Bond, Dr. John Adelman, and Dr. James Maylie.

ABSTRACT

The suprachiasmatic nucleus (SCN) of the anterior hypothalamus is the central circadian pacemaker of the body. Besides several neuropeptides, SCN neurons express the neurotransmitter γ–aminobutryic acid (GABA), and local GABAergic nerve terminals are abundant within the SCN. Despite the prevalence of GABA and GABA receptors in the SCN, the physiological and functional roles of GABA within the SCN remain unclear. GABA signaling has been proposed to mediate synchrony, desynchrony, phase shifts, synaptic gain, and has been observed to be both inhibitory and excitatory within the SCN neural network. My dissertation work has investigated the physiological and functional roles of GABA transmission in the SCN.

The results presented in Chapter 2 provide new insight into the functional role of SCN GABA transmission. I show that that genetic deletion of the vesicular GABA transporter (VGAT), and therefore disruption of synaptic release of GABA from SCN neurons, results in the deterioration of behavioral rhythmicity *in vivo* and concurrent cellular desynchonry *in vitro.* Therefore, the results presented here indicate that local GABA transmission is essential for the synchronization of SCN neurons that is necessary for coherent circadian output.

In the central nervous system, GABA transmission is normally inhibitory, but several groups have observed excitatory GABA transmission in the adult SCN. However, studies across labs have disagreed on the circadian phase, neuronal location and prevalence of excitatory GABA transmission. GABA has been reported to be exclusively inhibitory, inhibitory during the day and excitatory during the night, and excitatory during the night and inhibitory during the day. The intracellular concentration

of chloride ($[Cl^-]_i$) is the ultimate determinant of GABA's physiological action. In Chapter 3, I present results obtained from two independent techniques to address the regulation of $[Cl^-]_i$ in SCN neurons. Together, my results indicate that the potassium-chloride cotransporters (KCCs) have a significant role in SCN $[Cl^-]_i$ regulation, while the sodium-potassium-chloride cotransporter type 1 (NKCC1) has a relatively minor role. Further, I have observed that $[Cl^-]_i$ is differentially regulated in AVP- and VIP-expressing neurons, and have found direct evidence for a circadian component to $[Cl^-]_i$ regulation in AVP-expressing neurons.

Membrane excitability has been linked to the molecular clock in SCN neurons. Therefore, the regulation of $[Cl^-]_i$ in SCN neurons addressed in Chapter 3 may be a key regulator of the circadian synchrony of SCN neurons investigated in Chapter 2. Both of these projects have made use of novel genetic approaches to address complex questions in SCN physiology. These techniques represent the forefront of neuroscience research, and have once again been shown to be invaluable for dissecting neural circuitry.

CHAPTER 1: INTRODUCTION

1.1 Circadian rhythms and health

It is not surprising that life forms organize their behavior according to the presence of the sun—certainly the most salient stimulus to terrestrial organisms. What is surprising however, is that organisms maintain daily fluctuations in behavior and physiology in the absence of this rhythmic stimulus. These endogenous rhythms were named circadian rhythms for their approximate daily periodicity ('circa' approximate, 'dian' referring to the day). First described by Jean Jacques d'Ortous de Mairan in 1729, circadian rhythms have since been found in creatures from unicellular organisms to man.

Circadian organization of behavior provides adaptive advantage to organisms, preparing them for upcoming changes in their environment. In mammals, essential body functions including sleep, growth, metabolism, core body temperature, fluid regulation, and cardiac output display circadian organization. Just as circadian organization is adaptive, disruption of circadian physiology can be highly deleterious. Shift work and the accompanying circadian misalignment have been identified to be risk factors for cardiovascular, gastrointestinal, and metabolic diseases as well as obesity and even cancer (Smith and Eastman, 2012). Therefore, in our modern 24/7 'always on' society, understanding circadian physiology has become increasingly crucial.

1.2 The molecular clock

Remarkably, circadian rhythmicity exists within individual cells in what is referred to as the molecular clock. The molecular clock in mammals is a transcriptional-translation feedback loop composed of multiple interacting 'clock genes'. Generally speaking, cell processes including transcription, translation, nuclear translocation and protein degradation collectively give rise to the emergent circadian period. The transcription factors CLOCK and BMAL1 makeup the 'engine' or positive limb of the feedback circuit. After dimerization, the CLOCK:BMAL1 complex initiates transcription at E-box elements found in promoters throughout the genome. Among these members are the *Per* (*Per1* and *Per2*) and *Cry* (*Cry1* and *Cry2*) genes. The PER and CRY proteins inhibit the activity of the CLOCK:BMAL1 complex through either epigenetic modifications at E-box elements, or through direct protein-protein interactions. In this way, PER and CRY inhibit their own expression, and therefore constitute the negative limb of the feedback circuit. Additionally, PER2 contributes to the rhythmic expression of BMAL1. Increased levels of BMAL1 will in turn promote PER2 expression, thereby restarting the transcription cycle (Reppert and Weaver, 2001; Hastings et al., 2003).

Accessory feedback loops have also been identified in the molecular clockwork. CLOCK:BMAL1 dimers also initiate transcription of *Ror* and *Rev-erb*. These transcription factors compete for regulatory binding sites within the promoter of *Bmal1*, where ROR initiates and REV-ERB inhibits transcription. Knockouts of these genes do not result in drastic circadian phenotypes, and therefore are not considered to be core components of the molecular clock. However, the REV-ERB/ROR accessory loop as well others interact with the primary transcription-translation feedback loop at critical

points, regulating features such as timing precision and rhythm amplitude (Buhr and Takahashi, 2013).

1.3 The discovery of the SCN and the circadian organization of the body

The circadian clock's sensitivity to light lead researchers to the suprachiasmatic nucleus (SCN), now considered the master clock of the circadian system. Looking for non-image forming projections from the retina, neuroanatomist Robert Moore identified several structures in the anterior hypothalamus that receive direct innervation from the retina, including the suprachiasmatic nucleus (SCN) which was named for its location above ('supra') the optic chiasm (Moore and Lenn, 1972). That same year, two lesioning studies identified the SCN as necessary for circadian rhythms in behavioral activity, water consumption, and adrenal corticosterone (Moore and Eichler, 1972; Stephan and Zucker, 1972). When the SCN was lesioned, these behaviors were arrhythmic in constant conditions. Subsequent characterization of intrinsic circadian rhythms present in *ex vivo* SCN tissue (e.g. action potential discharge, neuropeptide secretion, etc.) further supported the SCN's defining role in circadian rhythm generation, but the SCN's sufficiency to drive circadian rhythms was not adequately established until years later by clever transplant experiments, where rhythmicity was rescued in SCN-lesioned animals. SCN from mutant hamsters displaying 20 hour circadian rhythms were transplanted into SCN-lesioned wild type hamsters. Remarkably, the period of the donor SCN determined the resultant behavioral period in the animal, arguing for the supremacy of the SCN in the circadian organization of the body (Ralph et al., 1990; Vogelbaum and Menaker, 1992).

More recently, the SCN's reign of supremacy has been challenged by the observed presence of circadian rhythmicity in several peripheral tissues *ex vivo*, without any possible input from the SCN. However, these peripheral circadian rhythms dampen after a few cycles—much more quickly than the SCN, which can persist for weeks. This observation has lead the field to conclude that the SCN is not solely responsible for circadian rhythm generation, but rather provides amplification and timing cues to intrinsic molecular clocks throughout the body. Indeed, a major role of the SCN is to synchronize the body to the environment in a process called entrainment. The SCN adjusts its phase (e.g. locomotor activity onset, firing frequency or clock gene expression) in response to sensory cues such as the light/dark cycle, food presentation, locomotor activity, stress, and social interaction. These cues are referred to as zeitgebers ("time givers") and circadian rhythms are often plotted in relation to these stimuli (zeitgeber time, or ZT). The difference in time of a phase marker between one cycle and the next is referred to as a phase shift. These phase shifts occur within the SCN, and are subsequently relayed to the rest of the body through neural, endocrine, and paracrine signaling. In this way, the SCN synchronizes the body to the environment, and ensures proper circadian organization within the body.

1.4 Cell autonomy and cell coupling

As described above, the molecular clock is an intracellular phenomenon found in cells throughout the body. The molecular clock does not require input from other cells or surrounding tissue in order to cycle—it is a cell-autonomous self-sustaining oscillator. In dispersed culture, individual SCN neurons display rhythmicity in action potential

discharge, intracellular calcium concentration, and clock gene expression. So if the molecular clock exists within individual cells, why is the SCN necessary for the circadian organization of the body? As mentioned, the SCN mediates entrainment, whereby the body is synchronized to the environment through sensory input. Similarly, a key role of the SCN neural network is to mediate circadian synchrony, where cell-autonomous molecular clocks are synchronized in period and phase with each other. Neurons in dispersed culture display a wide range of periods, yet in an intact SCN slice, they demonstrate a narrow distribution close to 24 hours (Welsh et al., 1995). Interestingly, the density of the dispersed cell culture has been related to the degree of period variability (Aton and Herzog, 2005; Webb et al., 2009). Further insight into the role of the SCN neural network has come from genetic ablations of clock genes. The circadian rhythms of single SCN neurons are more susceptible to genetic perturbations than the intact SCN (Liu et al., 2007). Therefore, the SCN neural network provides robustness and stability to the cell-autonomous molecular clock and generates rhythmic output that is more precise than that provided by an individual neuron (Herzog et al., 2004).

Together, these studies hint that some signaling factor or factors are mediating cell coupling within the SCN neural network. Indeed, TTX provokes desynchronization among SCN neurons, speaking to the necessity for synaptic transmission (Honma et al., 2000; Yamaguchi et al., 2003). The potential correlation between circadian firing rate and synaptic connectivity was investigated in a multi-electrode study by Shirakawa et al. The majority of neuron pairs analyzed demonstrated no correlation in the phase of their circadian firing rhythm. Similarly, no synaptic interaction could be detected in these pairs. However, in the 45 pairs that did show circadian synchrony, a synaptic

relationship was detected (Shirakawa et al., 2000). Therefore, synaptic transmission seems to be necessary for SCN cell coupling, and yet the substance mediating this synchrony has remained elusive. Vasoactive intestinal polypeptide (VIP), gastrin-release peptide (GRP), neurotensin (NT) and gamma-Aminobutyric acid (GABA) have all been implicated in cell coupling. In recent years, understanding the mechanisms mediating SCN synchrony has been a major focus in the field of chronobiology. The second chapter of this work uses new techniques to address GABA's role in mediating SCN synchrony.

1.5 SCN neuroanatomy

1.5.1 Afferents

The SCN is defined as the bilateral region of high neuronal density located above the optic chiasm and flanking the third ventricle. This location situates the SCN in an ideal position to receive extensive input from both optic nerves via the retinohypothalamic tract (RHT). Indeed, a major source of input to the SCN comes from specialized intrinsically-photosensitive retinal ganglion cells. Melanopsin confers these retinal ganglion cells with the unique ability to sense environmental light information directly, independent of rod and cone photosensitivity. This retinal light information is conveyed to the SCN by synapses containing glutamate and pituitary adenylate cyclase activating peptide (PACAP). Ambient light information phase-locks the SCN in a process called entrainment. Light is the most important zeitgeber, but as mentioned, the SCN can also be entrained by a variety of non-photic sensory inputs. Major sources of these non-photic stimuli originate from the intergeniculate leaflet (IGL) of the

thalamus and the dorsal raphe nucleus. The IGL conveys GABAergic and neuropeptide Y (NPY) input, while that from the raphe nuclei is serotonergic. Besides these primary three input streams, numerous less significant afferents have been identified through retrograde tract tracing studies (Krout et al., 2002).

1.5.2 Neuropeptide expression and partitioned framework

Heterogeneity is a noteworthy feature of the SCN. SCN neurons express several neuropeptides, including vasopressin (AVP), vasoactive intestinal polypeptide (VIP), gastrin releasing peptide (GRP), substance P (SP), neurotensin (NT), enkephalin (ENK), somatostatin (SS) and cholecystokinin (CCK). Immunohistochemical staining for these peptides reveals regional clustering of neurons within the nuclei. Furthermore, certain genes other than neuropeptides (such as calbindin and calretinin) display regional expression throughout the SCN. Colocalization studies indicate that some neurons are positive for multiple neuropeptides antigens, adding an additional layer of complexity to SCN organization. Strikingly, the regional expression of VIP within the ventrolateral SCN correlates with the axon terminal fields of several key inputs into the SCN (see above), leading researchers to impose a dichotomy unto the SCN whereby neurons in the ventrolateral “core” receive sensory input from the RHT and IGL, which is then conveyed to output neurons in the dorsomedial “shell.” Although this framework has been a useful framework for SCN analysis, it may be limiting researchers from a more complete understanding of SCN organization (Morin, 2007).

1.5.3 Cytoarchitecture and local connections

Like other regions of the hypothalamus, the SCN has no clear laminar structure. An extensive morphological study classified SCN neurons as either radial multipolar, bipolar, or monopolar (Van den Pol, 1980). SCN neurons have one to three dendrites that average ~180 um in length, rendering a total dendritic field of approximately 350 μm (Jobst et al., 2004). Dendrites sprawl in all directions, although there is some preference for a dorsomedial orientation. Therefore, dendritic fields are capable of spanning the entire nuclei. Most SCN neurons have short axons of approximately 50 μm—much shorter than their dendrites. The majority of these axons have axon collaterals that terminate within the SCN (Van den Pol, 1980; Card and Moore, 1984; Van den Pol and Gorcs, 1986). Collectively, these cytoarchitectural descriptions portray the SCN as a diffuse and complex interconnected synaptic network. Indeed, an extensive confocal microscopy study found dense reciprocal innervation between nearly all immunoreactive subpopulations of SCN neurons examined, leading the authors to describe the SCN as an "oscillatory/reverberative [network] generated by a non-linear self-organizing system" (Romijn et al., 1997; LeSauter et al., 2002). This model is supported by an electrophysiological study that demonstrated functional local activity using focal application of glutamate and glutamate uncaging, supporting the model of the SCN as a network of local inhibitory circuits (Strecker et al., 1997). Despite the wealth of information describing the anatomy and physiological activity of the local SCN "meshwork," the functional role of interneuronal communication within the SCN remains unclear. In this dissertation, I have addressed a possible functional role of local GABA communication between SCN neurons.

1.5.4 Efferents

The SCN projects to numerous downstream targets, most of which are in the hypothalamus (Watts and Swanson, 1987; Kalsbeek et al., 1993; Morin, 1994). Despite this divergence, three significant pathways stand out: 1) an anterior projection to the ventral lateral septum, bed nucleus of the stria terminalis and anterior paraventricular thalamus; 2) a projection running along the third ventrical to nearby hypothalamic targets including the subparaventricular zone, the paraventricular nuclei, the ventromedial and dorsomedial nuclei, the preoptic area, and the premammillary area and 3) a posterior projection to the posterior paraventricular thalamus, precommissural nucleus and olivary pretectal nucleus (Morin, 2013).

In addition to these neural pathways, the SCN probably orchestrates some degree of signaling through paracrine or humoral factors. Indeed, the SCN is poised to mediate paracrine signaling through ventricular secretion. The exact nature of these signals remains uncertain, but transplants of SCN tissue encapsulated in membranes that permit diffusion of small molecules but prevent neurite outgrowth are able to partially rescue behavioral (but not endocrine) rhythms in SCN-lesioned animals, arguing for a role of diffusible molecules from the transplant (Silver et al., 1996).

1.6 GABA machinery in the SCN

GABA is the primary inhibitory neurotransmitter in the mammalian central nervous system. GABA is synthesized from glutamate by glutamic acid decarboxylase (GAD). The mammalian genome encodes two GAD isoforms, encoded by two separate

genes, GAD65 and GAD67, named for their protein molecular weight. SCN neurons are considered to be GABAergic as nearly all neurons in the SCN express GAD and there is ubiquitous staining for GABA throughout the SCN (Okamura et al., 1989; Moore and Speh, 1993; Castel and Morris, 2000; Belenky et al., 2003; Jobst et al., 2004). Interestingly, GAD expression and activity may be under circadian control (Cagampang et al., 1996; Huhman et al., 1996; Huhman et al., 1999; Panda et al., 2002), which could explain the observed rhythmicity of GAD activity (Aguilar-Roblero et al., 1993) and GABA-mediated synaptic currents (Itri and Colwell, 2003; Itri et al., 2004).

Once synthesized, GABA molecules are loaded into synaptic vesicles by the vesicular GABA transporter (VGAT), also known as the vesicular inhibitory amino acid transporter (VIAAT) due to its additional ability to transport glycine (Jonas et al., 1998). Protein-protein interactions exist between GAD65 and VGAT, suggesting that the synthesis and transport of GABA are coupled processes (Jin et al., 2003). VGAT uses the electrochemical gradient for H^+ and possibly Cl^- to load GABA into synaptic vesicles (Hsu et al., 1999; Riazanski et al., 2011).

Following vesicle fusion, GABA reaches concentrations in the synaptic cleft in the range of 1.5 to 3 mM (Mozrzymas et al., 2003; Barberis et al., 2004), and binds to its cognate receptors, the ionotropic $GABA_A$ receptors or the metabotropic $GABA_B$ receptors. $GABA_A$ receptors are pentameric structures composed of 19 possible subunits: α(1–6), β(1–3), γ(1–3), δ, ε, θ, π, and ρ(1–3). Despite the propensity for receptor diversity, the observed subunit compositions are limited by several factors including 1) cell-type specific expression 2) preferential assembly interactions and 3) interactions with proteins involved in assembly, transport, subcellular targeting, and

synaptic anchoring (Mortensen et al., 2012). Most commonly, synaptic $GABA_A$ receptors are composed of two α subunits, two β subunits, and a γ subunit. In SCN neurons, three α (α2, α3, and α5), two β (β1 and β3), and two γ (γ1 and γ2) $GABA_A$ receptor subunits have been identified (Gao et al., 1995; O'Hara et al., 1995; Naum et al., 2001; Belenky et al., 2003; Jobst et al., 2004). Interestingly, certain $GABA_A$ subunits may be under circadian regulation in the SCN (Naum et al., 2001).

While αβγ hetero-pentamers are found both synaptically and extrasynaptically, $GABA_A$ receptors containing the δ subunit are generally restricted to extrasynaptic sites. These extrasynaptic αβδ receptors often include a specialized α subunit—usually either α4 or α6. αβδ receptors exhibit high sensitivity to GABA and slow rates of desensitization. This combination of properties bestows αβδ receptors with the unique ability to mediate tonic GABA currents. Currently, there is only indirect evidence for the presence of tonic GABA currents in SCN neurons (Ehlen and Paul, 2009; McElroy et al., 2009).

$GABA_A$ receptor gating opens an anion-selective pore which is permeable to both Cl^- and the bicarbonate ion (HCO_3^-). Approximately 80% of the current is carried by Cl^-. Therefore, the reversal potential for $GABA_A$ receptors (E_{GABA}) is primarily determined by the reversal potential for Cl^-, E_{Cl}. E_{Cl} critically depends on the intracellular concentration of chloride, $[Cl^-]_i$. In neurons, $[Cl^-]_i$ is established by a family of cation chloride cotransporters (CCCs) which use the concentration gradients of Na^+ or K^+ ions to transport Cl^- ions—the CCCs are secondary active transporters, relying on the potential energy established by the Na^+/K^+ ATPase in order to transport Cl^- against its electrochemical equilibrium (Blaesse et al., 2009). Originally studied in non-neuronal

cells for their roles in cell volume regulation, more recently, they have gained attention for their roles in neuronal Cl^- regulation. For most mature neurons, $[Cl^-]_i$ is low, resulting in Cl^- influx upon $GABA_A$ receptor activation and classical inhibitory neurotransmission. This gradient is established by the activity of the potassium-chloride-cotransporters (KCCs), which remove one K^+ ion and one Cl^- ion with a 1:1 stoichiometry (Blaesse et al., 2009). Four KCCs have been identified in the mammalian genome, KCC1-4. All four are expressed in the CNS, but KCC2 expression is exclusively neuronal. Therefore, the uniquely low $[Cl^-]_i$ observed in neurons has been largely attributed to the activity of KCC2.

During embryonic development and early neonatal life, GABA transmission is excitatory in central neurons. This period of excitatory GABA correlates with elevated brain expression of the sodium-potassium-chloride cotransporter 1, NKCC1 (Hubner et al., 2001; Yamada et al., 2004). However, this idea has been contested (Clayton et al., 1998; Yan et al., 2001; Mikawa et al., 2002; Wang et al., 2002). NKCC1 mediates Cl^- uptake, transporting one Na^+ and one K^+ with every two Cl^- ions. Therefore, increased neonatal activity of NKCC1 relative to KCC2 may underlie neonatal excitatory GABA. Excitatory GABA transmission has also been observed in several regions of the adult brain, including the dentate gyrus, the auditory brainstem, the supraoptic nucleus, the paraventricular nucleus, and the suprachiasmatic nucleus (see below)(Wagner et al., 1997; Price and Trussell, 2006; Chiang et al., 2012; Haam et al., 2012). Further, several studies have described an excitatory effect of GABA input onto axons of central and peripheral neurons. Ascription of NKCC1 to excitatory GABA in these regions has been mixed. For example, NKCC1 activity was responsible for excitation in the

paraventricular nucleus, but was not found to contribute to Cl^- accumulation in the calyx of Held (Price and Trussell, 2006).

E_{GABA} varies widely between neurons and even within neurons. Notably, E_{GABA} rarely coincides with the thermodynamic equilibrium of either the KCCs or NKCC1 (Ebihara et al., 1995; Martina et al., 2001; Balakrishnan et al., 2003; Yamada et al., 2004; Tyzio et al., 2008; Glykys et al., 2009; Dzhala et al., 2010). Further, a push-pull relationship between NKCC1 and KCC2 is not energetically favorable. A suitable explanation for these issues may be found in the kinetic regulation of CCC activity. The kinetics of membrane Cl^- transport will depend on the number of functional membrane transporters as well as their intrinsic transport rates (Blaesse et al., 2009). The phosphorylation state of the CCC determines the rate of transport: generally, phosphorylation enhances NKCC1 activity, while phosphorylation inactivates the KCCs (Kahle et al., 2010). The signaling pathways and kinases regulating CCC phosphorylation state is an emerging field of study that is likely to provide key new insight into $[Cl^-]_i$ regulation.

1.7 Excitatory GABA transmission in the SCN

Early reports investigating the effect of GABA on SCN neurons observed the normal inhibitory action (Liou and Albers, 1990; Mason et al., 1991; Bos and Mirmiran, 1993; Chen et al., 1996; Liu and Reppert, 2000). Further, these studies indicated that the efficacy of GABA-mediated inhibition was constant throughout the day. In 1997, Wagner et al. were the first to observe excitatory GABA transmission in the adult SCN. They concluded that GABA was predominantly excitatory during the day—bath

application of GABA increased action potential discharge in 71% of neurons during the day, but decreased firing in 56% of neurons during the night (Wagner et al., 1997). Two years later, a collaboration of three labs using independent electrophysiological techniques published a rebuttal, insisting that GABA is exclusively inhibitory in the SCN (Gribkoff et al., 1999). To further complicate the issue, the next major study addressing excitatory GABA transmission in the SCN concluded that GABA can be depolarizing, but that depolarization is more common during the night, contradictory to Wagner's initial findings (De Jeu and Pennartz, 2002). Albus et al. added a layer of anatomical complexity to the issue, observing that GABA was exclusively inhibitory in the ventral SCN, but is excitatory in the ventral SCN during the late day and early night (Albus et al., 2005). Choi et al. used extracellular recordings to characterize the effect of GABA by cell location, retinal innervation, and ZT, concluding that an excitatory action of GABA is present across all of these variables, although minor (Choi et al., 2008). Irwin and Allen re-examined GABA transmission in the SCN using Ca^{2+} imaging. In a subset of neurons, GABA was sufficiently depolarizing to elicit Ca^{2+} transients mediated by voltage-sensitive Ca^{2+} channels. These GABA-induced Ca^{2+} transients were observed both in the day (46%) and the night (66%), and were most prevalent in the dorsomedial SCN (Irwin and Allen, 2009). An extensive gramicidin perforated-patch study described both regional and circadian regulation of E_{GABA} in the SCN. In their model, during the day GABA is excitatory in the dorsal SCN but inhibitory in the ventral SCN, and during the night, GABA is inhibitory in the dorsal SCN but excitatory in the ventral SCN (Alamilla et al., 2014). When characterizing fast synaptic connections between SCN neurons using multi-electrode arrays, Freeman et al. concluded that approximately 40%

of GABAergic connections were excitatory and remained excitatory throughout the day (Freeman et al., 2013). Using optogenetic techniques, Fan et al. found that approximately 56% of day neurons and 43% of night neurons increased their firing rate upon optical stimulation of VIP-expressing neurons (Fan et al., 2015). Interestingly, excitatory GABA transmission has also been found to depend on photoperiod. GABAergic excitation was most prominent in animals entrained to long days (Farajnia et al., 2014). In conclusion, GABA has been reported to be exclusively inhibitory, inhibitory during the day and excitatory during the night, and excitatory during the night and inhibitory during the day.

Some of the discrepancies between these studies may be attributed to differences in the definition of excitation. Strictly speaking, inhibition reduces the probability of a neuron reaching AP threshold, whereas excitation increases that probability. Regardless of the value of E_{GABA}, activation of $GABA_A$ receptors will increase membrane conductance, resulting in shunting inhibition. Shunting inhibition acts by decreasing the temporal and spatial summation of excitatory input. Even if E_{GABA} is depolarizing, this shunting effect will be functionally inhibitory. Therefore, whether GABA is ultimately excitatory or inhibitory will depend on the method used to draw the conclusion—techniques that measure AP discharge may be the most physiologically relevant. Regardless of the specifics, it is clear that GABA can be excitatory in the adult SCN.

1.8 Mechanisms of excitatory GABA transmission in the SCN

Although depolarizing GABA has been reported by several labs, the mechanisms underlying E_{GABA} regulation have received less attention. Secondary to any shunting inhibition, the voltage effects of $GABA_A$ receptor activation will depend on the location of V_m relative to E_{GABA}. The resting membrane potential has been shown to be under circadian regulation in SCN neurons (Colwell, 2011). Therefore, circadian variation in V_m may be partially responsible for excitatory GABA transmission. Accumulating evidence indicates that E_{GABA} is also under circadian control. Using a series of voltage-clamp protocols, Wagner et al. characterized two Cl^- transport mechanisms—one that replenishes the cell after Cl^- depletion, and a second that extrudes Cl^- after Cl^- loading. They observed that the 'replenishing' transport process was less effectual during the night, explaining the prevalence of GABAergic excitation during the day. Shimura et al. described a dependence of E_{GABA} on the animal's time of death when measured in acutely dissociated neuronal cultures (Shimura et al., 2002), but this observation is difficult to interpret as SCN neurons are known to continue cycling in culture.

New insights into SCN Cl^- regulation came from molecular anatomy. Key determinants of neuronal chloride demonstrated differential expression throughout the SCN. KCC2 expression abounds in the ventrolateral SCN, but is deficient in the dorsomedial SCN (Kanaka et al., 2001; Belenky et al., 2008). Instead, KCC3 and KCC4 are prominent in dorsomedial SCN. NKCC1 was shown to be expressed throughout the SCN, with particularly high density in the dorsomedial SCN (Belenky et al., 2010). The differential expression of CCCs throughout the SCN suggests that $[Cl^-]_i$ (and E_{GABA}) may vary throughout the SCN. Further, CCC expression correlated with neuropeptide

content, suggesting that $[Cl^-]_i$ may vary according to cell identity. Western blot analysis of SCN tissue further implicated NKCC1 in SCN chloride regulation: NKCC1 expression was highest in the dorsomedial SCN during the night (Choi et al., 2008). Further, three groups have agreed that blocking NKCC1 with bumetanide decreased the amplitude of GABA-induced Ca^{2+} transients (Choi et al., 2008; Irwin and Allen, 2009; Farajnia et al., 2014). WNK3, a chloride-sensitive serine-threonine kinase known to regulate CCC kinetics was identified in soma and dendrites throughout the SCN. Therefore, WNK3 may execute circadian regulation of $[Cl^-]_i$ in the SCN. Collectively, these results imply unique features of Cl^- regulation in the SCN, suggesting that $[Cl^-]_i$ may vary in relation to cell type or time of day.

1.9 Functional roles of GABA in the SCN

Most hypothalamic neurons express a neuropeptide in addition to a fast neurotransmitter such as glutamate or GABA. While ablation studies can reveal relationships between groups of neurons and particular behaviors, parsing out the roles of the various signaling molecules within the targeted neurons remains challenging (Schone and Burdakov, 2012). This problem is compounded in the hypothalamus where neural circuits lack clear organization, signal processing is non-linear, and nuclei lack the laminar organization found in other parts of the brain. Such complexity is especially profound in the SCN where cellular heterogeneity abounds. And yet, GABA expression is common to SCN neurons. Here, I discuss some of the roles ascribed to GABA's function in the SCN.

1.9.1 Retinohypothalamic tract synaptic regulation

$GABA_B$ receptors regulate glutamate release from retinohypothalamic tract terminals synapsing onto SCN neurons (Shibata et al., 1986; Jiang et al., 1995). Subsequent research has indicated that these presynaptic $GABA_B$ receptors mediate this effect by inhibiting RHT terminal calcium channels (Moldavan et al., 2006) and that this regulation is sensitive to circadian changes in ambient GABA concentration (Moldavan and Allen, 2013). Consistent with these physiological data, $GABA_B$ receptor agonists attenuate light-induced phase delays in the early night while $GABA_B$ antagonists facilitate these phase delays (Gillespie et al., 1997).

1.9.2 Phase shifts

As discussed, several zeitgebers are able to adjust the phase of the internal circadian clock. Light is the most well-studied zeitgeber, and yet the signaling pathway from light information to clock gene expression is not fully resolved. In part, glutamatergic fibers from the retina excite SCN neurons leading to Ca^{2+} influx, a rise in cAMP, activation of cAMP response element-binding protein (CREB), and induction of period genes. Therefore, post-synaptic effects of GABA on V_m or Ca^{2+} entry is likely to influence the phase of SCN neurons. In a study using multi-electrode arrays to track the firing rate of individual neurons over several days, treatments with the $GABA_A$ receptor agonist muscimol elicited phase-shifts in a phase-dependent manner (Liu and Reppert, 2000). Similarly, behavioral studies have found roles for GABA signaling in phase resetting. During the day, $GABA_A$ receptor activation elicits phase advances in nocturnal rodents, but phase delays in diurnal species (Smith et al., 1989; Novak and

Albers, 2004). During the night, $GABA_A$ receptor activation attenuates the ability of light to induce either phase advances or delays (Gillespie et al., 1996; Gillespie et al., 1997). Conversely, blocking $GABA_A$ receptors with bicuculline potentiated photic phase shifts (Gillespie et al., 1996). Similar effects of GABA were observed when phase was monitored with clock gene expression instead of behavior. Light-induced clock-gene expression was inhibited by $GABA_A$ receptor activation (Ehlen et al., 2008). Therefore, GABA opposes the phase-shifting effects of light at both the behavioral and molecular levels. Together, these studies indicate that $GABA_A$ receptors regulate the efficacy and gating of phase-shifts in the SCN.

1.9.3 Firing frequency

GABAergic IPSPs are prevalent in SCN neurons (Kim and Dudek, 1992; Strecker et al., 1997); (Jiang et al., 1997; Itri and Colwell, 2003; Gompf and Allen, 2004; Itri et al., 2004; Gompf et al., 2006). Kononenko and Dudek demonstrated that this constant bombardment of inhibitory input is responsible for the irregular firing observed in a population of SCN neurons—application of GABAergic antagonists increased the regularity of action potential discharge (Kononenko and Dudek, 2004).

1.9.4 Circadian synchrony or 'coupling'

SCN neurons do not synchronize their AP discharge on a millisecond timescale as observed in other regions of the brain. However, the SCN does display a circadian rhythm in AP discharge, with peak firing frequency occurring around the middle of the day, indicating that SCN neurons do coordinate their firing patterns, albeit on a relatively

slow timescale. As discussed previously, synaptic connectivity is essential for this circadian synchrony among SCN neurons. Several lines of evidence suggest that synaptic GABA transmission coordinates phase synchrony between SCN neurons. In phase-dispersed cultures, long duration applications of GABA were found to synchronize circadian firing frequencies (Liu and Reppert, 2000). Using multi-unit *in vitro* recording, Albus et al. found a single peak in AP discharge in control slices, but two peaks in AP discharge in rats subjected to a 6 hour phase delayed. One peak corresponded to the middle of the day in the new phase-delayed light-dark cycle, while the other peak corresponded to the middle of the day in the prior light-dark cycle. GABAergic synaptic signaling was required for the ventral SCN to convey phase information to the dorsal SCN (Albus et al., 2005). Together, these two studies indicate that GABA is able to synchronize SCN neurons. However, GABA's role in orchestrating circadian synchrony has been contested. Two reports have concluded that GABA does not contribute to circadian synchrony (Aton et al., 2006; Freeman et al., 2013). In fact, these studies found that GABA destablized circadian rhythms in either AP discharge or clock gene expression, concluding that GABA signaling dampens circadian rhythms and introduces 'jitter' into the network, rendering it more susceptible to entrainment signals. Therefore, the most parsimonious explanation is that GABA signaling is sufficient but not necessary for circadian synchrony.

A new experimental model has helped to resolve some of these seemingly contradictory findings. In this model, the phase of individual neurons was analyzed relative to the average phase of the SCN. After long day photoperiods, SCN explants showed a greater degree of phase dispersion compared to slices from mice entrained to

12:12 light-dark cycles. The phase relationship showed a regional pattern, where the dorsal SCN phase-led the ventral SCN. Over time in culture, the phase relationship from long day animals gradually adjusted to match that from 12:12 entrained mice. $GABA_A$ signaling was found to be essential for this adjustment of phase relation, leading the authors to conclude that "$GABA_A$ signaling promotes network synchrony in an antiphase state, but opposes network synchrony in a steady-state configuration" (Evans et al., 2013).

1.10 Specific aims

Therefore, due to the importance of GABA in the SCN, this dissertation presents experiments designed to investigate the physiological and functional roles of GABA transmission in the SCN.

1.10.1 The functional role of GABA transmission in the SCN

Elucidating the *in vivo* role of GABA transmission within the SCN has been challenging. Global knockouts of GABA transmission are lethal, and results from intracranial cannulation can be difficult to interpret. The recent dawning of intersectional genetics has provided new techniques to deconstruct neural circuits. Using such approaches, I have produced a local depletion of GABA transmission in the SCN neural network to test for GABA's role in mediating circadian synchrony.

1.10.2 Cl^- regulation in SCN neurons

Previous studies have shown that $GABA_A$ receptor activation can be either excitatory or inhibitory in SCN neurons, suggesting that the Cl^- reversal potential may be under circadian regulation. In a series of electrophysiological and fluorometric experiments, I have investigated the role of key chloride cotransporters in regulating the intracellular Cl^- concentration. The activity of NKCC1 and KCC2 were assessed during the day and night, and in genetically-defined subpopulations of SCN neurons.

CHAPTER 2: LOCAL GABA TRANSMISSION IS REQUIRED FOR SUPRACHIASMATIC NUCLEUS CIRCADIAN OUTPUT

Nathan J. Klett[1,2], Heinrich S. Gompf[3]*, Charles N. Allen[1], Olga Cravetchi[1], William Todd[3], Clifford B. Saper[3], Patrick M. Fuller[3]

[1]Oregon Institute for Occupational Health Sciences, [2]Neuroscience Graduate Program, Oregon Health & Science University,
Portland, OR 97239 USA

[3]Department of Neurology, Division of Sleep Medicine, and Program in Neuroscience
Beth Israel Deaconess Medical Center, Harvard Medical School
Boston, MA 02215 USA

*Present address:
Department of Neurobiology, Physiology, and Behavior
University of California at Davis
Davis, CA 95616 USA

2.1 Abstract

The neurotransmitter γ–aminobutryic acid (GABA) is expressed in most neurons of the brain's master biological clock, the suprachiasmatic nucleus (SCN). The function of GABAergic signaling within the SCN neural network, however, remains poorly understood. Here we show that genetic deletion of the vesicular GABA transporter (VGAT), and hence disruption of synaptic release of GABA from SCN neurons, results in the deterioration of behavioral rhythmicity *in vivo* and concomitant cellular desynchonry *in vitro.* These findings suggest that GABAergic signaling is essential for proper SCN network function and coherent rhythmicity.

2.2 Introduction

The master mammalian circadian oscillator, located in the suprachiasmatic nucleus (SCN) of the hypothalamus, is composed of cell-autonomous neuronal oscillators (Hastings et al., 2003; Roenneberg et al., 2003; Aton et al., 2005; McDearmon et al., 2006; Mohawk and Takahashi, 2011). When cultured at low density, individual SCN neurons exhibit a range of circadian periods; *in vivo* they are synchronized to a common period via poorly understood intercellular signaling mechanisms (Welsh et al., 2010). Furthermore, the network properties of the SCN provide stability for circadian rhythms against mutations that affect the transcription-translation feedback loops of the molecular clock (Liu et al., 2007). Thus, intercellular signaling within the SCN network is critical for the generation and maintenance of behavioral circadian rhythms.

SCN neurons differ in their expression of several neuropeptides, but all synthesize the fast-acting neurotransmitter GABA and its receptors (Abrahamson and Moore, 2001). Still, the functional role of GABA transmission from SCN neurons has remained elusive. Anatomical studies report that SCN neurons have GABAergic terminals both within and afferent to the SCN (Moore and Speh, 1993; Castel and Morris, 2000; Abrahamson et al., 2001). An important role of the SCN neural network is to mediate neuronal cell coupling (Welsh et al., 1995; Aton and Herzog, 2005). Blocking action potentials with tetrodoxin (TTX) provokes desynchronization of SCN neurons, suggesting that synaptic transmission is necessary for synchrony (Honma et al., 2000; Yamaguchi et al., 2003). *In vitro* studies have provided mixed results concerning GABA's role as a synchronizing agent within the SCN (Liu and Reppert, 2000; Albus et al., 2005; Aton et al., 2006; Evans et al., 2013; Freeman et al., 2013). In SCN neuronal cultures, applications of GABA were found to synchronize circadian firing frequencies (Liu and Reppert, 2000). Albus et al. reported that GABA signaling was required for the ventral SCN to synchronize to the dorsal SCN after a phase delay (Albus et al., 2005). However, two reports have concluded that GABA does not contribute to circadian synchrony (Aton et al., 2006; Freeman et al., 2013). Recently, it was proposed that GABA signaling promotes synchrony in an antiphase state, but opposes synchrony in a steady-state configuration (Evans et al., 2013).

A major barrier to understanding the role of GABA in the SCN has been the lack of methods to produce long-term modulation of the GABA system. Global knockouts of GABAergic transmission in the CNS are lethal (Wojcik et al., 2006). Further, the $GABA_A$ receptor is a pentamer assembled from a family of at least 18 possible subunits, but

none are exclusive to the SCN. To better understand GABA's role in SCN function and circadian rhythmicity, we selectively disrupted GABA transmission in SCN neurons of adult mice. Our results indicate that SCN GABA transmission is required for coherent physiological and behavioral rhythmicity *in vivo* and contributes to the synchronization of SCN neurons *in vitro*.

2.3 Methods

2.3.1 Mice and animal care

We used mice with three different transgenic mouse lines in this study. In the *Vgat*$^{lox/lox}$ mice, *Vgat* has been modified to contain loxP sites flanking the gene's translational start site in the second exon (Tong et al., 2008). In the PER2::LUC reporter line, luciferase is fused in-frame to the endogenous PER2 gene (Yoo et al., 2004). For *mPer1*-Venus fluorescence imaging experiments, mice contained the *Per1*^{Venus} allele in which Venus is inserted into the promoter region of *mPer1* (Cheng et al., 2009). Genotyping was performed by an external facility (Transnetyx, Inc). All transgenic mice were on a C57BL/6 genetic background. Unless otherwise mentioned, mice were housed in 12:12 light-dark (LD) cycles. All tissue was prepared during the animal's light cycle and data were plotted relative to time of lights on (zeitgeber time or ZT, lights on = ZT0). The age of the mice used in these experiments ranged from four to six months old. All procedures were performed in accordance with the guidelines of the Animal Care and Use Committees of Oregon Health & Science University and Beth Israel Deaconess Medical Center.

2.3.2 Intracranial viral injections

Adult mice were anaesthetized with an isoflurane/oxygen mixture. Throughout the surgery, the depth of anesthesia was monitored by assessment of the rate of respiration and anesthesia was confirmed by the absence of a withdrawal reflex in response to tail pinch. Once anesthesia was established, mice were placed on a heating pad, and immobilized in a stereotaxic frame. The head was positioned with ear bars, and isoflurane was delivered to the nosecone. The surgical area was shaved, and treated with ethanol and betadine. The scalp was incised (about 5 mm) and a small burr hole was drilled in the skull. A glass micropipette (tip diameter 3-5 μm) was then lowered to the designated coordinates, and the AAV injected with either an air pressure device (Picospritzer, General Valve Corporation) or a pneumatic injection unit (Nanoject, Drummond Scientific). Coordinates for SCN injection were ±0.15 lateral, −0.45 posterior, and −5.5 mm ventral to bregma. Coordinates for SPZ injection were identical but −5.0 mm ventral to bregma. The injection volume ranged from 100 – 200 nL (titer: approximately 2-10^{12} particles/mL). Mice received either AAV-Cre, AAV-Cre-GFP, AAV-GFP (serotypes 10, Boston Children's Hospital Viral Vector Core), or AAV-Cre-mCherry (serotype 8, University of North Carolina Viral Vector Core) according to the experiment. After injection, the pipette was withdrawn, and the wound was sealed with surgical glue. Betadine and triple antibiotic ointment were applied to the surrounding area. Anesthesia was discontinued, and the mouse was moved to a heated recovery cage. Once awake, the mouse was transferred to its home cage. Most mice used in this study were injected in Boston at Beth Israel Deaconess Medical Center under the direction of Dr. Patrick Fuller. After a minimum of two weeks after

surgery, mice were shipped to Oregon Health & Science University and quarantined for three weeks prior to any experimentation. Mice used for *mPer1*-Venus experiments were injected at Oregon Health & Science University by the author.

2.3.3 Electrophysiology

Mice were entrained to a LD 12:12 cycle, with lights on at 10 AM. Mice were removed from housing, anaesthetized with isoflurane, and decapitated. The brain was quickly removed and submerged in an ice-cold slicing solution consisting of (in mM): 126 NaCl, 26 $NaHCO_3$, 11 dextrose, 4 $MgCl_2$, 2.5 KCl, 1.2 NaH_2PO_4, and 0.5 $CaCl_2$, saturated with 95% O2, 5% CO2, ~300 mOsm. The brain was blocked and 250 µm thick coronal slices were prepared with a Leica VT1000S vibratome. Slices were then transferred to an aCSF containing (in mM): 132.5 NaCl, 22 $NaHCO_3$, 11 dextrose, 2.5 KCl, 2.4 $CaCl_2$, 1.2 $MgCl_2$, and 1.2 NaH_2PO_4 and allowed to incubate at 36°C for 1-4 hours before recording. Brain slices were visualized under epifluorescence to verify successful transduction of AAV-Cre-GFP in the SCN. For whole-cell patch clamp recording, slices were imaged under DIC optics and single cells were targeted from the dorsomedial SCN with boroscillicate glass pipettes (4-7 MΩ) filled with (in mM): 145 KCl, 10 HEPES, 4 Mg-ATP, 2 NaCl, and 1 EGTA. Following gigaseal formation, the cell membrane was ruptured and allowed to equilibrate for 5 minutes before the onset of recording. To isolate miniature $GABA_A$-mediated post-synaptic currents (mGPSCs), 10 µM CNQX and 0.5 µM TTX was added to the recording solution. These currents were confirmed to be GABAergic as application of picrotoxin at the end of several recordings completely eliminated synaptic activity. A high concentration of intracellular Cl^- was

used to facilitate the detection of synaptic currents. Because these currents were inward, we elected to refer to them as mGPSCs instead of inhibitory post-synaptic currents. All experiments were done at 32°C with a 1-2 mL/min flow rate. Whole-cell recordings were performed with a Axopatch-1D amplifier, filtered at 2 kHz, digitized at 5 kHz, and acquired with Patchmaster v5.3. Cells were voltage-clamped at −60 mV, and cells with holding currents less than −50 pA were excluded from analysis. A small voltage step was used to monitor series resistance. Only cells with stable (less than 20% change) series resistance values less than 40 MΩ were kept for analysis of mGPSCs.

mGPSCs detection and analysis was performed with custom macros for Igor Pro (Version 6.22A; Wavemetrics). To detect mGPSCs, a threshold filter (−3 nA/s) was applied to the first derivative of the current trace. Events exceeding this threshold were considered to be mGPSCs and were kept for subsequent analysis. For each cell, average amplitude was obtained from a composite mGPSC.

2.3.4 Behavior

Adult mice were housed individually in cages equipped with a running wheel, and maintained in climate-controlled environmental chambers (Percival Scientific). Housing light intensity was approximately 300 lux. Wheel rotations were monitored through magnetic induction and acquired every 5 minutes with Vitalview software. Time series data were imported into Clocklab (Actimetrics) for analysis of behavioral rhythmicity. Actograms were double-plotted and ‘scaled’ was selected for the display setting. Chi-square periodograms were generated from 10 days of wheel-running data in constant

darkness with a 1 min block size (Sokolove and Bushell, 1978). The dashed line indicates a *p*-value of 0.05. The largest peak in the periodogram in the range of 12-36 hours was selected as the dominant circadian period. The amplitude of this peak for the behavior of each mouse was used to compare between genotypes.

2.3.5 Luminometry

Vgat$^{lox/lox}$, *Per2*^{Luc} mice were entrained to a 12:12 LD cycle and killed during the animal's light cycle as described above. Using sterile techniques, brains were quickly removed and submerged in sterile-filtered (0.2 µm) chilled 1x Hanks' buffered salt solution (HBSS; 10x HBSS without Ca^{2+}, Mg^{2+} and $NaHCO_3$, Life Technologies, #14065; supplemented with 4.5 mM $NaHCO_3$, 10 mM HEPES, 100 u/mL penicillin and 100 u/mL streptomycin). Cultures were prepared as described previously (Yamazaki et al., 2000; Abe et al., 2002). Briefly, the brain was blocked and 300 µm coronal slices were prepared with a vibratome (VT1000S; Leica-Microsystems). SCN slices were trimmed to remove surrounding hypothalamic tissue, and positioned unto Millicell cell culture inserts. Inserts were placed in 35 mm culture dishes containing 1.2 mL culture medium and sealed with sterile vacuum grease. Culture medium consisted of DMEM supplemented with B27, 20 mM glucose, 10 mM HEPES, 4.2 mM $NaHCO_3$, 25 µg/mL penicillin, 25 µg/mL streptomycin, and 0.1 mM beetle luciferin. Dishes were placed into an Actimetrics Lumicycle and photons were counted for 75 seconds every 10 minutes. Data was imported into the Actimetrics Lumicycle Analysis program, smoothed at a value of 5, and 24 and 3 hr running averages were exported for subsequent analysis. In order to control for variability in the number of PER2-expressing neurons within a slice,

individual traces were normalized to the amplitude of the first bioluminescent peak. After normalization, the value of the third peak in culture was used to compare between genotypes.

2.3.6 mPer1-Venus imaging

Organotypic slice cultures were prepared as described under luminometry. Coronal slices were sectioned at 150 μm to minimize background fluorescence. The slices were placed on a membrane insert (Millicell Organotypic Cell Culture inserts, EMD Millipore) and the insert placed into a glass-bottomed 35 mm culture dish (MatTek Corp.) containing 1.2 ml of culture media. Sealed dishes were placed in a 36°C temperature-controlled chamber (ibidi GmbH). Venus fluorescence measurements were obtained by excitation at 500/20 nm with a 515 nm long pass dichroic and a 535/30 nm emission filter (Chroma Technology). Excitation light was supplied via a Lambda LS (Sutter Instrument) comprising a Xenon Arc Lamp and filter wheel. Acquisition duration was limited to avoid photobleaching, but ranged from 500 to 1500 ms. Light passed through a Nikon Eclipse TE2000 microscope using a 10x/0.3 Plan Fluor Nikon objective. Images were captured using a cooled charge-coupled device camera (CCD, Evolve 512 EMCCD, Photometrics) controlled via the digital imaging software Metafluor (Molecular Devices). 16 bit images were acquired every 5 or 10 minutes.

Optical data were converted to relative fluorescence intensity units for each cell or region of interest using ImageJ (v1.48) (U. S. National Institutes of Health) and the Plugins Speckle TrackerJ (v0.87) and Speckle_Intensity (Smith et al., 2011).

Subsequent analysis was performed using Excel (v14.4, Microsoft), Igor Pro (v6.3, Wavemetrics) and R (v3.02, R Foundation for Statistical Computing). The background signal for each frame was subtracted with ImageJ using a sliding paraboloid radius of 50 pixels. The time and amplitude of the peak fluorescence for each cell or region of interest was determined using a custom script written in Matlab (The MathWorks, Inc.). Data were plotted using KaleidaGraph (version 3.6; Synergy Software), and R. Rhythmicity was determined by visual inspection. We used the Raleigh test derived from circular statistics to determine the degree of phase synchrony between individual SCN neurons (Batschelet, 1981). The resulting Rayleigh Statistic, R (here referred to as the "synchrony index"), quantifies the degree of phase cohesion among cells: a value of 1 indicates perfect synchrony (all cells are phase-matched) while a value of 0 indicates the absence of synchrony (the phases of individual neurons are uniformly distributed throughout the day). Rayleigh analysis was performed in R using the package "Circular" written by Ulric Lund and Claudio Agostinelli (Jammalamadaka, 2001).

2.4 Results

2.4.1 Genetically-driven disruption of SCN GABAergic transmission in vitro

To disrupt GABAergic neurotransmission in SCN neurons, we implemented an intersectional strategy, using Cre-lox technology to mediate local *Vgat* deletion. We used *Vgat*$^{lox/lox}$ mice in which the gene for the vesicular GABA transporter (VGAT, encoded by *Vgat*) has been modified to contain loxP sites flanking the gene's translational start site in the second exon (Tong et al., 2008). Cre-mediated

recombination results in an excision of *Vgat*'s translational start site, halting VGAT production. To introduce Cre recombinase into the SCN, we performed stereotaxic injections of adeno-associated viral vectors (AAV-Cre, serotype 10). In this vector, Cre is downstream of the CMV promoter, providing constitutive expression of Cre in transduced neurons. VGAT is required for synaptic release of GABA (Wojcik et al., 2006) and is expressed by nearly all SCN neurons (Figure 2.1 A). Bilateral transduction of AAV-Cre produced substantial loss of *Vgat* mRNA in the SCN (Figure 2.1 B & C). Accordingly, SCN *Vgat* deletion resulted in a decrease in the frequency of miniature $GABA_A$-mediated post-synaptic currents (mGPSCs) recorded from SCN neurons. Specifically, Cre-mediated disruption of GABAergic transmission produced a 37% reduction in mGPSC frequency from 8.1 to 5.1 Hz ($p<0.05$ using generalized estimating equations, Figures 2.1 E & F). Because a substantial proportion of the GABAergic inputs received by SCN neurons comes from other SCN neurons (Belenky et al., 1996), we attribute this decrease in mGPSC frequency to reflect a decrease in local GABAergic synaptic activity. We also noticed a small increase in average mGPSC amplitude (23.4%, $p<0.05$ using generalized estimating equations, Figures 2.1 G & H). Closer examination of the mGPSC amplitude distribution revealed that, compared to uninjected controls, SCN neurons from AAV-Cre injected $Vgat^{lox/lox}$ mice exhibited a reduction in the proportion of small amplitude mGPSCs (less than 50 pA) and a concomitant increase in the proportion of mGPSCs between 50 to 150 pA (Figure 2.1 H). Collectively, these *in vitro* findings confirm that our manipulation is able to disrupt synaptic GABA transmission in SCN neurons, and that this disruption can be observed within the local SCN network.

2.4.2 Loss of physiological rhythmicity in vivo

To assess the behavioral consequences of vesicular GABA depletion in the SCN, we monitored wheel-running activity in Cre-injected *Vgat*$^{lox/lox}$ mice. Under a 12:12 LD cycle, most Cre-injected mice exhibited normal locomotor rhythmicity, with wheel-running activity consolidated in the dark phase (Figures 2.2 A, C & E). Several Cre-injected mice displayed substantial daytime running, but the average percentage of daytime running did not significantly differ between groups (11.6 ± 3.4% for Cre-injected mice (n=22), vs 5.2 ± 2.8% for Cre-null mice (n=11); p=0.22, Student's *t*-test). Upon release into constant darkness (DD), several Cre-injected mice exhibited immediate fragmentation of their locomotor activity, with wheel-running distributed throughout the day (Figures 2.2 C & E). Because the degree of fragmentation demonstrated variability, we used the peak amplitude of chi-square periodogram obtained from 10 days of activity in constant darkness to compare the strength of rhythmicity between Cre-null and Cre-injected mice. Control mice had an average amplitude of 5234 ± 760 (n=5) while Cre-injected mice had an average amplitude of 2898 ± 257 (n=17) ($p<0.001$, Student's *t*-test, Figure 2.3). Cre-injected *Vgat*$^{lox/-}$ mice had an average amplitude of 3233 ± 402 (n=4), suggesting that loss of VGAT expression from a single allele is sufficient to elicit behavioral fragmentation. Collectively, these behavioral results indicate that SCN GABAergic transmission is necessary for the SCN to orchestrate coherent circadian rhythmicity.

In a separate set of experiments, my collaborators monitored animal body temperature (T_b) and locomotor activity rhythms via telemetry. As observed in the

wheel-running experiments, Cre-injected *Vgat*$^{lox/lox}$ mice demonstrated normal entrainment to the LD cycle, but became arrhythmic in DD (Figures 2.4 B & C). The disintegration of rhythmicity was rapid, but also variable. In some cases, release into DD resulted in an apparent phase shift, or rapid phase inversion, suggesting that the apparent entrainment in LD had been light masking, and not true photoentrainment. Collectively, these behavioral results indicate that SCN GABAergic transmission is necessary for the SCN to orchestrate coherent circadian rhythmicity.

2.4.3 Behavioral rhythmicity after disruption of subparaventricular zone GABA transmission

The subparaventricular zone (SPZ) is a major target of SCN efferents. Because injections targeting the SCN gave some expression in the SPZ, my collaborators asked whether loss of GABA transmission from SPZ neurons may have contributed to the observed behavioral arrhythmicity. We recorded LMA and T_b rhythms from *Vgat*$^{lox/lox}$ mice with Cre injections targeted to the bilateral SPZ. Cre-injected *Vgat*$^{lox/lox}$ mice demonstrated normal behavior in both LD and DD, and demonstrated no differences in phase angle of entrainment, period length, or cosinor amplitude when compared to injected controls (Figure 2.5).

2.4.4 Per2 rhythmicity intact in vitro

The observed behavioral fragmentation in constant conditions can be attributed to either a loss of rhythmicity within the SCN, or a loss of signaling from a rhythmic SCN—i.e. the locus of circadian disruption could be within the SCN itself or efferent to

the SCN. We investigated rhythmicity within the SCN using luminometry of the PER2::LUC reporter. My collaborators generated *Vgat*$^{lox/lox}$, *Per2*^{Luc} mice and injected AAV-Cre-GFP into the bilateral SCN. After recovery from surgery, shipment to OHSU, and entrainment to the light-dark cycle, I prepared organotypic SCN slices from these *Vgat*$^{lox/lox}$, *Per2*^{Luc} mice and placed them in the LumiCycle for *in vitro* monitoring of PER2 bioluminescence. To our surprise, PER2 rhythmicity could be detected in behaviorally arrhythmic mice (Figure 2.6 B). To quantify the degree of synchrony within the culture, we used the rate of damping as an index of coherent rhythmicity (Maywood et al., 2011; Mieda et al., 2015). Specifically, traces were normalized to the amplitude of the first peak in culture, and the normalized amplitude of the third peak was compared between groups. We found no difference in the third peak amplitude (0.32 ± 0.06 for Cre-injected *Vgat*$^{lox/lox}$ (n=12); 0.28 ± 0.05 for Cre-null mice (n=10); $p>0.05$, Student's *t*-test). Further, we found no difference in period between groups (24.82 ± 0.14 hrs for Cre-injected *Vgat*$^{lox/lox}$ (n=10); 24.38 ± 0.08 hrs for Cre-null mice (n=11); $p>0.05$, Student's *t*-test). We interpret these results to indicate that *Vgat* deletion within the SCN is not sufficient to disrupt the molecular clock.

2.4.5 Desynchrony of SCN neurons

Although rhythmicity was intact in SCN slices from Cre-injected *Vgat*$^{lox/lox}$ mice, it is possible that individual neurons were desynchronized within the slice. To investigate synchrony after VGAT depletion, we monitored *mPer1*-Venus fluorescence from individual neurons in organotypic slice cultures for several days (Cheng et al., 2009). *Vgat*$^{lox/lox}$, *Per1*^{Venus} mice received SCN injections of AAV-Cre-mCherry (serotype 8).

Red fluorescence was used to determine the location and precision of the injection. Most (78/101) Per1-expressing neurons were rhythmic in Cre-null control mice. To measure the degree of synchrony or phase cohesion amongst individual SCN neurons, we used the Rayleigh analysis (Batschelet, 1981). Rayleigh analysis produces a Synchrony Index which quantifies the degree of synchrony between individual neurons such that a value of 1 indicates perfect synchrony (all oscillators are phase-matched) while a value of 0 indicates the absence of synchrony (the phases of individual oscillators are uniformly distributed throughout the day). During the first cycle in culture, the three Cre-null explants had Synchrony Indexes of 0.87, 0.96, and 0.82, indicating a high degree of synchronization among neurons. Two days later, the Synchrony Indexes had dropped to 0.76, 0.61, and 0.61, indicating that desynchronization had occurred over time *in vitro*, as previously reported (Brancaccio et al., 2013; Freeman et al., 2013; Herzog et al., 2015). When cells from all three experiments were grouped together, the Synchrony Index was 0.88 for the initial peak and 0.6 for the third peak (Figures 2.7 D & E). In explants from Cre-injected mice, a smaller proportion of Per1-expressing neurons were rhythmic (36/77). Compared to Cre-null mice, the synchrony between rhythmic neurons was also reduced in Cre-injected mice. The three Cre-injected slices had an average Synchrony Index of 0.64 at the time of first peak, and 0.40 at the time of third peak, indicating that disrupting local GABA transmission decreased synchrony throughout the recording (Figures 2.7 H & I). In a Cre-injected mouse that missed the SCN, rhythmicity and synchrony were similar to that observed in the Cre-null mice (data not shown).

These results indicate that local GABA transmission contributes to the synchronization of neurons in the SCN neural network. SCN neurons may use GABA to mediate interneuronal synchronization. Synchronization is required to generate the high-amplitude output signals necessary to drive behavioral rhythms. Therefore, the observed desynchrony between SCN neurons of Cre-injected mice can explain the observed behavioral arrhythmia. The remaining rhythmicity in Cre-injected mice may reflect incomplete loss of VGAT from the SCN. To what extent the differences in rhythmicity between the PER2::LUC luminometry and *mPer1*-Venus fluorescence may represent divergent functionality of the *mPer1* and *mPer2* genes will require further research.

2.5 Discussion

Here we show that acute local deletion of *Vgat* in the SCN disrupts behavioral and physiological circadian rhythms. Cre-mediated excision of *Vgat* severely reduced GABA transmission in the SCN. VGAT depleted mice exhibited normal activity when housed in light-dark cycles, but fragmentation when housed in constant conditions, demonstrating that the acute behavioral effects of light (i.e. masking) were intact, and circadian rhythms alone were disrupted. PER2::LUC luminometry indicated that Per2 rhythmicity was unaffected by disrupting local GABAergic transmission. However, effective SCN signaling requires synchronization of cell-autonomous molecular clocks, and we were not able to track bioluminescence from individual neurons with our equipment. We turned to single-cell imaging to determine the degree of phase

cohesion among individual SCN neurons. Depleting SCN VGAT reduced the proportion of rhythmic neurons and increased the phase dispersion of rhythmic SCN neurons.

Circadian rhythms in mammals are generated by highly conserved auto-regulatory transcriptional/translational feedback loops in neurons of the hypothalamic SCN. However, it has become clear that SCN network activity is essential for proper function of the circadian clock. GABAergic neurotransmission has been proposed to play an important role in the coupling of SCN neurons, but this role has remained controversial. While daily application of GABA synchronized the circadian rhythm of firing frequency in dispersed cell culture (Liu and Reppert, 2000; Shirakawa et al., 2000), blocking GABA receptors had no effect on the synchronization of *Per1* expression (Aton et al., 2006). Freeman et al. concluded that $GABA_A$ receptor activation actually elicits desynchrony in the SCN (Freeman et al., 2013). A recent study has offered a new model of GABA's contributing to synchrony, suggesting that GABA signaling promotes network synchrony in an antiphase state, but opposes network synchrony in a steady-state configuration (Evans et al., 2013). Similarly, it has been proposed that fast GABAergic transmission introduces "jitter" into the SCN network (Freeman et al., 2013). GABA tone may provide SCN neurons with the pliancy necessary for autonomous cellular clocks to synchronize with their neighbors.

In addition to GABA, several lines of evidence have implicated VIP in mediating SCN synchrony. VIP knockout mice have a shortened circadian period and reduced rhythmicity in constant darkness (Colwell et al., 2003). Mice lacking the VIP receptor ($VPAC2^{-/-}$) have compromised photoentrainment to light-dark cycles, but demonstrate robust activity patterns once entrained. In DD, $VPAC2^{-/-}$ mice display short free-

running periods and compromised rhythmicity (Hughes et al., 2008). *In vitro*, SCN neurons from VPAC2$^{-/-}$ mice show reduced amplitude of Per1-bioluminiescence rhythms and desynchrony between cells (Maywood et al., 2006; Brown et al., 2007). Vasopressin receptor knockout mice (V1a$^{-/-}$) have normal photoentrainment and locomotor rhythmicity in LD, but compromised rhythmicity in DD (Li et al., 2009b). Importantly, rhythmicity is never completely abolished in these animal models. We interpret these findings to signify that neuropeptides contribute to—but are not required for—circadian synchrony. Because SCN neurons co-express neuropeptides along with GABA, there may be possible antagonistic or cooperative interactions between these two classes of signaling molecules. We propose that SCN circadian output is an emergent property that surfaces from a combination of fast GABA transmission and slow neuromodulation.

In conclusion, we found that long-term disruption of SCN GABA transmission elicited a reduction of circadian rhythmicity *in vivo* and desynchrony of Per1 expression *in vitro*. Our data provide the first *in vivo* evidence that GABA signaling is required for proper function of the SCN.

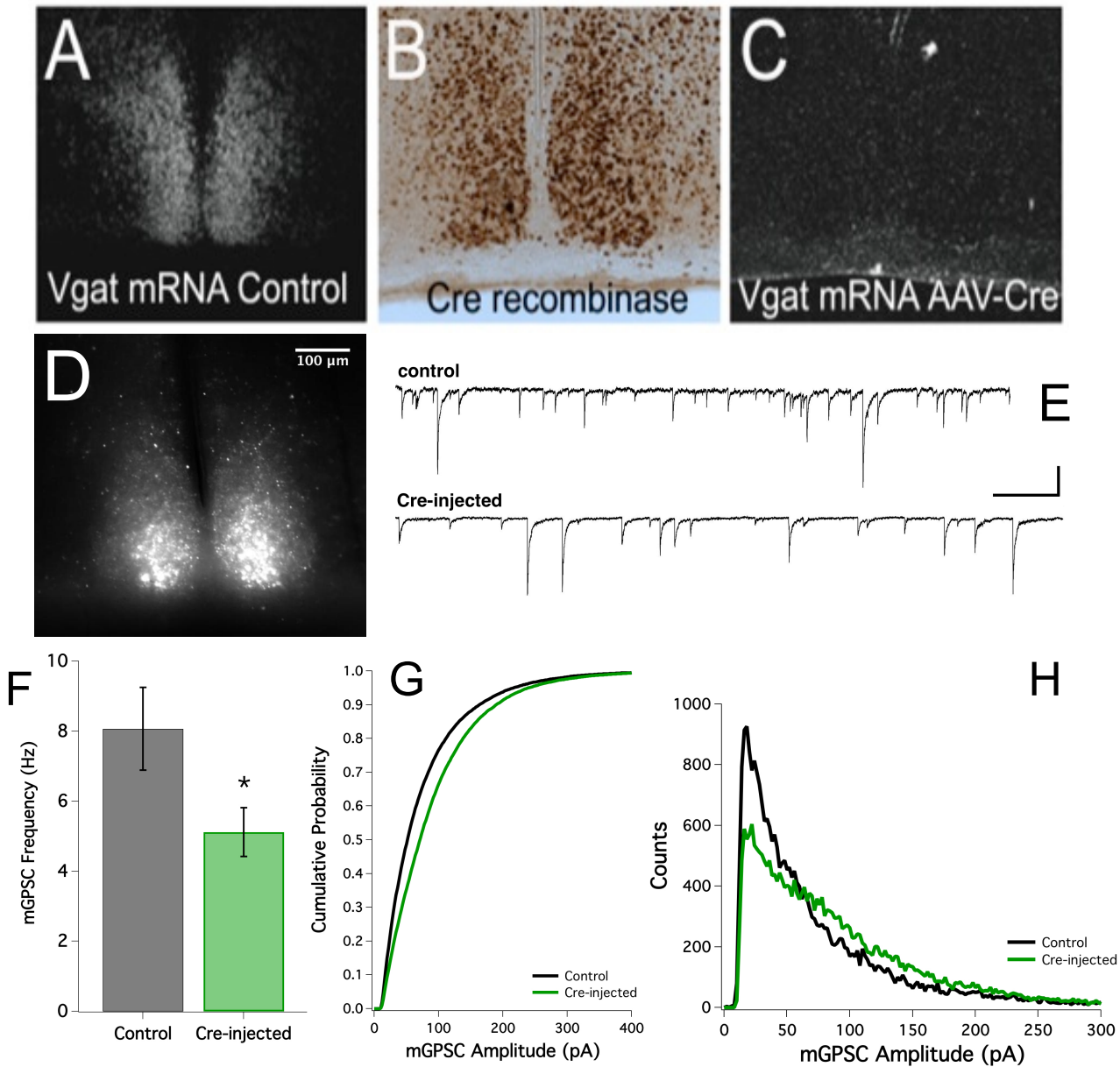

Figure 2.1: Reduction of GABA transmission in the SCN of Cre-injected *Vgat*$^{lox/lox}$ mice.

(A) *Vgat in situ* hybridization in the SCN of an uninjected control mouse. (B) After bilateral injections of AAV-Cre into the SCN of a *Vgat*$^{lox/lox}$ mouse nearly every neuron in the SCN expressed Cre (immunostaining), and (C) there was no *Vgat* mRNA expression remaining in the SCN. (D) Example fluorescent image of the SCN from a mouse injected with AAV-Cre-IRES-GFP. (E) Representative 5 second traces of mGPSCs recorded from control (top trace) and the Cre-injected SCN shown in D (bottom trace). The scale bar is 100 pA vertical and 0.5 sec horizontal. (F) The frequency of miniature GABA-mediated post-synaptic currents (mGPSCs) was reduced by 37% in Cre-injected SCN (8.1 vs 5.1 Hz; $p < 0.05$, generalized estimating equations). (G) The cumulative probability plot of mGPSC amplitude was shifted toward larger amplitude events in Cre-injected SCN (green line) compared to uninjected SCN (black line). (H) mGPSC event amplitude distribution for Cre-injected (green line) and uninjected SCN (black line). Electrophysiological recordings were obtained from 12 Cre-injected (100 neurons) and 12 uninjected *Vgat*$^{lox/lox}$ mice (98 neurons). In (H), the number of events for each group was matched for display purposes.

*Figures 2.1 A, B, & C were contributed by my collaborators Heinrich Gompf, Patrick Fuller, and Cliff Saper.

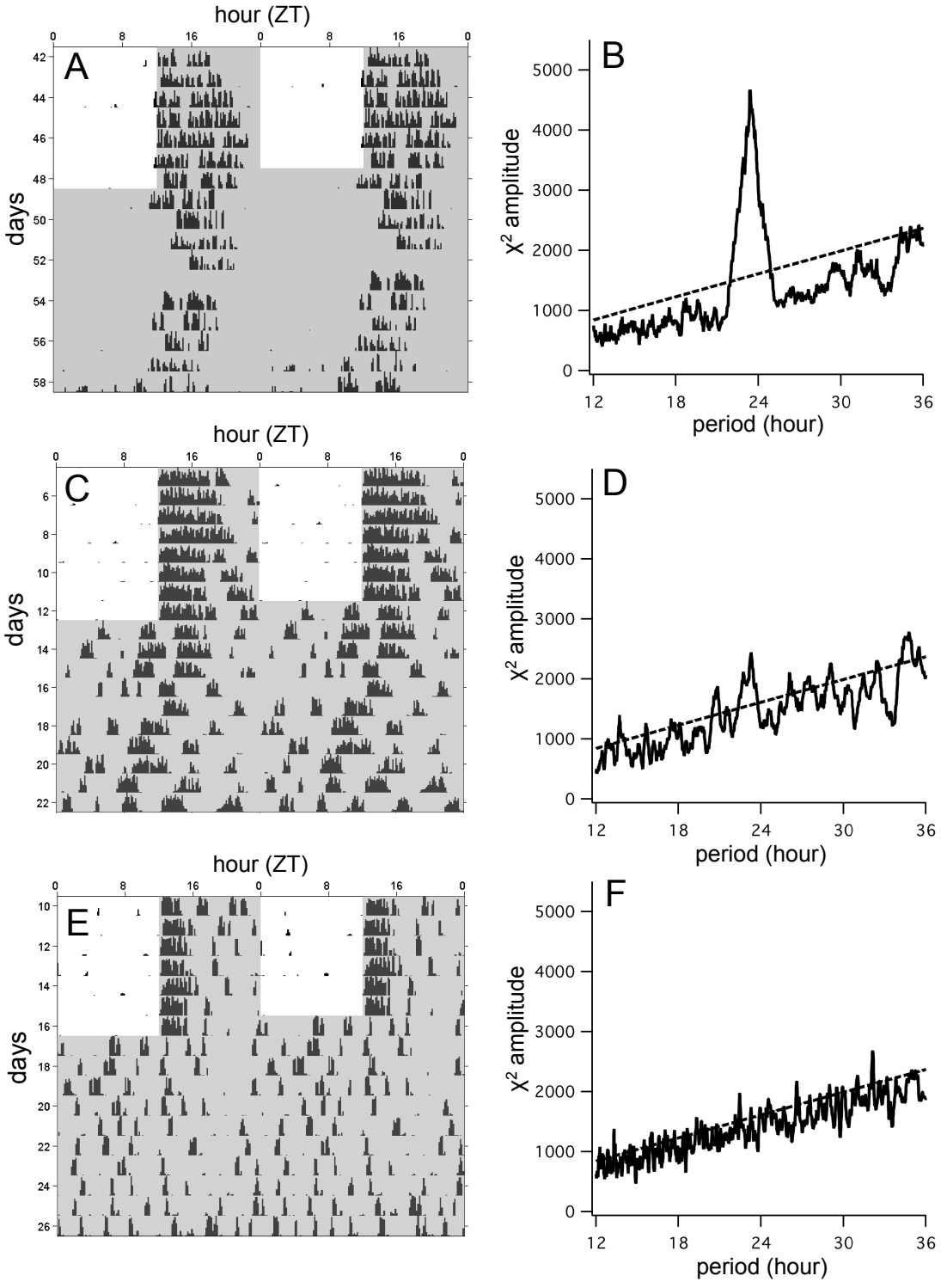

Figure 2.2: The circadian rhythm of wheel-running activity is disturbed in Cre-injected *Vgat*$^{lox/lox}$ mice.
Top row: double-plotted actogram (A) and corresponding χ^2 periodogram (B) from a Cre-injected *Vgat*$^{lox/lox}$ mouse displaying normal circadian rhythmicity when housed in constant darkness. The dashed line indicates a *p*-value of 0.05. A clear circadian peak in the behavior can be seen at 23.7 hours. Middle and bottom rows: double-plotted actograms (C and E) and corresponding χ^2 periodograms (D and F) from Cre-injected *Vgat*$^{lox/lox}$ mice demonstrating fragmented behavior in constant conditions. These mice exhibited normal diurnal activity under a light-dark cycle, but arrhythmia when released into constant darkness. Only small circadian amplitudes could be detected in the χ^2 periodograms obtained from these two mice.

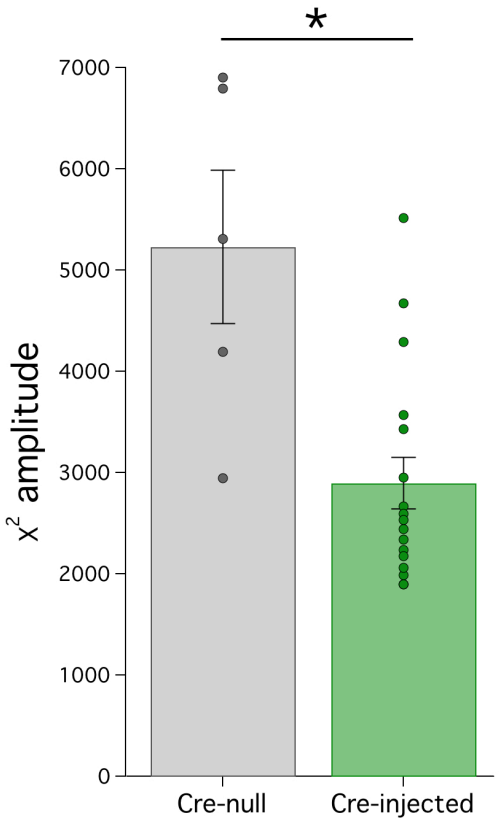

Figure 2.3: Summary data for wheel-running activity.

Circadian amplitude values obtained from χ^2 periodogram analysis of wheel-running behavior in constant darkness. Points represent values from individual mice while bars represent averages (± standard error) from Cre-null (gray) and Cre-injected *Vgat*$^{lox/lox}$ mice (green). The average amplitude from Cre-injected mice was significantly lower than that from Cre-null mice ($p < 0.001$, using the Student's *t*-test) indicating that SCN *Vgat* deletion compromised circadian rhythmicity of wheel-running activity.

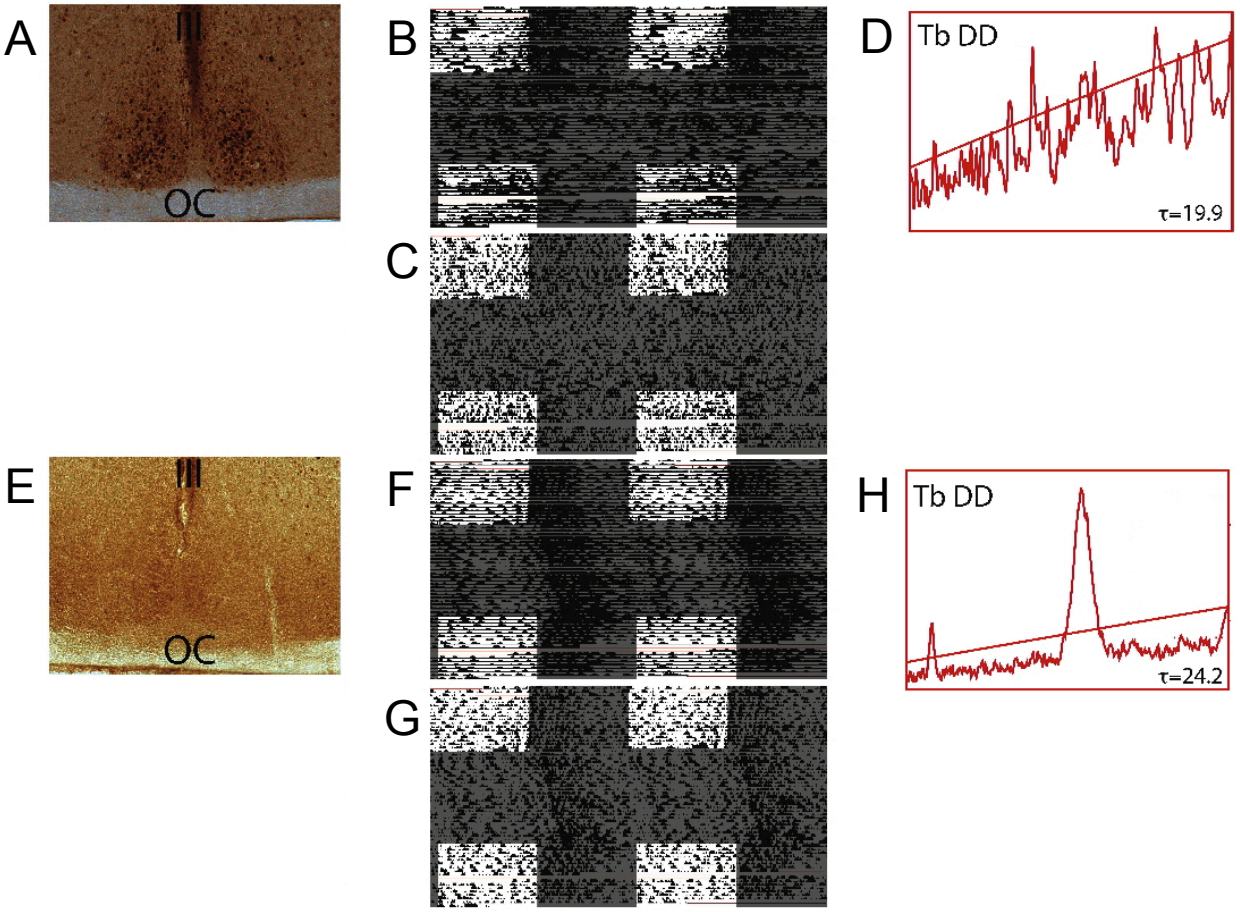

Figure 2.4: Disruption of GABA release by SCN neurons induces behavioral and physiological fragmentation in vivo. (A) photomicrograph (25x) of the SCN from a AAV-Cre-GFP injected *Vgat*$^{lox/lox}$ mouse showing that Cre transduction was restricted to the SCN. Double-plotted body temperature (T_b) (B) and locomotor (C) actograms from the mouse in (A). Periods of darkness are denoted with shading. The Cre-injected mouse showed entrainment to a 12:12 LD cycle but arrhythmia in constant darkness. (D) Periodogram analysis of T_b from 10 days in DD exhibited no prominent circadian peak. The straight line indicates a *p*-value of 0.05. (E) Lack of Cre expression in the SCN of a AAV-GFP injected *Vgat*$^{lox/lox}$ control mouse. Double-plotted T_b (F) and locomotor (G) actograms from the mouse in (E). (H) Periodogram analysis of T_b from 10 days in DD had a clear circadian peak.

*This figure was contributed by my collaborators Heinrich Gompf, Patrick Fuller, and Cliff Saper.

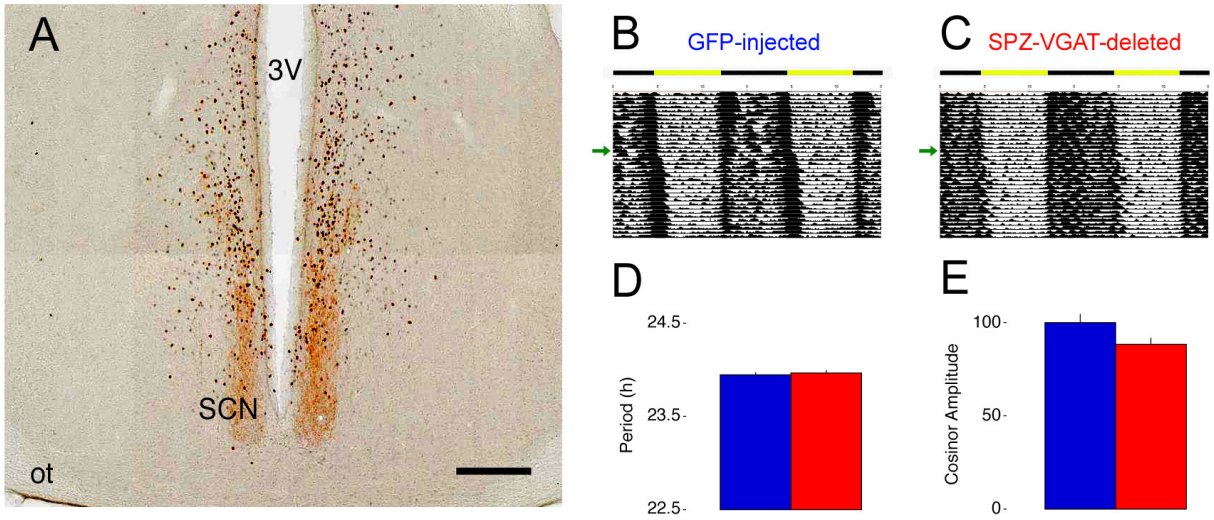

Figure 2.5: *Vgat* deletion in the subparaventricular zone (SPZ) does not affect circadian rhythms.
Photomicrograph depicting Cre-labeled cells (black) within the SPZ and vasoactive intestinal peptide-expressing fibers (brown) from the suprachiasmatic nucleus (SCN). Scale bar = 200 μm. 3V, third ventricle. ot, optic tract. (B) Double-plotted actograms depicting T_b rhythms in *Vgat*$^{lox/lox}$ mice injected with either AAV-GFP (B) or AAV-Cre-GFP (C). Green arrows denote the beginning of constant darkness. SPZ *Vgat* deletion (red) did not significantly affect the period length (D) or cosinor amplitude (E) of T_b circadian rhythms of compared to control (blue). n = 9 per group.

*This figure was contributed by my collaborators Heinrich Gompf, Patrick Fuller, and Cliff Saper.

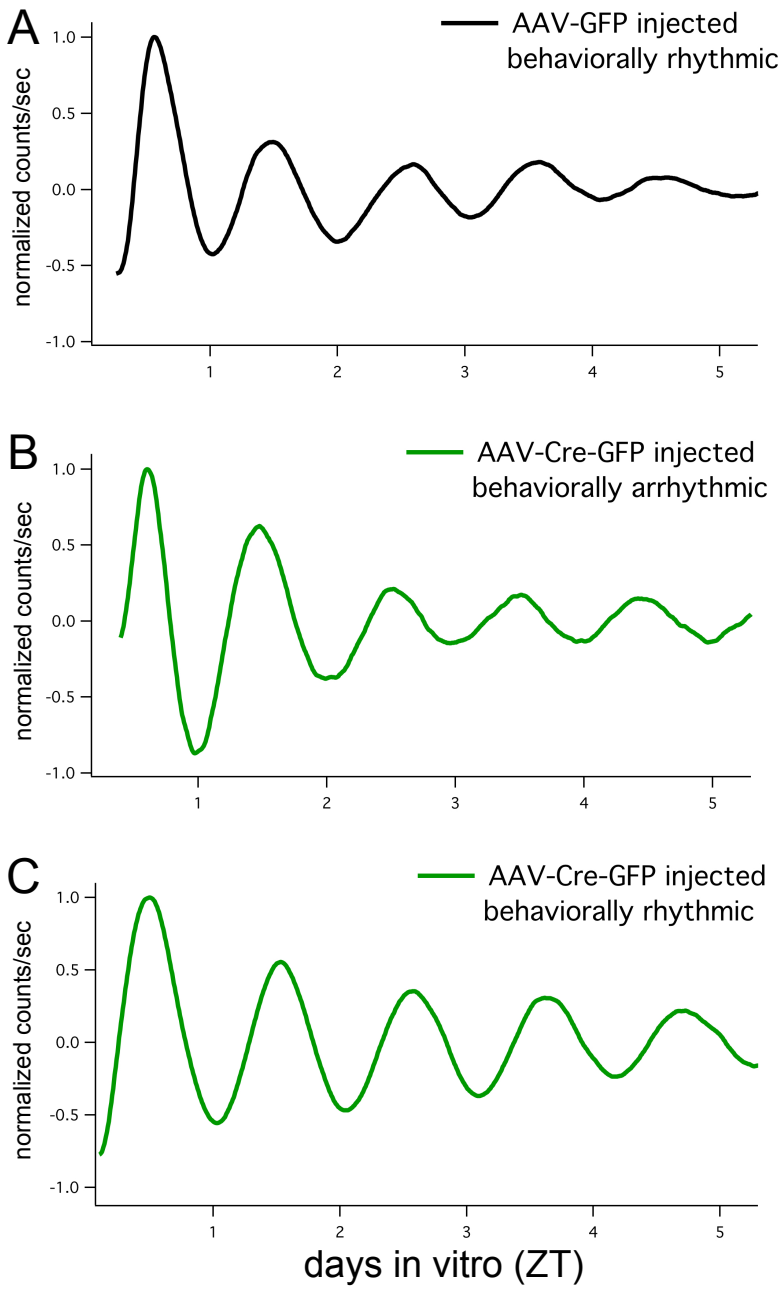

Figure 2.6: The molecular clock is undisturbed in Cre-injected *Vgat*$^{lox/lox}$ mice.
PER2::LUC bioluminescence rhythms obtained from organotypic slice cultures obtained from *Vgat*$^{lox/lox}$ mice injected with either AAV-GFP (A) or AAV-GFP-Cre (B and C). Individual traces are normalized to the amplitude of the first peak in culture. To measure the rate of damping, we compared the normalized amplitude of the third peak in culture between groups. Cre-injection did not overtly disrupt the rate of damping (third peak in culture was 0.32 ± 0.06 for Cre-injected *Vgat*$^{lox/lox}$ (n = 12) and 0.28 ± 0.05 for Cre-null mice (n = 10); $p > 0.05$ using a Student's *t*-test) or the period (24.82 ± 0.14 hours for Cre-injected *Vgat*$^{lox/lox}$ (n = 10); 24.38 ± 0.08 hours for Cre-null mice (n = 11); $p > 0.05$ using a Student's *t*-test) of the PER2::LUC bioluminescent signal. The trace in Figure B was recorded from the same mouse whose wheel-running behavior is shown in Figure 2.2 C; the trace in Figure C was obtained from the same mouse whose behavior is shown in Figure 2.2 A.

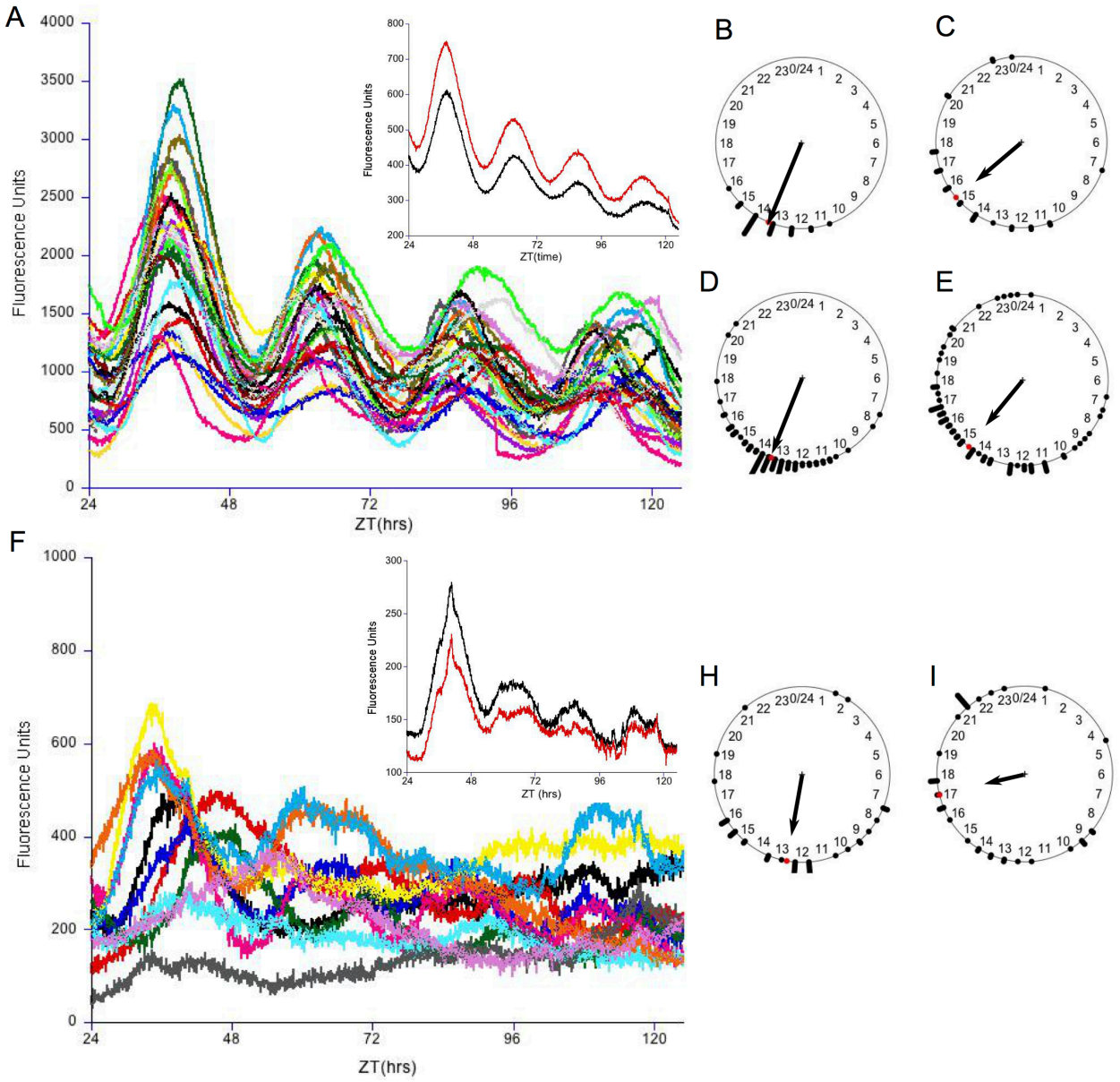

Figure 2.7: Time-lapse imaging of individual neurons following Cre-injection into the SCN of *Vgat*$^{lox/lox}$, *mPer1*-Venus mice reveals reduced rhythmicity and synchrony of SCN neurons.

(A) Individual *mPer1*-Venus recordings from a Cre-null mouse. Insert: the fluorescence intensity of the left (red) and right (black) lobes of the SCN. (B, C) Rayleigh plots from the slice shown in A at the time of first (B) and third (C) peak in culture. Each point represents the peak time for an individual neuron. The direction of the arrow denotes the dominant phase of the group while the length of the arrow represents the Synchrony Index. (D, E) Rayleigh plots of the imaged neurons (n = 101) from three Cre-null slices at the time of first (D) and third peak (E) in culture. (F) Individual Per1-Venus recordings from an SCN that received bilateral AAV-Cre-mCherry injection. Insert: the intensity of the left (red) and right (black) SCN. Note that the slice continued to have low amplitude rhythmic activity even though a significant number of neurons were arrhythmic. (H, I) Rayleigh plots of the imaged neurons (n = 77) from three AAV-Cre-mCherry slices at the time of first (H) and third (I) peak in culture.

CHAPTER 3: INTRACELLULAR CHLORIDE REGULATION IN NEURONS OF THE SUPRACHIASMATIC NUCLEUS

Nathan J. Klett[1] and Charles N. Allen[1,2]

[1]Neuroscience Graduate Program, [2]Oregon Institute for Occupational Health Sciences,
Oregon Health & Science University,
Portland, OR 97239

3.1 Introduction

In addition to several neuropeptides, SCN neurons express and package the fast-acting neurotransmitter GABA. GABA transmission is normally inhibitory, but several groups have observed excitatory GABA transmission in the SCN (Wagner et al., 1997; Wagner et al., 2001; De Jeu and Pennartz, 2002; Albus et al., 2005; Choi et al., 2008; Irwin and Allen, 2009; Freeman et al., 2013; Alamilla et al., 2014; Farajnia et al., 2014; Fan et al., 2015). Studies across labs have disagreed on the circadian phase, neuronal location and prevalence of excitatory GABA transmission. GABA has been reported to be exclusively inhibitory, inhibitory during the day and excitatory during the night, and excitatory during the night and inhibitory during the day. However, there is some agreement that GABA is more often depolarizing in the dorsomedial SCN during the night (Choi et al., 2008; Irwin and Allen, 2009).

The effect of $GABA_A$ receptor activation depends on the intracellular concentration of chloride ($[Cl^-]_i$). $[Cl^-]_i$ is regulated by a family of cation chloride cotransporters (CCCs) which use the concentration gradients of Na^+ and K^+ ions to transport Cl^- ions into (the sodium-potassium-chloride cotransporter 1, NKCC1) or out (the potassium-chloride cotransporters, KCC) of neurons. Normally, $[Cl^-]_i$ is kept low in neurons by the action of the neuron-specific isotonically-active KCC2. However, a role for NKCC1 in $[Cl^-]_i$ regulation has been demonstrated in the SCN (Choi et al., 2008; Irwin and Allen, 2009; Alamilla et al., 2014; Farajnia et al., 2014). Interestingly, a recent study has demonstrated differential expression of the chloride transporters throughout the SCN (Belenky et al., 2010). KCC2 expression was found in the ventrolateral SCN, but KCC3 and KCC4 were found in the dorsomedial SCN. Further, NKCC1 was

expressed throughout the SCN, but was concentrated in the dorsomedial SCN. The differential expression of CCCs throughout the SCN suggests that $[Cl^-]_i$ and the GABAergic reversal potential (E_{GABA}) may vary regionally throughout the SCN.

In this work, I have examined potential regional and circadian regulation of $[Cl^-]_i$, and have investigated the relative contributions of NKCC1 and KCC2 to setting $[Cl^-]_i$ in SCN neurons. I have used two independent techniques to address $[Cl^-]_i$ in genetically-defined populations of SCN neurons. Using gramicidin perforated-patch recordings, I have tested for regional activity of the CCCs in setting the GABAergic reversal potential. Similarly, using ratiometric imaging of Cl^- Sensor, I have investigated the contributions of NKCC1 and KCC2 to $[Cl^-]_i$ regulation. Together, my results indicate that KCC2 has a significant role in $[Cl^-]_i$ regulation in SCN neurons, while NKCC1 has a relatively minor role. Further, I have observed that $[Cl^-]_i$ is differentially regulated between AVP- and VIP-expressing neurons, and have found direct evidence for a potential circadian component to intracellular chloride in AVP-expressing neurons.

3.2 Methods

3.2.1 Animal strains and housing

Both rats and mice were used in this study. All electrophysiological experiments were done with male Wistar rats, 8 to 24 weeks old. Wild-type rats were obtained from Charles River Labs while the data presented in Figure 3.4 made use of a transgenic rat line in which eGFP is fused to AVP (AVP-eGFP; Ueta et al., 2005). These rats were bred in-house, but tail snips were sent to an external facility for genotyping (Transnetyx, Inc). Genomic DNA was screened for eGFP by PCR analysis.

Cl^- imaging experiments were performed with C57BL/6 mice in which a floxed Cl^- Sensor allele was inserted into the Rosa26 locus (Batti et al., 2013). We crossed these mice with either AVP-IRES-Cre (Harris et al., 2014) or VIP-IRES-Cre (Taniguchi et al., 2011; Harris et al., 2014) to yield AVP-Cl Sensor or VIP-Cl Sensor mice. Genotyping was performed by Transnetyx, Inc. Mice were heterozygous for both the Cl^- Sensor and Cre transgenes. Tissue was prepared from adult male and female mice between two and six months old.

All animals were entrained to 12:12 light-dark (LD) cycles. Were applicable, data were plotted in relation to time of lights on (zeitgeber time or ZT, lights on = ZT0). All procedures were performed in accordance with the guidelines of the Animal Care and Use Committees of Oregon Health and Science University.

3.2.2 Acute slice preparation and solutions

During their light phase, animals were removed from housing, anaesthetized with isoflurane, and decapitated. The brain was quickly removed and submerged in an ice-cold slicing solution consisting of (in mM): 111 NaCl, 26 $NaHCO_3$, 11 dextrose, 6 Na-gluconate, 4 $MgCl_2$, 3 KCl, 1 NaH_2PO_4, and 0.5 $CaCl_2$, saturated with 95% O_2, 5% CO_2. The brain was blocked and 175 µm thick coronal slices were prepared with a Leica VT1000S vibratome. Slices were incubated in slicing solution for 1-4 hours at 36°C before recording.

Experiments were continuously perfused at 1-2 mL/min with an artificial cerebrospinal fluid (aCSF) with Cl^- set to a physiologically-relevant concentration (122 mM; Schrock and Kuschinsky, 1989). aCSF contained (in mM): 114 NaCl, 26 $NaHCO_3$, 11 dextrose, 6 Na-gluconate, 2.7 KCl, 2 $CaCl_2$, 1 $MgCl_2$, and 1 NaH_2PO_4, saturated with

95% O_2, 5% CO_2. Recordings from AVP-eGFP rats and Cl^- imaging experiments where indicated were performed in HEPES-buffered aCSF containing (in mM): 114 NaCl, 22 Na-gluconate, 12.5 HEPES, 7.5 Na-HEPES, 5 dextrose, 2.7 KCl, 2 $CaCl_2$, 1 $MgCl_2$, and 1 NaH_2PO_4, For this solution, pH adjusted to 7.40 with NaOH, and gassed with 100% O_2. The bath was maintained at 36°C for all experiments and tetrodotoxin (TTX) was included in the recording solution to eliminate any possible polysynaptic effects of GABA agonists.

3.2.3 Electrophysiology

Recordings were performed with an Axopatch-1D amplifier (Axon Instruments), filtered at 2 kHz, digitized at 5 kHz, and acquired with Patchmaster v5.3 (HEKA Elektronik). For whole-cell recordings, pipette solution contained (in mM): 120 K-gluconate, 9 KCl, 10 HEPES, 2 NaCl, 1 EGTA, and 4 Neurobiotin-Cl. For some experiments, KCl was replaced with K-gluconate to yield a 15 mM $[Cl^-]_p$ pipette solution. For perforated-patch recordings, pipette solution contained (in mM): 120 KCl, 20 K-gluconate, 15 HEPES, 2 NaCl, 1 EGTA. For all solutions, pH was adjusted to 7.26 with KOH. Perforated-patch pipette solutions included either 0.2 mM Lucifer Yellow or Texas Red. Gramicidin (Sigma) was dissolved in DMSO to a concentration of 50 mg/mL, aliquoted, and frozen. Before an experiment, this stock solution was diluted to a 30-100 μg/mL in pipette solution. A drop of gramicidin-free pipette solution was first applied to the backend of the pipette. After capillary action filled the pipette tip, the pipette was back-filled with the gramicidin-containing solution moments before submersion into the recording chamber. After seal formation, series resistance (R_s) was

monitored with a −5 mV voltage step to monitor the progress of perforation. Only recordings with R_s less than 100 MΩ and were used for experiments. Cells were voltage clamped at −60 mV and cells with holding currents less than −30 pA were discarded.

The GABAergic reversal potential (E_{GABA}) was determined with one of two voltage-clamp protocols. For whole-cell recordings, the membrane potential was sequentially stepped to test potentials in 10 mV increments every 10 seconds. After a delay, 1 mM GABA was puff applied near the soma of the neuron at 5 psi for 5 to 20 ms. To obtain the GABA-evoked current, peak current was subtracted from the baseline current before application of GABA. To calculate E_{GABA}, the GABA-evoked current amplitude (y-axis) was plotted against the command potential (x-axis) and the data was fit by a linear function. E_{GABA} was taken to be the x-intercept of this fit. For perforated-patch recordings, E_{GABA} was determined using voltage ramp protocols. Every 10 seconds, a 400 ms voltage ramp protocol ($\Delta V \cong 60$ mV) was executed 100 ms after puff-application of GABA. A current trace recorded in the absence of GABA was subtracted from currents done in the presence of GABA. The subtracted current trace was then plotted against the ramp command potential, and E_{GABA} was calculated as previously. R_s offsets were not used to correct voltage values. Liquid junction potentials were not used to correct E_{GABA} measurements, but were accounted for in estimates of $[Cl^-]_i$. I used the Goldman-Hodgkin-Katz equation to estimate $[Cl^-]_i$, which accounts for the relative permeability of $GABA_A$ receptors for bicarbonate (0.2, E_{HCO3} = −20 mV).

3.2.4 Cl^- imaging from acute SCN slices

Animals were entrained to a LD 12:12 cycle, with lights on at 11 AM for 'day' animals and 1 AM for 'night' animals. Experiments were done during ZT2-8 for day mice and ZT12-18 for night mice. Cl^- Sensor fluorescent imaging was performed using epifluorescent methodology similar to that developed by Friedel et al. (2013). Excitation light was supplied by a monochrometer (Polychrome IV; Till Photonics) with a 10 nm bandwidth and passed through a UG11 optical filter. Excitation at 500 nm preceded excitation of CFP at 436 nm in order to minimize YFP_{Cl} inactivation (Friedel et al., 2013). Excitation durations ranged from 20 to 200 ms, with the excitation at 500 nm 1.5 times longer than that at 436 nm in order to give R_{Cl} values near 1. Fluorescent signal passed through a double bandpass emission filter [470(24) + 535(30) nm] (Chroma Technology Corporation). Imaging was performed with an upright fluorescent microscope and a 63x water-immersion objective, NA 0.90 (Leica). Images were acquired with a charge-coupled device camera (CCD, ORCA-ER 12 bit level; Hamamatsu). Camera gain was set to 100, and binning was 4x4. Equipment control and images processing were performed with Metafluor software (Molecular Devices). Regions of interest (ROI) were defined around neuronal soma, and a dim region of the field of view was selected to be background. Background values were subtracted for each wavelength independently. To obtain the chloride ratio (R_{Cl}), the fluorescent intensity after excitation with 436 nm was plotted over the intensity obtained after 500 nm light.

Because the YFP moiety of Cl^- Sensor is quenched by Cl^- ions, we choose to plot the emission following 436 nm excitation over that at 500 nm excitation so that R_{Cl} would be a proxy for $[Cl^-]_i$, with a higher ratio indicating higher $[Cl^-]_i$. When sampling at

2 and 5 second intervals, an exposure-dependent increase of R_{Cl} was observed, most likely due to an accumulation of Cl^- Sensor's YFP moiety in an inactivated state (Friedel et al., 2013). To correct for this instability, we fit our data with a single-exponential function, and subtracted the time-dependent term in order to detrend the data. This manipulation linearized the data and facilitated visual inspection. Despite this correction, we observed that steady-state R_{Cl} remained sensitive to exposure (Figure 3.5). We corrected for this exposure-dependent trend in AVP+ and VIP+ neurons independently and observed no difference in steady-state R_{Cl} between these two populations of neurons (Figure 3.5 E), allowing us to apply a combined exposure-dependent correction factor (0.0015/ms) to measures of R_{Cl}.

3.2.5 Calibration of Cl^- Sensor and estimation of $[Cl^-]_i$

To calibrate Cl^- Sensor, we made use of a 0 mM Cl^- solution consisting of (in mM): 120 Na-gluconate, 26 $NaHCO_3$, 11 dextrose, 2.7 K-gluconate, 2 Ca-gluconate, 1 $MgSO_4$, and 1 NaH_2PO_4, saturated with 95% O_2, 5% CO_2. This solution was mixed with bicarbonate-buffered aCSF to produce solutions of 0, 4, 20, 40, 60, and 80, and 123 mM Cl^-. 50 µM β-escin was added to all calibration solutions to permeabilize cells. AVP-Cl Sensor and VIP-Cl Sensor day- and night-entrained mice were used for analysis. R_{Cl} values were corrected for exposure as discussed. Average steady-state R_{Cl} was plotted against chloride concentration (Figure 3.10) and calibration data was fit with the following logistic dose-response sigmoidal curve:

$$R_{Cl} = R_{\max} + \frac{R_{\min} + R_{\max}}{1 + \left(\frac{[Cl^-]_i}{K_d} \right)^p}$$

Where R_{Cl} is the fluorescence intensity ratio (F_{436}/F_{500}) for chloride, K_d is the dissociation constant for Cl binding, R_{min} and R_{max} are the minimum and maximum asymptotic values of R_{Cl}, and p is the Hill coefficient (Batti et al., 2013). To obtain estimates of $[Cl^-]_i$, we re-arranged the equation for $[Cl^-]_i$:

$$[Cl^-]_i = K_d \cdot \left(\frac{R_{\min} - R_{\max}}{R_{Cl} - R_{\max}} - 1 \right)^{\frac{1}{p}}$$

After fitting the curve, we obtained the following values: K_d = 81.6 mM, R_{min} = 0.82 R_{max} = 1.94 and p = 2.65 (Figure 3.10). Our K_d is approximately 20 mM higher than previously-reported values (Markova et al., 2008; Waseem et al., 2010; Batti et al., 2013). The reason for this discrepancy will require further analysis but may be related to differences between calibration solutions.

3.2.6 Long term imaging of Cl^- Sensor

Using sterile techniques, brains were quickly removed and submerged in chilled Hanks' buffered salt solution (HBSS). Cultures were prepared as described previously (Yamazaki et al. 2000; Abe et al., 2002). Briefly, the brain was blocked and 200 µm coronal slices were prepared with a vibratome (VT1000S, Leica Biosystems). SCN slices were trimmed to remove surrounding hypothalamic tissue, and positioned unto membrane inserts (Millicell Organotypic Cell Culture inserts, EMD Millipore). Inserts were placed in glass-bottomed 35 mm culture dishes (MatTek Corp.) containing 1.2 mL culture medium and sealed with sterile vacuum grease. Culture medium consisted of DMEM (Sigma-Aldrich) supplemented with B27, 20 mM glucose, 10 mM HEPES, 4.2 mM $NaHCO_3$, 25 µg/mL penicillin, and 25 µg/mL streptomycin. Sealed dishes were

placed in a 36°C temperature-controlled chamber (ibidi GmbH), and imaged with an inverted fluorescent microscope (model ECLIPSE TE2000-U, Nikon), a CFP/YFP filter set (Chroma Technology, 51017) and an Evolve EMCCD camera (Photometrics). Excitation duration was between 500 and 1000 milliseconds. Images were acquired every 10 minutes with Metafluor software (Molecular Devices). Regions of interest (ROI) were defined around groups of fluorescent neurons on each side of the SCN. Background values were subtracted from each wavelength emission as above. Because experiments on organotypic slice cultures were done with different equipment (e.g. emission filters) from those done with acute slices, it is not possible to compare values of R_{Cl} between these two sets of experiments. Similarly, values of R_{Cl} can not be related to estimates of $[Cl^-]_i$ as calibration was only performed with acute SCN slices. Rhythmicity was determined with a nonparametric algorithm named JTK_Cycle run in R (R Foundation for Statistical Computing) (Hughes et al., 2010). A permutation-based *p*-value (ADJ.P) less than 0.05 was considered to indicate the presence of a statistically significant circadian rhythm.

3.2.7 Drugs

All drugs used in this study were acquired from Tocris Bioscience. Bumetanide and VU0240551 were dissolved in DMSO (Sigma-Aldrich) and stored as 10 mM stock solutions, and applied through the bath at 10 μM. A 100 mM stock of isoguvacine in water was diluted in ACSF to 1 mM and focally applied (5 psi) through a micropipette connected to a Picospritzer (General Valve Corporation).

3.2.8 Statistics and analysis

Igor Pro (Version 6.22A; Wavemetrics) was used for plotting, curve-fitting and data analysis. Data are presented as the mean ± standard error. For electrophysiological experiments, statistical significance was determined using either paired or unpaired Student's *t*-tests. For imaging experiments, generalized estimating equations (GEE) were used to determine statistical significance (Zeger and Liang, 1986). A *p*-value less than 0.05 was considered statistically significant.

3.3 Results 1: Electrophysiology

3.3.1 Whole-cell recordings from SCN neurons

Early investigations into $[Cl^-]_i$ regulation in SCN neurons were made with whole-cell patch clamp recording. Previous reports in the SCN and elsewhere have indicated that the pipette solution does not necessarily define $[Cl^-]_i$ (Wagner et al., 2001; Gonzalez-Islas et al., 2009). However, when using a pipette Cl^- concentration of 15 mM, E_{GABA} was measured to be −44.0 ± 2.1 mV (n=10, Figures 3.1 A & B), closely reflecting the GABAergic reversal potential predicted by the Goldman-Hodgkin-Katz equation for the $GABA_A$ receptor. Furthermore, E_{GABA} tracked with changes in pipette Cl^- concentration: changing pipette Cl^- from 15 to 6.2 mM produced an −18.2 mV change in E_{GABA} (E_{GABA} = −62.2 ± 1.2 mV, n=8, Figures 3.1 C & D), once again similar to that predicted by a Nernstian relationship. Therefore, in whole-cell recording, $[Cl^-]_i$ is largely clamped by the pipette's concentration of chloride. This methodological limitation could explain why blocking NKCC1 with bumetanide had no effect on E_{GABA} (−44.5 ± 1.5 mV when $[Cl^-]_p$ was 15 mM, n=8).

Although whole-cell recording was determined to be insufficient to assess resting $[Cl^-]_i$, whole-cell recording may still be informative of cell Cl^- transport mechanisms after $[Cl^-]_i$ manipulation (Wagner et al., 2001). Therefore, I performed whole-cell recordings of SCN neurons to manipulate $[Cl^-]_i$ and monitor the recovery process. A high concentration (1 mM) of GABA was dissolved in aCSF and brief (5-20 ms) puff applications of GABA were directed toward the neuronal soma every 10 seconds. These applications produced inward currents when cells were held at –60 mV. The response amplitude of these currents was monitored throughout the course of the experiment. After several baseline trials, the cell was challenged with a protocol designed to deplete $[Cl^-]_i$: the holding potential was hyperpolarized during a one second application of GABA. This protocol produced large inward currents indicative of Cl^- efflux. Following this large Cl^- efflux, test pulses of GABA were performed as previously to monitor the recovery of the response amplitude. In several experiments, the GABA-evoked current reversed direction, indicating successful manipulation of $[Cl^-]_i$ (Figure 3.1 F). The responses gradually recovered to their original amplitude with an average τ of recovery of 17.8 ± 1.5 seconds (n=6, Figure 3.1 E). This rate of recovery was assumed to reflect cell Cl^- loading mechanisms such as the activity of NKCC1. However, this recovery in GABA-mediated current amplitude may reflect a recovery from $GABA_A$ receptor desensitization. Therefore, the recovery after a minimal Cl^- flux was examined. In these experiments, 1 second of 1 mM GABA was directed to the cell as previously; however, the holding potential was maintained close to the cell's measured GABAergic reversal potential, inducing only minor Cl^- influx. Once again, the amplitude of the GABA-evoked current was seen to recover with a similar timecourse.

Therefore, the measured time constant of recovery not only represents homeostatic stabilization of $[Cl^-]_i$ but also the $GABA_A$ receptor's recovery from desensitization. Indeed, the recovery for desensitization for the $GABA_A$ receptor has been reported to have a time constant of 10 to 90 seconds, depending on cell type (Kaila, 1994; Barberis et al., 2011). Furthermore, the rate of recovery was not sensitive to bumetanide ($\boldsymbol{\tau}$ = 17.3 ± 2.6 seconds, n=6, $p>0.05$ using the Student's *t*-test). Collectively, these experiments indicated that the pipette solution clamped $[Cl^-]_i$ in whole-cell recordings, and argued for the need for techniques that would not perturb the native $[Cl^-]_i$.

3.3.2 Regulation of $[Cl^-]_i$ by NKCC1

The gramicidin ionophore is selectively permeable to cations but not anions. Therefore, perforation of the cell membrane with gramicidin provides electrical continuity with the cell without disrupting native $[Cl^-]_i$. The first set of perforated-patch recordings targeted neurons in the dorsomedial SCN during the animal's subjective night, as previous studies have observed that excitatory GABA transmission is more common in the dorsomedial SCN during the night (Albus et al., 2005; Choi et al., 2008; Irwin and Allen, 2009), and NKCC1 expression was found to be prevalent in the dorsomedial SCN (Belenky et al., 2010). After successful perforation of the membrane, E_{GABA} was monitored with voltage ramp protocols (Figure 3.2 A). Voltage ramp protocols were the preferred method of assessing E_{GABA} assessment as they minimize net Cl^- flux and are not sensitive to receptor availability (e.g., desensitization). GABA was puff-applied toward the soma to activate $GABA_A$ receptors, and a subsequent voltage ramp was administered. To quantify neuronal Cl^- influx mechanisms, a Cl^- depletion protocol was

implemented, similar to that described previously. Following Cl^- depletion, voltage ramps were run every 10 seconds to monitor the rate of E_{GABA} recovery (Figure 3.2). In control conditions, the average GABAergic reversal potential was −37.9 ± 1.9 mV (n=7) and the timecourse of recovery had an average **τ** of 28.2 ± 3.7 seconds (n=7). This protocol was repeated after the application of 10 μM bumetanide, to block NKCC1. Inhibiting NKCC1 with bumetanide was expected to hyperpolarize E_{GABA} and slow the rate of Cl^- loading following Cl^- depletion. However, bumetanide did not alter E_{GABA} or the rate of recovery (Student's *t*-test, $p>0.05$ for both parameters). In the presence of bumetanide, the average GABAergic reversal potential was −32.8 ± 4.9 mV (n=7, Figure 3.1 F) and the timecourse of recovery following Cl^- depletion had an average **τ** of 23.2 ± 3.2 seconds (n=7, Figure 3.1 G).

In a separate set of experiments, the contribution of NKCC1 to SCN Cl^- regulation was investigated in dorsomedial neurons recorded during the animals' subjective day. The GABAergic reversal potential measured during the day (E_{GABA} = −39.0 ± 3.5 mV, n=11) did not differ from that measured during the night. Once again, 10 μM bumetanide did not alter E_{GABA} or the timecourse of recovery (E_{GABA} = −38.8 ± 2.3 mV (n=11); **τ** = 23.4 seconds ± 2.8 (n=11) in control and 21.9 ± 1.5 seconds in bumetanide). Collectively, these results argue that NKCC1 is not involved in setting $[Cl^-]_i$ or mediating homeostatic Cl^- influx in dorsomedial neurons in either the day or the night. Alternatively, if NKCC1 is constitutively active in SCN neurons, other Cl^- uptake pathways could be masking or compensating for the loss of NKCC1. Further experiments will be necessary to address these possibilities.

3.3.3 Regulation of $[Cl^-]_i$ by KCC2

To test for the activity of KCC2 in setting $[Cl^-]_i$, gramicidin perforated patch recordings were targeted to neurons in the ventrolateral SCN, as a greater density of KCC2 expression was observed in the ventrolateral SCN (Belenky et al., 2008). Recordings were performed during the day, as previous studies have observed that excitatory GABA transmission is more common at night. Therefore, KCC2, which keeps $[Cl^-]_i$ low and GABA inhibitory, may be most active during the day. As discussed, voltage ramp protocols were used to monitor E_{GABA} (Figure 3.3 A). Interestingly, E_{GABA} was significantly more hyperpolarized in ventrolateral neurons compared to dorsomedial neurons (day recordings, $E_{GABA} = -52.7 \pm 4.7$, n=11, $p<0.05$, *t*-test). To test for the activity of KCC2 in setting resting $[Cl^-]_i$, KCC2 was blocked by adding 20 μM VU0240551 (VU) to the bath. VU depolarized E_{GABA} to -25.6 ± 5.0 mV (n=7, $p<0.001$, paired *t*-test, Figure 3.3 F), indicating that KCC2 is involved in setting resting $[Cl^-]_i$.

To test for the activity of KCC2 in homeostatic Cl^- efflux, E_{GABA} was assessed every 10 seconds after a Cl^- loading protocol (Figure 3.3 B). In control conditions, the time constant of recovery was 55.2 ± 17.2 seconds (n=5). Blocking KCC2 with 20 μM VU, slowed the recovery process slowed to 111.9 ± 38.1 seconds (n=5, $p<0.05$, paired *t*-test, Figure 3.3 E & G), indicating that VU contributes to Cl^- efflux after a large Cl^- influx. Collectively, these results indicate that KCC2 is involved in setting $[Cl^-]_i$, and contributes to homeostatic Cl^- efflux.

3.3.4 Regulation of $[Cl^-]_i$ in AVP+ neurons

Previous studies have observed that GABAergic excitation is more common in the dorsomedial region of the SCN (Choi et al., 2008; Irwin and Allen, 2009), which is populated with vasopressin-expressing (AVP+) neurons. Interestingly, in the nearby paraventricular zone, AVP+ neurons have been shown to have depolarized E_{GABA} values compared to the AVP^- neurons within the nuclei (Haam et al., 2012). Therefore, we used a transgenic rat line where eGFP is fused to AVP (Ueta et al., 2005) to target recordings to AVP+ neurons in the SCN. For these recordings, bicarbonate was removed from the extracellular solution to minimize any influence of the bicarbonate/chloride exchangers on $[Cl^-]_i$. Instead, pH buffering was accomplished with 20 mM HEPES. Furthermore, $[Cl^-]_o$ was adjusted to 122 mM in order to mimic physiological extracellular chloride concentrations (Schrock and Kuschinsky, 1989; Delpire and Staley, 2014). $[Cl^-]_p$ was adjusted to 122 mM and red dye was added to the pipette solution in order to ensure the integrity of the perforated patch.

E_{GABA} was measured with voltage ramp protocols as previously discussed. AVP+ neurons demonstrated no circadian change in E_{GABA} (Figure 3.4 A). In order to test for a role of NKCC1 in setting $[Cl^-]_i$ in AVP+ neurons, 40 μM bumetanide was added to the bath in a subset of neurons. Since little effect was observed previously at 10 μM, the concentration of bumetanide was increased to 40 μM to ensure full blockade of NKCC1 (Haam et al., 2012). On average, bumetanide decreased E_{GABA} by 3.8 mV ($p < 0.001$, *t*-test, Figure 3.4 B). The effect of bumetanide cannot be attributed to gradual loss of the perforated patch over time because dialyzation of the pipette solution would be expected to increase E_{GABA}. Interestingly, blocking NKCC1 did not hyperpolarize

E_{GABA} below V_m, suggesting that other Cl^- uptake mechanisms besides that mediated by NKCC1 underlie the relatively depolarized value of E_{GABA}. Indeed, the resting E_{GABA} had no relation to the change in E_{GABA} after bumetanide (Figure 3.4 C).

3.4 Results 2: Cl^- imaging

3.4.1 Abstract

Several reports have described excitatory GABA transmission in the SCN. Unfortunately, these reports have disagreed on the circadian phase and neuronal location of the phenomenon—therefore, the nature of excitatory GABA transmission in the SCN has remained elusive. Here, using newly developed Cl^- imaging techniques, we show that activation of $GABA_A$ receptors elicits Cl^- influx in both AVP and VIP-expressing SCN neurons. The intracellular chloride concentration $[Cl^-]_i$ was found to be regulated by KCC2 to a greater degree than by NKCC1, suggesting that the KCCs sets $[Cl^-]_i$ in SCN neurons. Interestingly, $[Cl^-]_i$ demonstrated a circadian rhythm in AVP+ neurons, but not VIP+ neurons. We conclude that GABA is inhibitory in both AVP+ and VIP+ neurons, but is under circadian regulation in AVP+ neurons.

3.4.2 Introduction

The suprachiasmatic nucleus (SCN) of the anterior hypothalamus is the master pacemaker of the circadian system. Besides a cohort of neuropeptides, SCN neurons express and package the neurotransmitter GABA. GABA transmission has been implicated in regulating synaptic input from the RHT (Moldavan et al., 2006), mediating

phase shift (Gillespie et al., 1996; Gillespie et al., 1997), regulating firing frequency (Kononenko and Dudek, 2004), and contributing to circadian synchrony (Liu and Reppert, 2000; Albus et al., 2005; Evans et al., 2013; Freeman et al., 2013).

GABA is the primary inhibitory neurotransmitter in the CNS, but has been observed to be excitatory during embryonic and neonatal development, in certain pathologies, as well as in several areas of the adult brain (Gamba, 2005; Blaesse et al., 2009; Ben-Ari et al., 2012). Interestingly, several reports have described excitatory GABA transmission in the mature SCN (Wagner et al., 1997; Wagner et al., 2001; De Jeu and Pennartz, 2002; Albus et al., 2005; Choi et al., 2008; Irwin and Allen, 2009; Freeman et al., 2013; Alamilla et al., 2014; Farajnia et al., 2014; Fan et al., 2015). Unfortunately, these reports have disagreed on the circadian phase and neuronal location of the phenomenon—therefore, the nature of excitatory GABA transmission in the SCN has remained elusive.

We re-examined excitatory GABA transmission in the SCN using ratiometric Cl^- imaging. The $GABA_A$ receptor is permeable to Cl^- ions, and whether GABA is depolarizing or hyperpolarizing depends on the intracellular concentration of chloride ($[Cl^-]_i$). Cl^- imaging allows estimation of $[Cl^-]_i$ from multiple cells simultaneously without disrupting the cellular milieu. Furthermore, transgenic strategies offered us the ability to measure $[Cl^-]_i$ in genetically-defined subpopulations of SCN neurons. Cl^- Sensor is composed of a CFP moiety linked to a YFP moiety whose emission is sensitive to chloride with a K_d of approximately 50 mM. Using epifluorescence microscopy, we were able to elicit and detect both fast and slow changes of $[Cl^-]_i$ in SCN neurons. Our results indicate that GABA transmission is inhibitory in AVP+ and VIP+ neurons in the

SCN, but that $[Cl^-]_i$ is differentially regulated between these two populations of neurons. Further, we show that $[Cl^-]_i$ demonstrates a circadian rhythm in AVP+ neurons.

3.4.3 Results

Vasoactive intestinal peptide (VIP) and vasopressin (AVP) mark the "core" and "shell" partition that has been a useful anatomical model for dissecting SCN function. Generally, sensory inputs project to the SCN core, while core neurons synapse unto neurons in the shell. Several reports have suggested that excitatory GABA transmission may correlate with this anatomical feature. Therefore, we performed Cl^- imaging in VIP+ and AVP+ neurons of the SCN to look for differences in $[Cl^-]_i$ regulation between these two populations of neurons. To image Cl^- fluxes in neurons, we used a newly-developed Cre-inducible mouse line, with a floxed Cl^- Sensor allele inserted into the Rosa26 locus (Batti et al., 2013). To obtain Cl^- Sensor expression in the SCN, we crossed these mice with either VIP-IRES-Cre mice or AVP-IRES-Cre mice to give Cl^- Sensor expression in either VIP+ or vasopressin AVP+ neurons (Taniguchi et al., 2011; Harris et al., 2014). The resultant VIP-Cl Sensor mice displayed Cl^- Sensor expression in the ventrolateral SCN, while the AVP-Cl Sensor mice displayed Cl^- Sensor expression in the dorsomedial SCN, as previously reported for VIP and AVP expression (Figure 3.5, Van den Pol, 1986).

We used epifluorescent microscopy to monitor $[Cl^-]_i$ in SCN neurons of acute brain slices. We excited the sample with 500 nm light followed by 436 nm light and monitored emission through a double-bandpass filter, after the method developed by (Friedel et al., 2013). To obtain the chloride ratio (R_{Cl}), we plotted the emission from

436 nm excitation light over that at 500 nm light, so that an increase in R_{Cl} indicates an increase in $[Cl^-]_i$. Several reports have described regional variability of excitatory GABA transmission, with some agreement that it is more common in the dorsal SCN, suggesting that this phenomenon may be specific to AVP+ neurons. Indeed, in the nearby paraventricular nucleus, Haam et al. observed that AVP+ neurons had a more depolarized E_{GABA} relative to their AVP− neighbors (Haam et al., 2012). To determine whether AVP+ neurons demonstrate higher $[Cl^-]_i$ relative to VIP+ neurons, we compared R_{Cl} between VIP+ and AVP+ neurons. After correcting for differences in exposure, there was no difference in steady-state R_{Cl} between VIP+ or AVP+ neurons. Average R_{Cl} was 0.84 (n=258, standard deviation: 0.14) and 0.86 (n=320, standard deviation: 0.26) in AVP+ and VIP+ neurons respectively (Figure 3.5 E). These values correspond to $[Cl^-]_i$ estimates of 19.3 (AVP+) and 23.1 (VIP+) mM.

To examine whether $[Cl^-]_i$ may be under circadian regulation, we performed long-term imaging of SCN slice cultures, to monitor R_{Cl} over several days in VIP+ and AVP+ neurons. We found no circadian variation in R_{Cl} when monitored in VIP+ neurons but a small amplitude circadian rhythm in AVP+ neurons ($p < 0.001$ with JTK_CYCLE). Figure 3.6). In AVP+ neurons, R_{Cl} was found to peak near ZT12, indicating that $[Cl^-]_i$ is elevated during the late day and early night. Because our calibration curve was performed with different equipment (e.g. emission filters) than these long-term imaging experiments, it is not possible to relate these measures of R_{Cl} to estimates of $[Cl^-]_i$.

A hyperpolarizing action of GABA will involve Cl^- influx, while a depolarizing action will involve Cl^- efflux. To assess the polarity of GABA transmission in SCN neurons, we returned to acute SCN slices. Upon puff application of a high

concentration of the $GABA_A$ agonist isoguvacine, R_{Cl} increased in AVP+ neurons during the day and night, indicative of Cl^- influx and normal inhibitory GABA transmission (Figure 3.7, top row). Cl^- influx was also observed in VIP+ neurons in both the day and the night (Figure 3.7, bottom row). These results indicate that GABA is inhibitory in both AVP+ and VIP+ SCN neurons.

$GABA_A$-induced Cl^- transients lasted on the order of minutes. The long recovery time of R_{Cl} can be attributed to a slow washout of isoguvacine from the slice, slowly-desensitizing $GABA_A$-mediated Cl^- currents, and/or due to the action of the cation chloride cotransporters (CCCs), which transport Cl^- ions either into or out of neurons. Indeed, in other neurons it has been shown that transient shifts in GABA polarity can last for minutes (Staley and Proctor, 1999; Lamsa and Taira, 2003). In a separate set of experiments using gramicidin perforated-patch recording, the GABAergic reversal potential was found to require more than a minute to return to resting levels after a large Cl^- load (see Figure 3.3), indicating that the timecourse of these Cl^- transients may indeed reflect Cl^- transport.

We next tested the degree to which the CCCs set $[Cl^-]_i$ in SCN neurons. Since our $GABA_A$-induced Cl^- transients indicated inhibitory Cl^- influx upon $GABA_A$ receptor activation, we first tested the contribution of KCC2, the neuron-specific CCC considered responsible for keeping $[Cl^-]_i$ levels low in neurons throughout the brain. To test for the activity of KCC2, we used 10 μM of VU0240551, an antagonist of the KCCs (Delpire et al., 2009). VU increased R_{Cl} by approximately 0.18 in AVP+ and 0.27 in VIP+ neurons. VU had a significantly greater effect in VIP+ neurons compared to AVP+ neurons ($p<0.05$ with GEE), but there were no day/night differences within neuron type (Figure

3.8 B). Based on our calibration curve, we estimate the changes in R_{Cl} to reflect a 27 mM increase in $[Cl^-]_i$ in AVP+ neurons and a 33 mM increase in VIP+ neurons. We interpret these findings to indicate that the KCC family of chloride transporters plays a major role in $[Cl^-]_i$ regulation in SCN neurons. Interestingly, the mechanism mediating this increase in $[Cl^-]_i$ after blocking KCC is not likely to be mediated by NKCC1, as sensitivity to VU was unchanged in the presence of bumetanide (data not shown).

Previous studies have implicated NKCC1 in $[Cl^-]_i$ regulation in SCN neurons (Choi et al., 2008; Irwin and Allen, 2009; Belenky et al., 2010; Farajnia et al., 2014). Indeed, our estimates of $[Cl^-]_i$ suggested that there may be active uptake of Cl^- in SCN neurons. To test for a contribution of NKCC1 to resting $[Cl^-]_i$, we used the loop diuretic bumetanide which selectively targets NKCC1 when used at 10 μM (Russell, 2000). Bumetanide increased R_{Cl} in AVP+ neurons by approximately 0.04 and decreased R_{Cl} in VIP+ neurons by 0.04 units (Figure 3.9 C). These changes were small but significantly different from baseline ($p<0.005$ with GEE). Once again, we observed differential sensitivity between AVP+ and VIP+ neurons ($p<0.001$ with GEE), but no any day/night differences within neuron type. Based on our calibration curve, we estimate that bumetanide caused an increase in $[Cl^-]_i$ by 9 mM in AVP+ neurons, and a decrease by 15 mM in VIP+ neurons. Remarkably, bumetanide increased $[Cl^-]_i$ in AVP+ neurons, contrary to its expected role in blocking Cl^- uptake. This result may be due to off-target effects of bumetanide, which is known to inhibit KCCs at higher concentrations (K_i ~ 25-50 μm). In either case, we observed relatively small effects of bumetanide compared to VU, suggesting that the KCCs are the major regulator of $[Cl^-]_i$ in SCN neurons. Interestingly, we observed differential effects of bumetanide and VU between VIP+ and

AVP+ neurons, a finding which may be related to the observed cycling of $[Cl^-]_i$ in AVP+ SCN neurons.

3.4.4 Discussion

We performed somatic Cl^- imaging and showed Cl^- influx following puff application of GABA agonists. Our results suggest that GABA is inhibitory at all times of day in both the AVP+ and VIP+ SCN neurons in both day and night. Our results add to a group of studies that have concluded that GABA is exclusively inhibitory in the mature SCN (Liou and Albers, 1990; Mason et al., 1991; Bos and Mirmiran, 1993; Chen et al., 1996; Liu and Reppert, 2000). However, it should be remembered that the SCN is a very heterogeneous nuclei and that AVP and VIP-expressing neurons only constitute ~13% and ~9% of all SCN neurons respectively (Welsh et al., 2010; Lee et al., 2015), leaving open the possibility that our study overlooked the relevant population(s) of neurons with excitatory GABA.

Our methodology did not allow us to investigate subcellular changes in R_{Cl} after $GABA_A$ receptor activation. Therefore, it is possible that GABA transmission elicits $[Cl^-]_i$ efflux in either the axons or dendrites of SCN neurons. Indeed, intracellular Cl^- gradients have been reported in several types of neurons throughout the brain (see Wright et al. 2011 for review). For example, a two-photon Cl^- imaging study observed a somatodendritic chloride gradient in a class of retinal bipolar cells, concluding that Cl^- is 20 mM higher in dendrites relative to the soma (Duebel et al., 2006). A somatodendritic Cl^- gradient could explain why previous studies have shown GABA-evoked Ca^{2+} transients in SCN neurons, supporting an excitatory role of GABA, while we have

reported inhibitory Cl^- influx. While dendritic depolarization may be able to activate somatic voltage-gated calcium channels, Cl^- efflux at dendrites may not be registered by somatic Cl^- imaging. Similarly, somatodendritic Cl^- gradients could also explain why bumetanide had a relatively large effect on GABA-evoked Ca^{2+} transients but only small effects in our experiments. Higher-resolution imaging techniques will be necessary to address whether somatodendritic Cl^- gradients exist in SCN neurons.

We observed large changes in R_{Cl} after application of the KCC antagonist VU, but small changes after blocking NKCC1 with bumetanide. VU increased $[Cl^-]_i$ by approximately 20 mM, suggesting that the KCCs are the major determinants of $[Cl^-]_i$ in SCN neurons. For a neuron with a V_m of −55 mV, Cl^- is passively distributed at approximately 15 mM. Therefore, our estimates of resting $[Cl^-]_i$ (~20 mM) indicate that there are constitutively active uptake mechanisms in SCN neurons. In VIP+ neurons, blocking NKCC1 decreased $[Cl^-]_i$ supporting a role for NKCC1 in Cl^- uptake. However, in AVP+ neurons, bumetanide caused a decrease in $[Cl^-]_i$, suggesting that other uptake mechanisms are active in AVP+ neurons. This Cl^- uptake may be mediated by the anion exchangers, which transport intracellular bicarbonate for extracellular chloride (Alka and Casey, 2014).

Interestingly, we observed that $[Cl^-]_i$ is under circadian regulation in AVP+ neurons. $[Cl^-]_i$ was found to be elevated in the late day and reduced during the late night. This finding is in agreement with a recent gramicidin perforate patch study that concluded that during the day the GABAergic potential is approximately −30 mV, but is −60 mV during the night (Alamilla et al., 2014). We did not observe that $[Cl^-]_i$ was under circadian regulation in VIP+ neurons, highlighting that $[Cl^-]_i$ is differentially regulated

within the SCN. Accordingly, AVP+ and VIP+ neurons differed in their sensitivity to both VU and bumetanide. Previous in situ hybridization (Kanaka et al., 2001) and immunocytochemical (Belenky et al., 2008) studies have described regional expression of chloride transporters in the rat SCN. Specifically, KCC2 expression was limited to the ventrolateral SCN, and colocalized with neurons containing GRP or VIP. Markedly, KCC2 expression was absent from the dorsomedial SCN and did not colocalize with AVP—rather, KCC3 and KCC4 were found in the dorsomedial SCN (Belenky et al., 2010). Despite the paucity of KCC2 in the dorsomedial SCN, we observed that VU increased $[Cl^-]_i$ in AVP+ neurons. This result may be explained by non-specificity of VU for KCC2 (Delpire et al., 2009), suggesting that VU inhibited KCC3 or KCC4 in AVP+ neurons. Further, Belenky et al. reported a greater density of NKCC1 expression in the dorsomedial SCN. Together, these findings may explain the differential effects of VU and bumetanide in AVP+ neurons compared to VIP+ neurons.

Recently, the role of the CCC's in determining $[Cl^-]_i$ has come under scrutiny by compelling two-photon Cl^- imaging results which argue for the primacy of large intracellular anions in setting $[Cl^-]_i$ (Glykys et al., 2014). In their study, Glycks et al. observed little effect of blocking either NKCC1 or KCC2 in hippocampal and neocortical pyramidal neurons, while we found a small effect of bumetanide and a clear effect of VU. Neuron type could underlie this difference. Alternatively, while we monitored R_{Cl} continuously, Glycks et al. sampled R_{Cl} before and 30 minutes after application of bumetanide and VU, leaving open the possibility that secondary homeostatic mechanisms reset $[Cl^-]_i$ during that time.

Unfortunately, the descriptions of excitatory GABA transmission in the SCN have been riddled with discrepancies. Differences in methodology are likely to underlie some of these discrepancies. Whole-cell, perforated-patch, cell-attached, and multi-unit recording techniques as well as Ca^{2+} imaging have all been used to address the polarity of GABA transmission in the SCN. The complexities of intracellular Cl^- regulation may have also contributed to the inconsistencies between studies of SCN GABA transmission. Besides neurotransmission, $[Cl^-]_i$ is an important cellular feature linked to processes such as pH regulation, cell volume regulation, and even membrane potential (Gamba, 2005; Blaesse et al., 2009). Therefore, cell turgidity as well as the osmolarity and pH of solutions are all likely to influence measures of $[Cl^-]_i$ (Delpire and Staley, 2014). Further, $[Cl^-]_i$ has been shown to change after neuronal damage, and in relation to the proximity of cells to the surface of a brain slice (Kahle et al., 2008; Dzhala et al., 2012).

Studies have not adequately ruled out the possibility that disinhibition underlies the observed excitatory effects of GABA transmission in the SCN. The SCN network is known to have diffuse local connectivity. Therefore, polysynaptic effects must be considered when applying GABA agonists to SCN neurons. Without the inclusion of TTX, GABA-mediated inhibition of pre-synaptic inputs could be read out as excitation in the cell of interest. Further, some of the data in support of excitatory GABA transmission has been inferred by the effects of the $GABA_A$ antagonist bicuculline. Regrettably, these results are confounded by the off-target effects of bicuculline, which is known to antagonize SK channels at commonly used concentrations (Khawaled et al., 1999). Indeed, SK channels have been shown to contribute to the

afterhyperpolarization and spike-frequency adaptation in SCN neurons (Teshima et al., 2003).

We have successfully implemented Cl^- imaging techniques in SCN neurons, and have demonstrated their utility for monitoring both transient Cl^- fluxes and $[Cl^-]_i$ regulation. The development of genetically-encoded indicators and effectors has prompted unprecedented dissection of neural circuitry. Cl^- imaging offers several advantages over gramicidin perforated patch recording, facilitating cell-targeting strategies, large sampling, and long-term recording of $[Cl^-]_i$. Further, imaging leaves neuronal V_m unperturbed. However, Cl^- Sensor has room for improvement. Cl^- Sensor's sensitivity to Cl^- is not optimal for general neuronal concentrations of chloride. Further, the H^+ sensitivity of the indicator within a physiological pH range can complicate the interpretation of results. We also observed a markedly greater rate of photobleaching for YFP compared to CFP, making Cl^- Sensor difficult to use as a true ratiometric indicator.

3.4.5 Supplemental data

Due to the pH sensitivity of Cl^- Sensor, we performed a series of experiments in HEPES-buffered aCSF. HEPES has a greater buffering capacity than bicarbonate, thereby increasing pH stability in the brain slice preparation. HEPES offers the added benefit of reducing the bicarbonate conductance through the $GABA_A$ receptor. As previously discussed, we puff-applied isoguvacine to AVP+ and VIP+ neurons in acute SCN slices. Remarkably, $GABA_A$ receptor activation elicited decreases of R_{Cl} in both

AVP+ and VIP+ neurons in these experiments, indicative of Cl^- efflux and depolarizing GABA transmission (Figure 3.11).

Because we observed Cl^- efflux in the HEPES-buffered solution, but Cl^- influx in bicarbonate-buffered solutions, we wondered if $[Cl^-]_i$ was differently regulated in the HEPES. Therefore, we repeated experiments to block the action of the KCCs and NKCC1 with VU and bumetanide, respectively. Blocking KCC with VU gave a pattern of results similar to that observed with bicarbonate: VU elicited an increase in R_{Cl} in all conditions, indicative of $[Cl^-]_i$ increase (Figure 3.12 A). Once again, VU had a larger effect in VIP+ neurons compared to AVP+ neurons. Interestingly, the amplitude of VU effect in VIP+ neurons was similar to that observed in bicarbonate, but was smaller in AVP+ neurons. Blocking NKCC1 with bumetanide decreased R_{Cl} in all conditions (Figure 3.12 B), indicative of a reduction in $[Cl^-]_i$ as expected when blocking Cl^- uptake. This observation stands in contrast to bicarbonate-buffered experiments, where bumetanide increased R_{Cl} in AVP+ neurons. Still, bumetanide once again differentially effected R_{Cl} in AVP+ and VIP+ neurons, causing a greater decrease in VIP+ neurons. For an interpretation of these results, please see *Chapter 4, Discussion*.

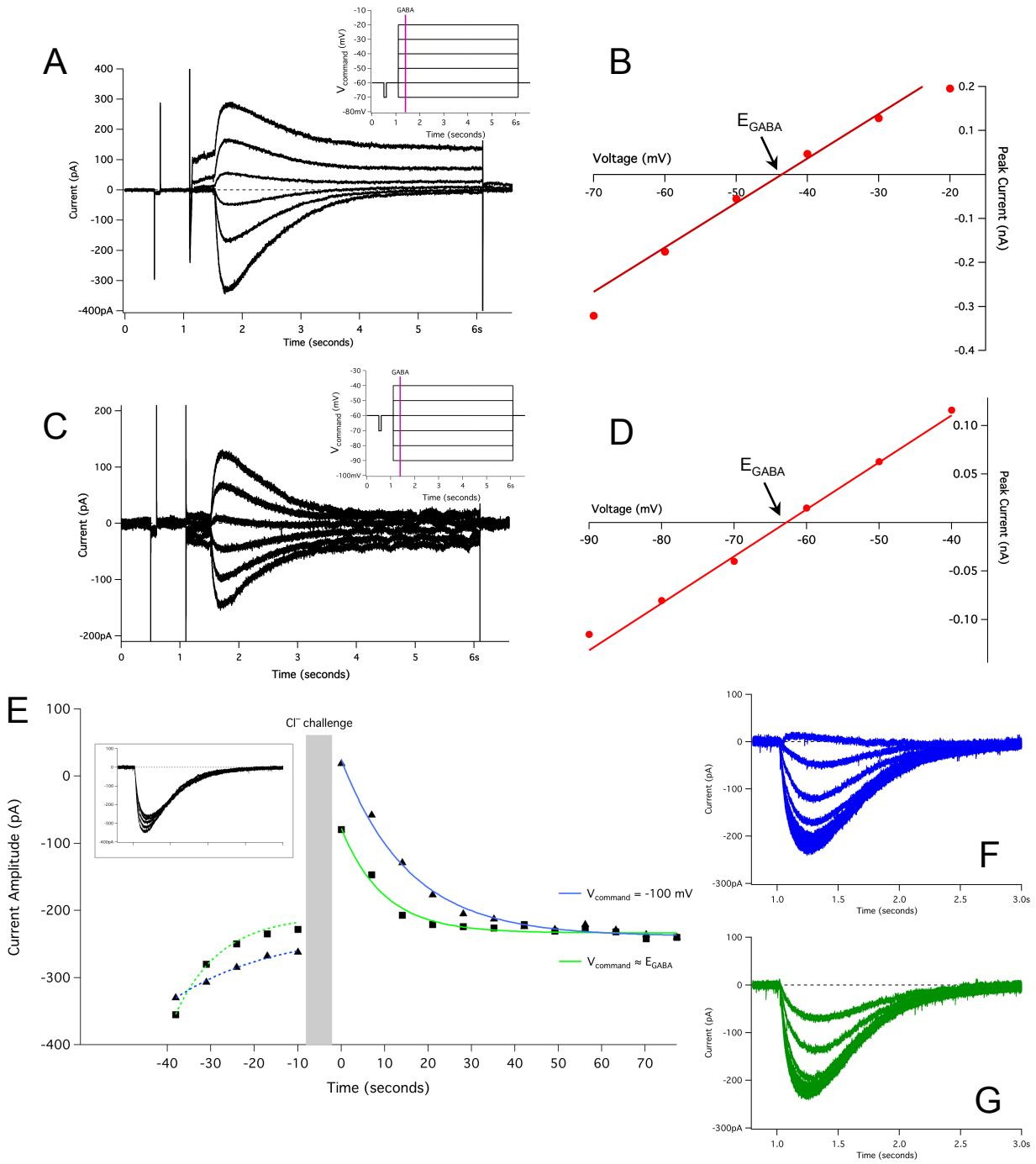

Figure 3.1: Whole-cell recordings from SCN neurons.

(A) Example voltage-clamp protocol (inset) and GABA-evoked currents used to determine E_{GABA} in an SCN neuron recorded with a pipette solution where $[Cl^-]_p$ = 15 mM. (B) IV relationship between $V_{command}$ and peak GABA-evoked current derived from Fig. A. E_{GABA} was determined as the point where the fit crossed the voltage axis. (C) Voltage-clamp protocol and GABA-evoked currents used to determine E_{GABA} in an SCN neuron recorded using a $[Cl^-]_p$ of 6 mM. (D) IV relationship derived from Fig. C. Note that E_{GABA} is hyperpolarized compared to Fig. B. (E) GABA-evoked current amplitudes plotted against time when $V_{command}$ was either negative to E_{GABA} (blue) or near E_{GABA} (green) during a long GABA application. GABA-evoked currents at baseline (E, inset) and during the recovery process (Figs. F and G). τ for these two examples are 15.5 and 9.7 seconds, respectively.

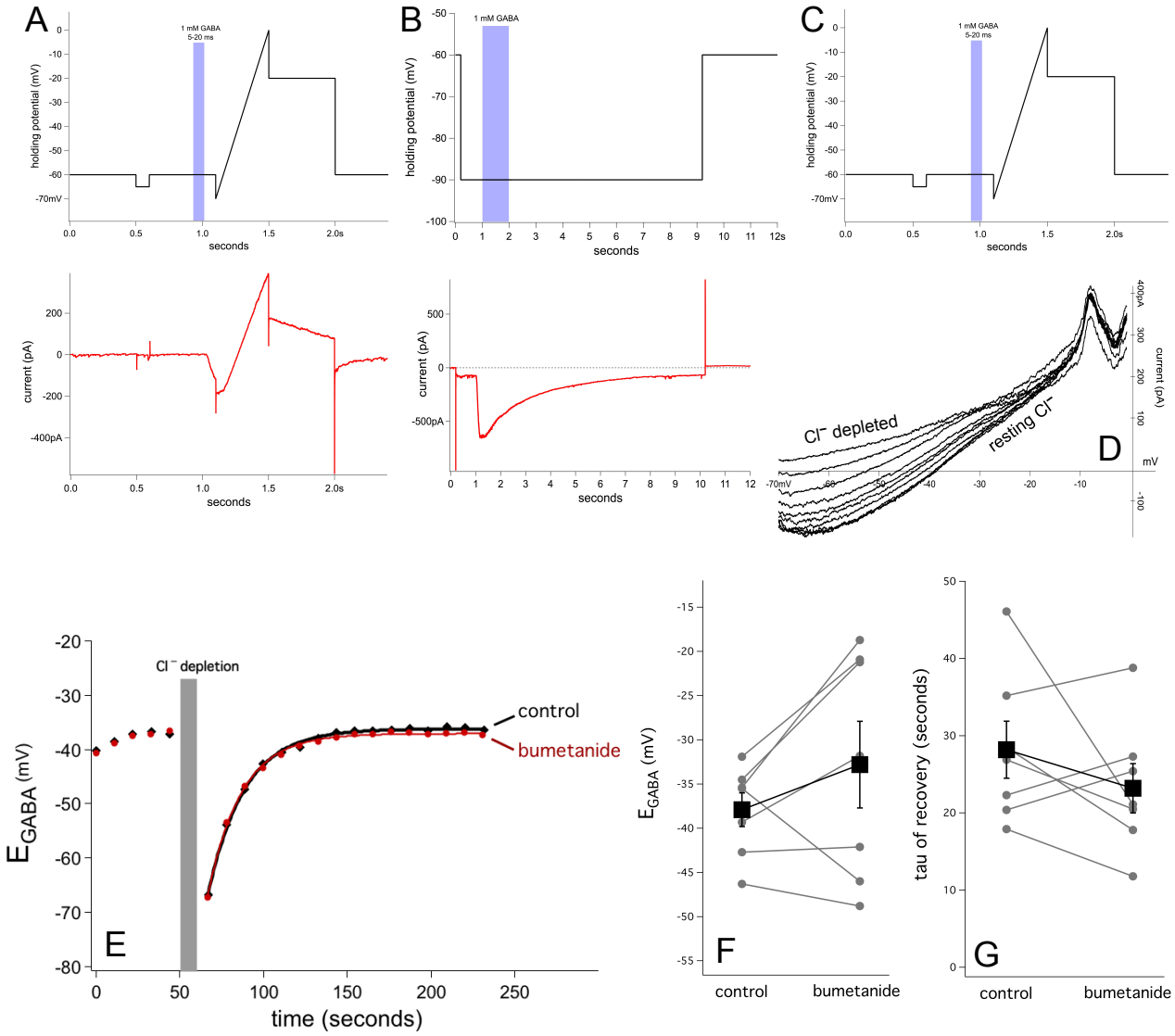

Figure 3.2: NKCC1 does not contribute to resting $[Cl^-]_i$ or the recovery following Cl^- depletion.
(A) Voltage ramp protocol (top) and example current trace (bottom) used to determine resting E_{GABA}. (B) Chloride depletion protocol (top) and resultant current trace (bottom). The cell was hyperpolarized in the presence of GABA in order to drive Cl^- efflux. (C) After the depletion event, voltage ramp protocols were again used to monitor the recovery of E_{GABA}. (D) IV plots derived from voltage ramp protocols recorded approximately every 10 seconds, before and after the chloride depletion event. Following the chloride depletion event, E_{GABA} is hyperpolarized and subsequently returns to its control value. (E) E_{GABA} plotted against time showing the recovery of E_{GABA} after the chloride depletion protocol. E_{GABA} values are fit with a monoexponential function before (τ = 21.9 s) and after the application of bumetanide (τ = 20.0 s). Bumetanide caused no significant change in either E_{GABA} (F) or the timecourse of recovery after depletion (G). Cells were selected from the dorsal SCN during the night.

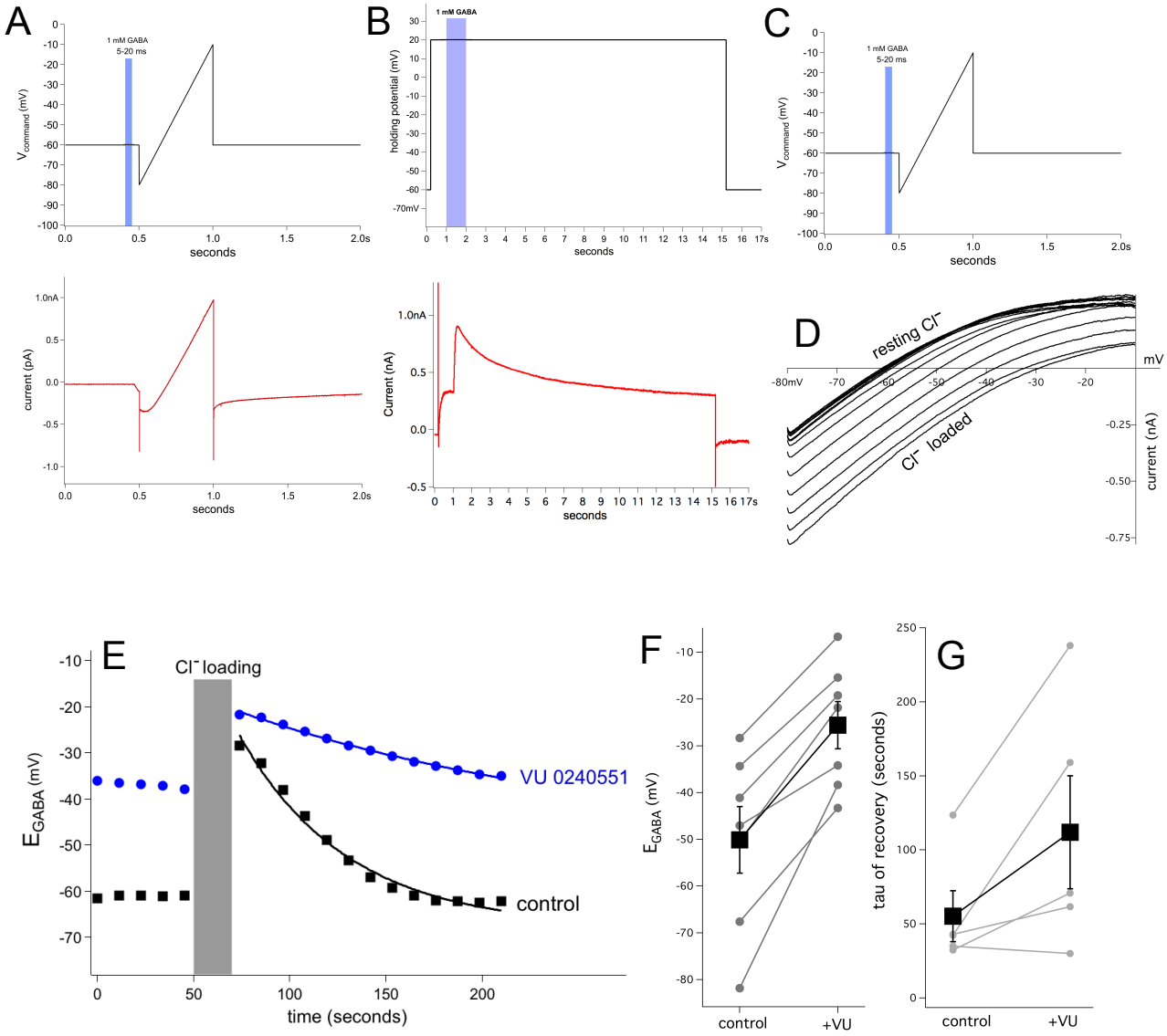

Figure 3.3: The KCCs regulate $[Cl^-]_i$ in SCN neurons.
(A) Voltage ramp protocol (top) and example current trace (bottom) used to determine native E_{GABA}. (B) Chloride loading protocol (top) and resultant current trace (bottom). (C) After the loading event, voltage ramp protocols were used again to monitor the recovery of E_{GABA}. (D) IV plots derived from the voltage ramp protocol recorded approximately every 10 seconds, before and after the loading event. Following the chloride loading event, E_{GABA} is depolarized and subsequently recovers to its control value. (E) Example experiment showing the recovery of the GABAergic reversal potential after the Cl^- loading protocol. E_{GABA} is plotted against time and fit with a monoexponential function before (τ = 56.2 s, black squares) and after the addition of 20 µM VU (τ = 197.9 s, blue circles). VU increased E_{GABA} (E, $p<0.001$, paired *t*-test) and slowed the timecourse of recovery (F, $p<0.05$, paired *t*-test). Cells were selected from the ventral SCN during the day.

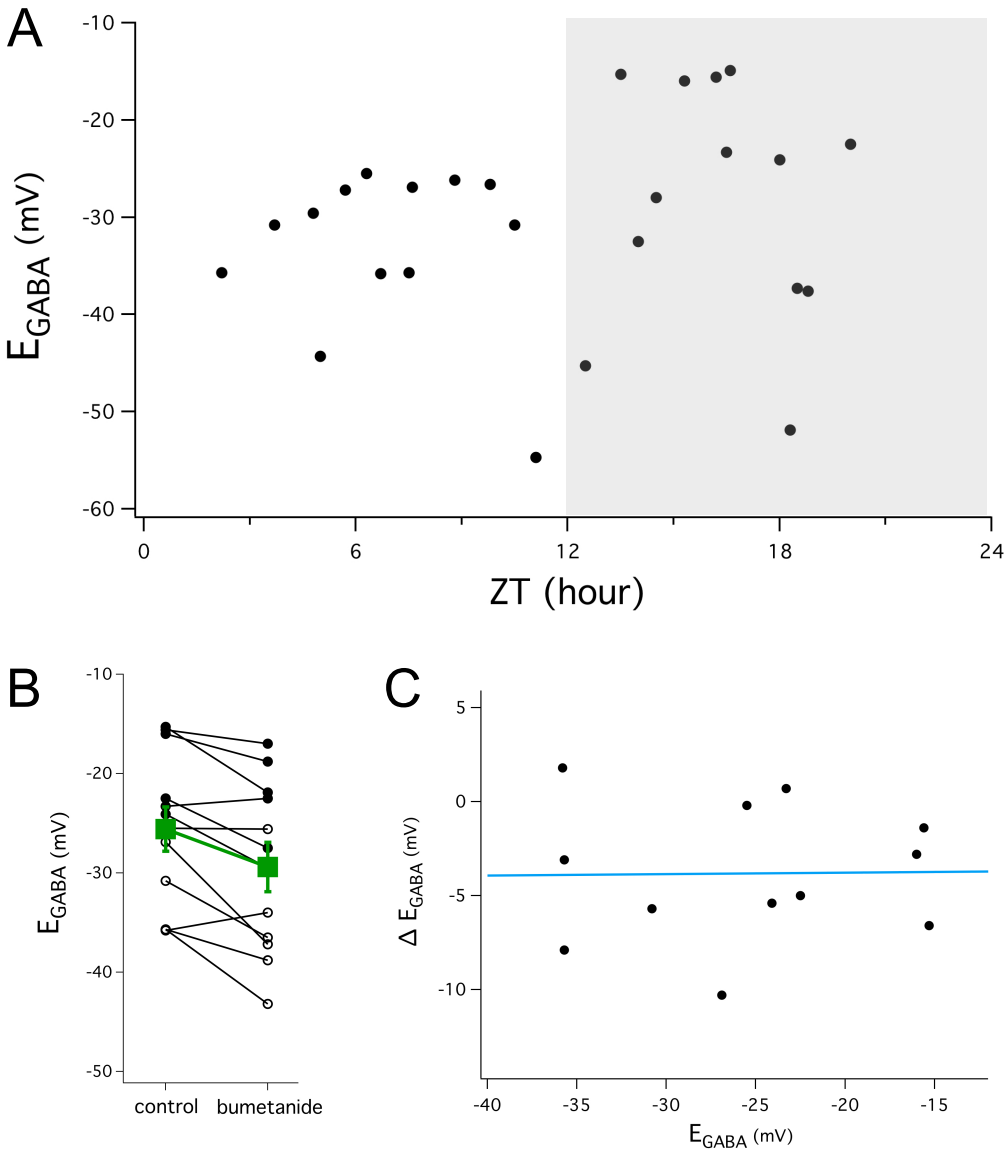

Figure 3.4: Perforated-patch recordings from AVP+ neurons.
(A) E_{GABA} was recorded from 26 AVP+ neurons, visually identified in slices from the AVP-eGFP rat line. E_{GABA} showed no clear relationship to the animal's light-dark cycle (ZT0 = time of lights on, ZT12 = time of lights off). (B) On average, 40 μM bumetanide hyperpolarized E_{GABA} by ~4 mV in AVP+ SCN neurons ($p<0.001$, *t*-test). The open circles represent cells recorded during the day, while the filled circles represent cells recorded during the night. (C) The resting E_{GABA} in AVP+ neurons showed no relationship to the change in E_{GABA} after bumetanide.

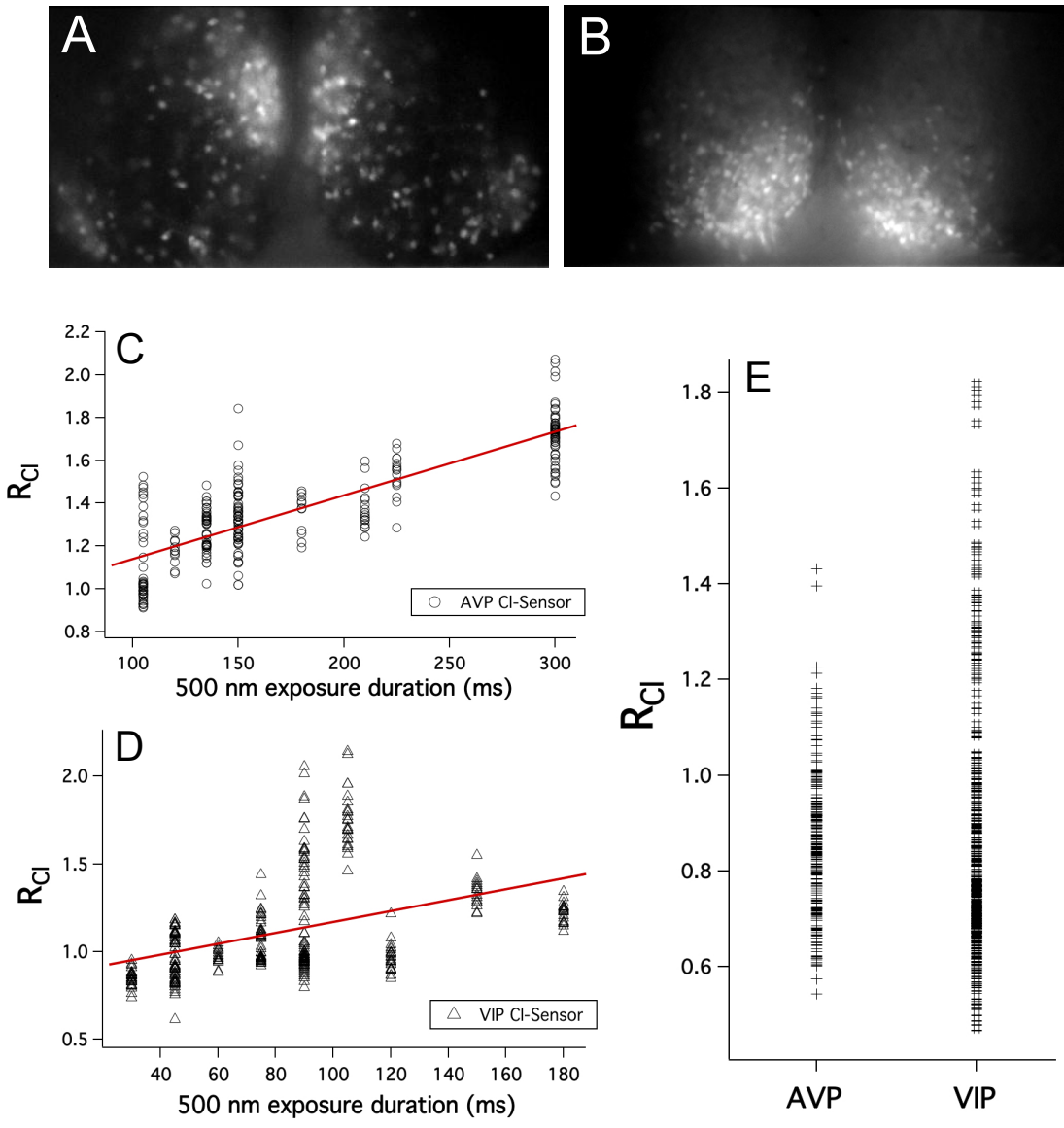

Figure 3.5: R_{Cl} did not vary by cell type.
Epifluorescent images demonstrating regional expression of Cl^- Sensor in the SCN of AVP-Cl Sensor (A) and VIP-Cl Sensor (B) mice. Steady-state R_{Cl} values obtained from AVP+ (C) and VIP+ (D) neurons were sensitive to exposure duration. Each point represents a single region of interest placed around a neuronal soma. (E) When correcting for this trend for each mouse independently, no difference in average R_{Cl} was found between the AVP+ and VIP+ neurons.

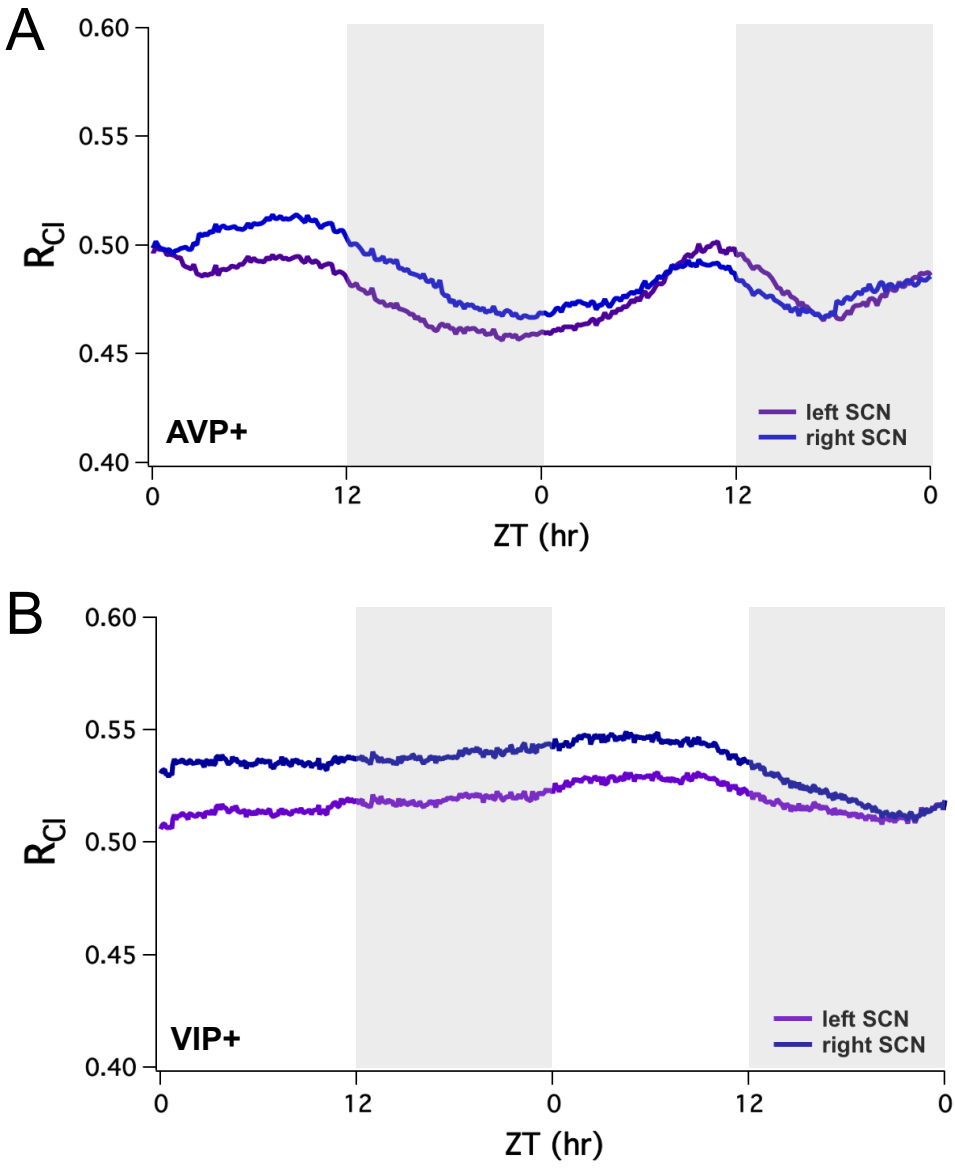

Figure 3.6: Long-term imaging of R_{Cl} from SCN explants.
(A) Long-term imaging of R_{Cl} from a AVP-Cl Sensor mouse. Each trace represents a measure of R_{Cl} from a cluster of AVP+ neurons in the left or right SCN. Circadian rhythmicity was detected with JTK_CYCLE ($p < 0.001$, period 23.0 hours). $[Cl^-]_i$ is high during the day and peaks near the time of lights off (ZT 12). (B) Long-term imaging of R_{Cl} from a VIP-Cl Sensor mouse. Each trace represents a measure of R_{Cl} from a cluster of VIP+ neurons in the left and right SCN. No rhythmicity was detected.

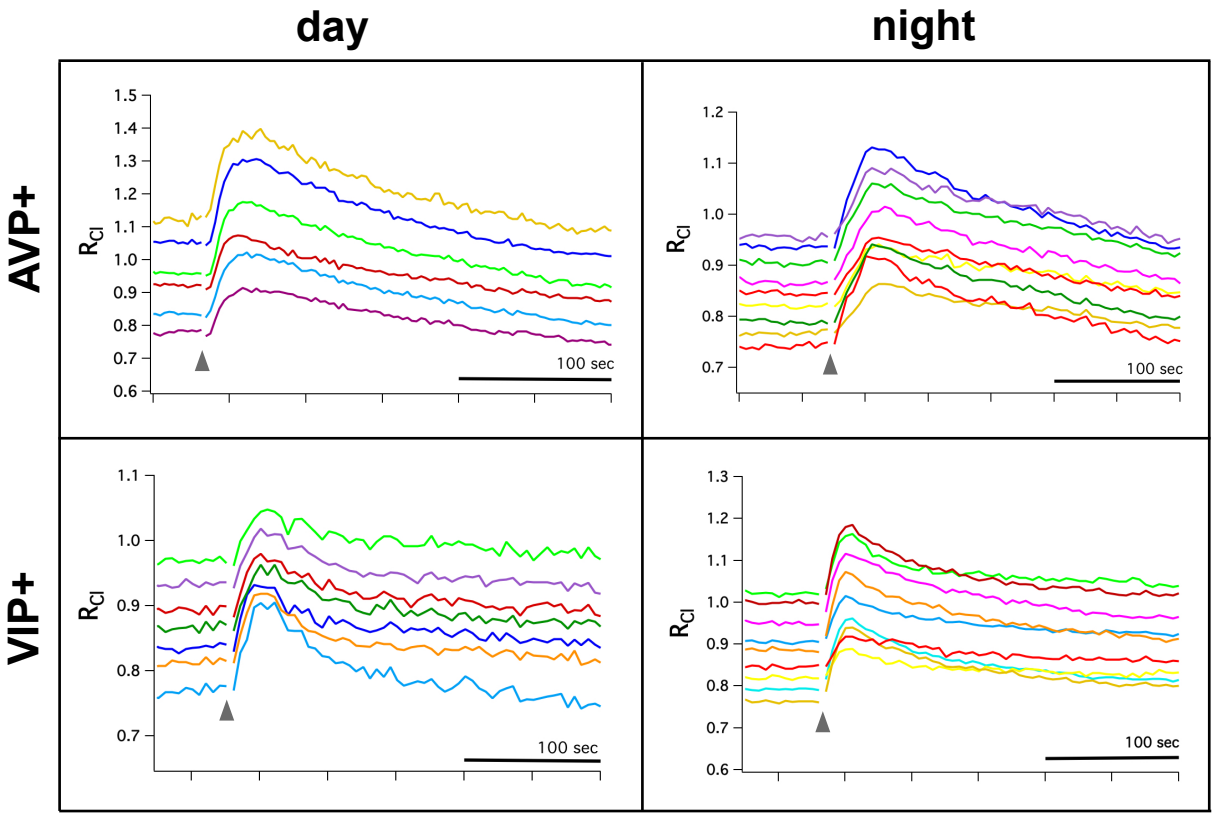

Figure 3.7: $GABA_A$ receptor-mediated Cl^- transients in AVP+ and VIP+ neurons.
Top row: AVP+ neurons from AVP-Cl Sensor mice tested during both subjective day and subjective night demonstrated an increase of R_{Cl} following puff application of the $GABA_A$ agonist isoguvacine (gray arrow), indicative of inhibitory Cl^- influx. Similarly, VIP+ neurons from VIP-Cl Sensor mice during both day and night responded to isoguvacine with an increase of R_{Cl} (bottom row). Each trace represents a R_{Cl} measurement obtained from a single neuronal soma.

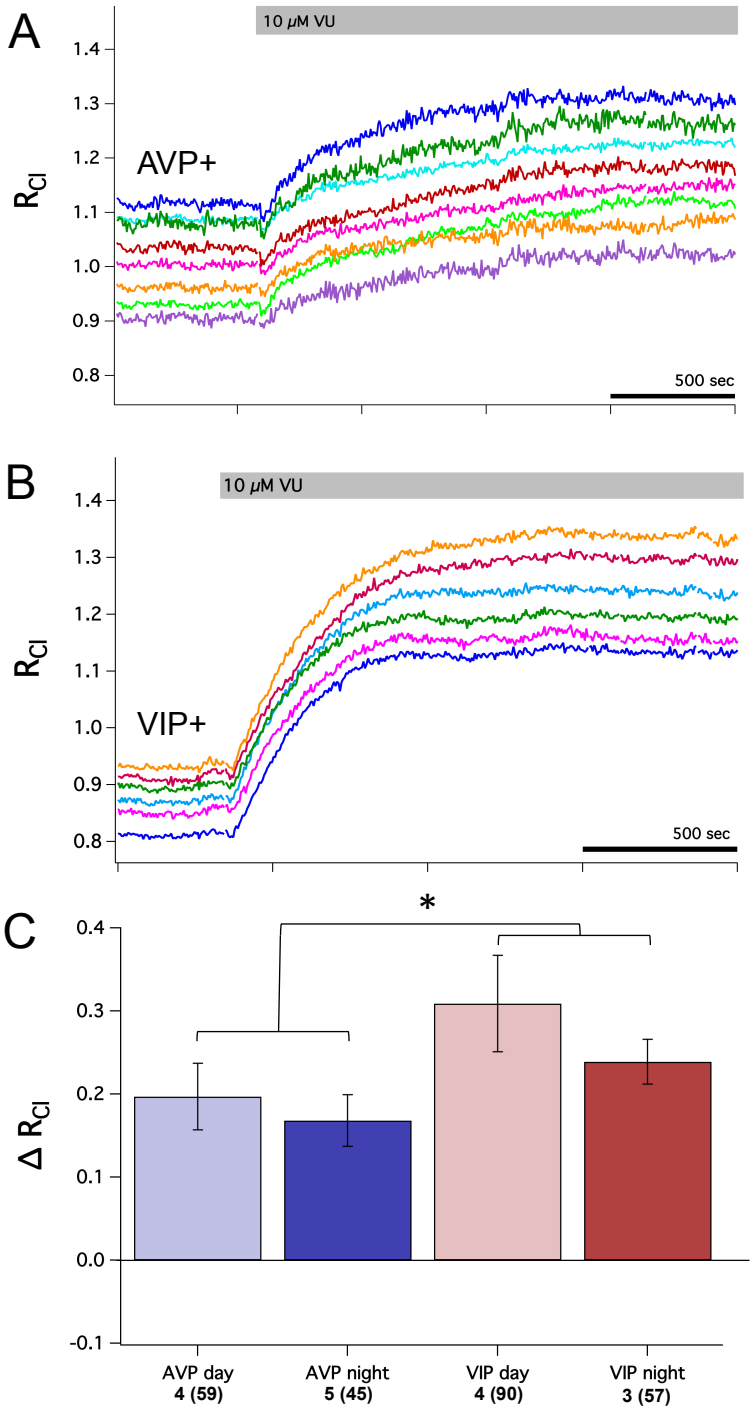

Figure 3.8: The KCCs contribute to $[Cl^-]_i$ regulation in SCN neurons.

(A) Example experiment from a VIP-Cl Sensor mouse after application of 10 μM the KCC antagonist VU. VU caused an increase in R_{Cl} indicative of a rise in $[Cl^-]_i$. Each trace represents a R_{Cl} measurement obtained from a single neuronal soma. (B) Example experiment from a AVP-Cl Sensor mouse after application of VU. VU caused an increase in R_{Cl} indicative of a rise in $[Cl^-]_i$. (C) Summary data of the average change in R_{Cl} after VU by neuron type and time of day. VU resulted in an increase in R_{Cl} in all conditions ($p<0.005$ with GEE), but had a significantly greater effect in VIP+ neurons compared to AVP+ neurons ($p<0.05$ with GEE). The number of slices and regions of interest is listed for each condition.

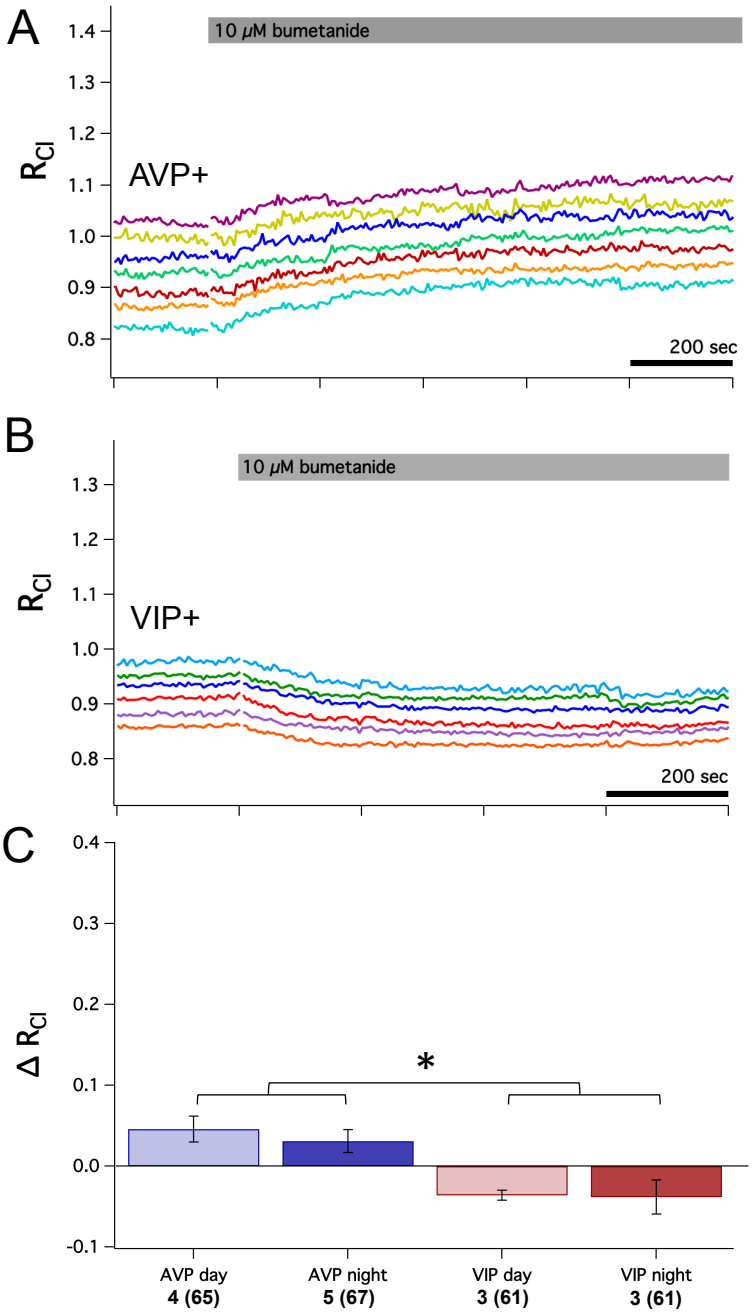

Figure 3.9: NKCC1 plays a minor role in setting $[Cl^-]_i$

(A) Example recording from a night-entrained AVP-Cl Sensor mouse showing the effect of blocking NKCC1 with 10 μM of bumetanide. Bumetanide caused a small increase in R_{Cl}. Each trace represents a R_{Cl} measurement obtained from a single neuronal soma. (B) Example recording from a night-entrained VIP-Cl Sensor mouse after application of bumetanide. Bumetanide caused a small increase in R_{Cl}. (C) Summary data of the average change in R_{Cl} after bumetanide by neuron type and time of day. Bumetanide elicited small but statistically significant changes in R_{Cl} in each condition ($p<0.005$). AVP+ and VIP+ neurons responded differently to bumetanide ($p<0.001$ with GEE), but there were no day/night differences within neuron types. Bumetanide statistically different effects on VIP+ neurons compared to AVP+ neurons. The number of slices and regions of interest is listed for each condition.

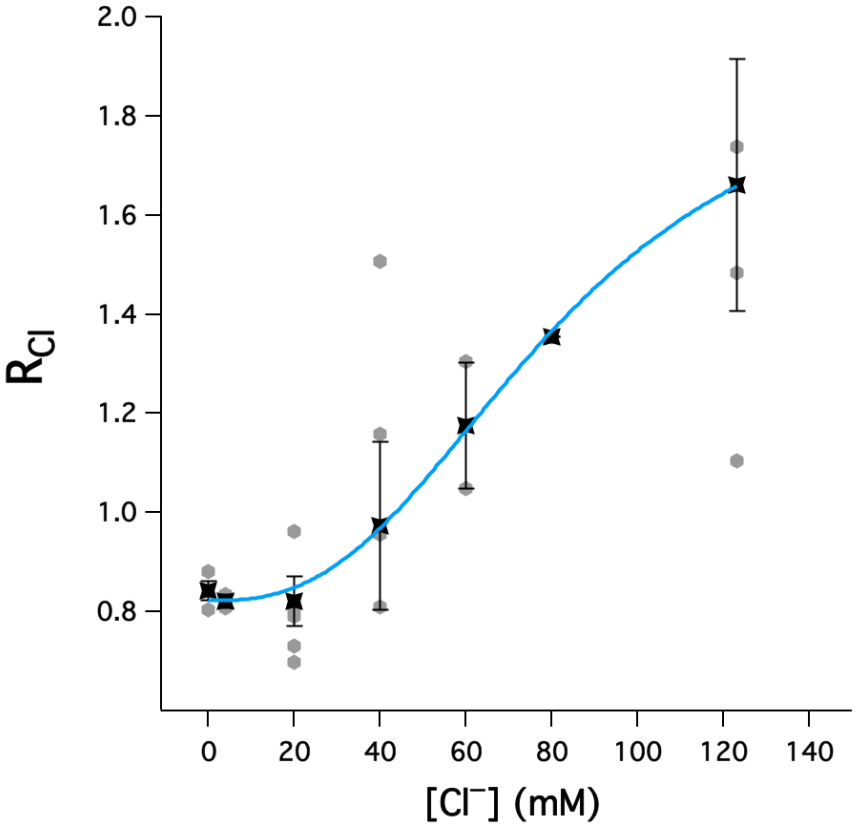

Figure 3.10: Calibration of Cl^- Sensor

To calibrate Cl^- Sensor, neurons were permeabilized with β-escin, and exposed to solutions in which NaCl was replaced with equimolar concentrations of Na-gluconate. Gray points represent average R_{Cl} values of individual trials obtained by averaging individual regions of interest; black dots represent average slice values ± standard error. Both AVP+ and VIP+ cells were used in calibration experiments. R_{Cl} was corrected for exposure duration as discussed (see methods). Averaged data were fit with a logistic dose-response sigmoidal curve, modeled after the Hill equation. Curve fitting yielded the following values: K_d = 81.6 mM, R_{min} = 0.82 R_{max} = 1.94 and p = 2.65.

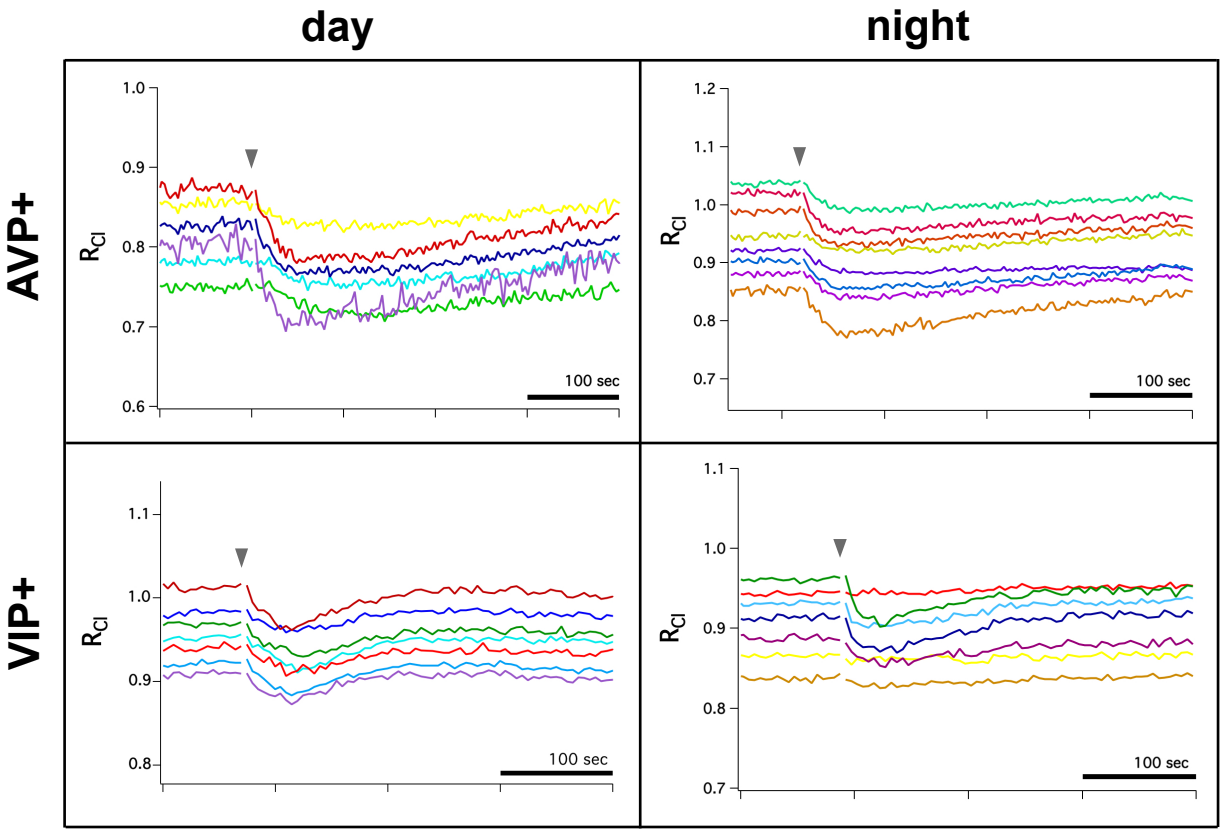

Supplemental Figure 3.11: $GABA_A$ receptor-mediated Cl^- transients in AVP+ and VIP+ neurons in HEPES-buffered aCSF. Top row: AVP neurons from AVP-Cl Sensor mice tested during both subjective day and subjective night demonstrated a decrease of R_{Cl} following puff application of the $GABA_A$ agonist isoguvacine (gray arrow), indicative of excitatory Cl^- efflux. Similarly, VIP+ neurons from VIP-Cl Sensor mice responded to isoguvacine with a decrease of R_{Cl} (bottom row). Each trace represents a R_{Cl} measurement obtained from a single neuronal soma.

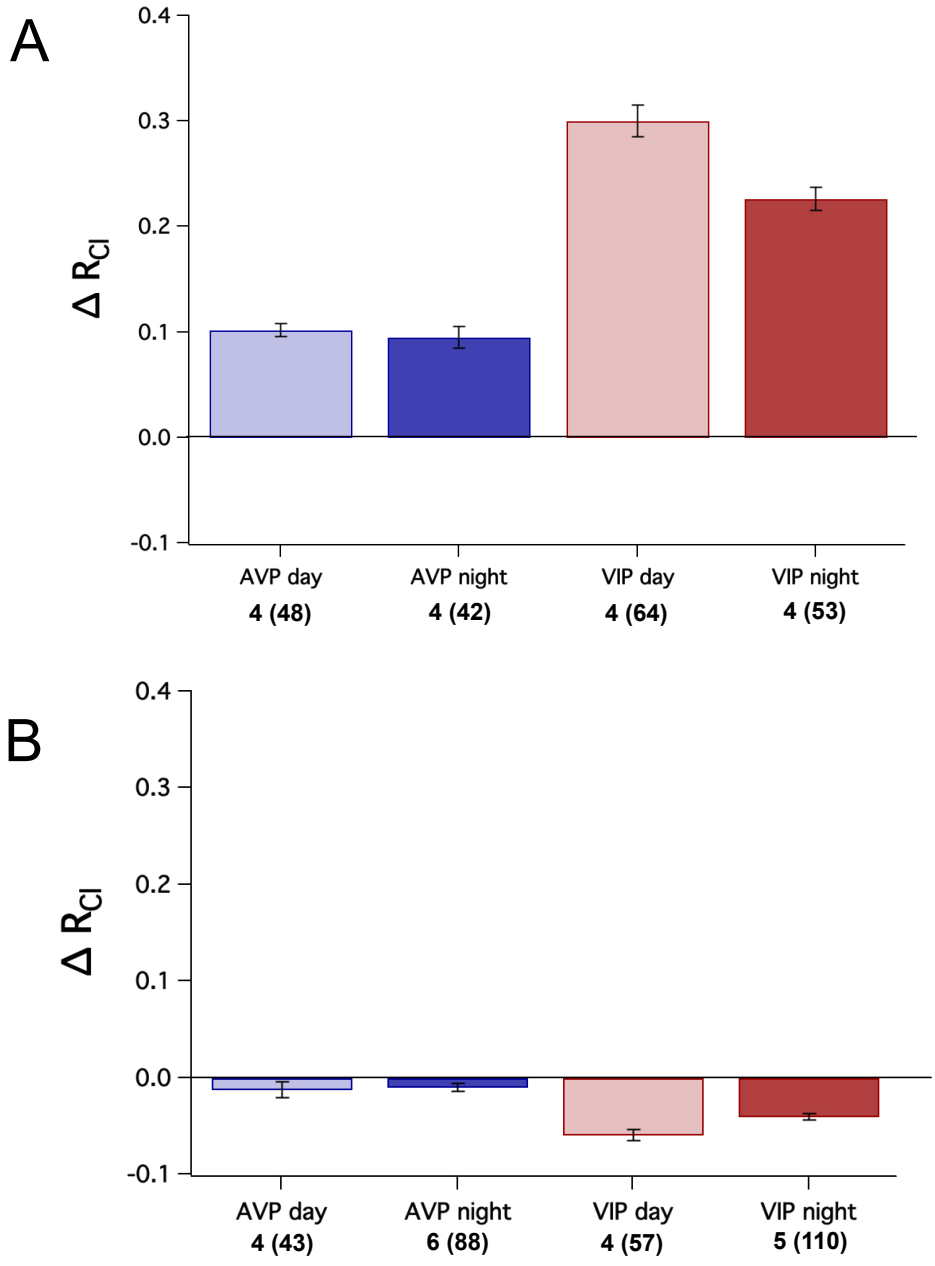

Supplemental Figure 3.12: Contributions of the chloride transporters to $[Cl^-]_i$ in HEPES-buffered aCSF. (A) Change in R_{Cl} after 10 μM of the KCC inhibitor VU. VU increased R_{Cl} in all conditions. (B) Change in R_{Cl} after 10 μM of the NKCC1 inhibitor bumetanide. Bumetanide caused a small reduction in R_{Cl} all conditions. The number of slices and regions of interest is listed for each condition.

CHAPTER 4: DISCUSSION

4.1 Overview

Despite the prevalence of GABA and GABA receptors in the SCN, the physiological and functional roles of GABA within the SCN have remained unclear. The results described in this dissertation have shed new light on the functional role of SCN GABA transmission, concluding that GABA transmission contributes to the synchronization of SCN neurons necessary for coherent circadian output. Further, I have used two independent techniques to study the intracellular chloride concentration in SCN neurons, which is the ultimate determinant of GABA's physiological action. These results have identified the molecular mechanisms of chloride transport in SCN neurons, and demonstrated differential chloride regulation in two genetically-defined populations of SCN neurons.

4.2 Local GABA transmission contributes to SCN synchrony

4.2.1 Deletion of Vgat and reduction of SCN GABA transmission

We successfully disrupted GABA transmission in SCN neurons. Generally, our results demonstrate the usefulness of our technique—local and acute disruption of GABAergic transmission is a valuable tool to dissect neural circuitry. Using an intersectional genetic strategy, we orchestrated local deletion of *Vgat*, the primary pathway for loading GABA into synaptic vesicles. *In situ* hybridization from Cre-injected $Vgat^{lox/lox}$ mice indicated that *Vgat* mRNA was dramatically reduced. We did not

demonstrate that VGAT protein was removed in Cre-transduced neurons. However, we observed a reduction in local synaptic GABA transmission. SCN neurons from Cre-injected mice had 37% fewer mGPSCs, suggesting that approximately 37% of GABAergic inputs were eliminated from SCN neurons. The remaining 63% of mGPSCs may be from SCN neurons with residual VGAT protein despite *Vgat* deletion, SCN neurons that did not receive AAV, or GABAergic inputs from outside of the SCN. Indeed, efferents from the IGL of the thalamus are a major input into the SCN and are known to be GABAergic (Card and Moore, 1982, 1989; Moore and Card, 1994). Notably, a 37% reduction in synaptic GABA tone was sufficient to elicit circadian disruption and cellular desynchronization, speaking to the importance of GABA transmission for SCN function.

The reduction in mGPSC frequency was paired with an increase in mGPSC amplitude. This increase in amplitude could reflect a homeostatic up-regulation of post-synaptic $GABA_A$ receptor expression or conductance. Alternatively, the increased amplitude might represent a difference between local and afferent GABAergic synapses present within the SCN. For example, GABAergic terminals from the intergeniculate leaflet may have a larger quantal size.

4.2.2 Behavioral disruption after VGAT depletion

We observed behavioral fragmentation of circadian rhythmicity in animals with disrupted SCN GABA transmission. Importantly, rhythmicity was maintained when mice were housed in light-dark cycles—arrhythmicity was only detected in constant darkness—indicating that this phenotype is due to circadian disruption. Arrhythmicity

was detected when measuring the animal's body temperature, wheel-running activity, and general locomotor activity. Certainly, it is reassuring to observe the same phenotype with different behavioral measures. Further, this concordance suggests a common point of origin upstream of these physiological outputs, which we regard to be the SCN.

Arrhythmicity was not observed in all Cre-injected *Vgat*$^{lox/lox}$ mice. As discussed above, this could be due to incomplete loss of SCN GABA transmission, or to variation in the location or extent of viral transduction. However, even mice with similar genotypes display diversity in their circadian phenotype. Interestingly, knockout mice for the VIP peptide, the VIP receptor, and the AVP receptor display varying degrees of rhythmicity in constant darkness with some mice being much more susceptible to genetic perturbation than others (Colwell et al., 2003; Hughes et al., 2008; Li et al., 2009a). The explanation for such behavioral variability warrants further research, but suggests that coherent SCN rhythmicity may require a threshold of synchronized SCN neurons.

Incredibly, GABA disruption demonstrated a more profound phenotype than deletion of certain clock genes. Rhythmicity is compromised but remains intact in *Clock*$^{-/-}$, *Cry1*$^{-/-}$, *Cry2*$^{-/-}$, *Per1*$^{-/-}$, *Per3*$^{-/-}$, *Rev-erbα*$^{-/-}$, *Rorα*$^{-/-}$, and *Rorβ*$^{-/-}$ mice. Double knockouts of these genes are often required to induce arrhythmicity (Lowrey and Takahashi, 2011). Therefore, the severity of circadian disruption observed after VGAT deletion speaks to the importance of GABA transmission for SCN function.

4.2.3 Interneuronal GABA transmission contributes to SCN synchrony

We attribute the observed behavioral fragmentation to desynchrony among rhythmic neuronal oscillators. Several studies have reported that genetic mutations elicit a severe disruption of rhythmicity in individual cells, but only a minor disruption of total SCN rhythmicity, concluding that cell coupling protects the SCN from perturbation (Liu et al., 2007; Abraham et al., 2010; Buhr et al., 2010; Ko et al., 2010). Candidate cell coupling signals include VIP, neurotensin, neuromedin S and GABA with compelling evidence supporting each (for review, see Welsh et al., 2010). Our evidence supports a role for GABA in cell coupling. We conclude that GABA facilitates synchrony of SCN neurons.

Luminometry from PER2::LUC SCN explants did not yield clear differences between Cre-injected and Cre-null *Vgat*$^{lox/lox}$ mice. The rate of damping was comparable between groups. Our method of damping analysis normalized the third PER2 peak to the first. Although this approach facilitated comparison between SCN slices with varied signal intensity, it removed amplitude from the analysis procedure. Signal amplitude is known to be crucial in orchestrating cohesive circadian rhythmicity. Therefore, it is possible that the VGAT-depleted mice had a smaller amplitude rhythm than the Cre-null mice, but that this difference could not be detected by our analysis procedure.

To monitor the molecular clock in individual neurons, we turned to fluorescent reporters. We used a mPER2 reporter to monitor total rhythmicity from SCN explants, but a mPER1 reporter to monitor rhythmicity in individual neurons. Though homologs with a similar phase relationship, important distinctions have been made between

mPER1 and mPER2. mPER1 and mPER2 expression is colocalized in some SCN neurons, but separate in others. Outside of the SCN, PER1 is mostly found in neurons, while PER2 is restricted to glia (Cheng et al., 2009). mPER1 and mPER2 demonstrated differential induction and localization in SCN tissue after mice were subject to phase-advancing and phase-delaying light exposures suggesting that mPER1 and mPER2 have different influences on the molecular clock (Yan and Silver, 2002). Another study concluded that mPER2 has greater influence on transcription, while mPER1 regulates post-translational modifications (Bae et al., 2001). Microarray analysis revealed that mPER1 and mPER2 regulate the expression of separate sets of clock-controlled genes (Zheng et al., 2001). Therefore, separate mPER1- and mPER2-driven molecular clocks may dominate in a given cell and total SCN timing may involve interneuronal interactions between these two molecular clocks. Future studies will be necessary to determine if GABA transmission selectively disrupts mPer1 intracellular signaling.

4.2.4 Future directions

Our results demonstrate circadian desynchrony of individual neuronal oscillators within the SCN. To measure synchrony, we monitored *mPer1*-Venus fluorescence intensity, which gives a readout of the molecular clock. I would like to see if the observed desynchrony of the molecular clocks is manifest in the circadian rhythm of action potential discharge rate, a significant physiologic output of the SCN. Individual SCN neurons demonstrate a circadian rhythm in firing frequency. In a preliminary set of experiments, I measured action potential discharge rate from 72 day and 93 night neurons, and observed the well-established day-night difference in firing frequency.

Unfortunately, I did not have the opportunity to record AP discharge from Cre-injected *Vgat*$^{lox/lox}$ mice. In my preliminary survey, I used cell-attached recordings to sample frequency from single neurons in a slice. However, to detect desynchrony it is best to track individual neurons over multiple circadian cycles. Therefore, I would like to monitor AP discharge from *Vgat*-deleted SCN slices with multi-electrode arrays.

Our technique allowed local and acute disruption of GABA transmission—*Vgat* was deleted in the adult SCN, avoiding any possible developmental effects. Although our viral-mediated recombination allowed local VGAT depletion, the injection procedure does introduce variability into the experimental design, and may not provide complete depletion of VGAT from SCN neurons (as discussed above). Recently, the gene for the dopamine receptor D1a (*Drd1a*) has emerged as a useful SCN targeting allele. In a recent optogenetics study, *Drd1a*-Cre mice were used to drive expression of channelrhodopsin (ChR2). ChR2 expression was observed in ~90% of AVP+ and VIP+ neurons, as well as in a high proportion of AVP-/VIP- SCN neurons (Jones et al., 2015). Therefore, although GABA transmission would be disrupted in *Drd1a*-expressing neurons throughout the brain, it would be interesting to look for a circadian phenotype in *Drd1a*-Cre, *Vgat*$^{lox/lox}$ mice.

Recently, I have crossed the AVP-Cre and VIP-Cre mice with *Vgat*$^{lox/lox}$ mice to remove GABA transmission from specific populations of SCN neurons. So far, I have observed no striking circadian phenotypes in either AVP-Cre, *Vgat*$^{lox/lox}$ mice or VIP-Cre *Vgat*$^{lox/lox}$ mice. These mice display normal entrainment to phase advances and phase delays, and normal rhythmicity under constant darkness. These preliminary results suggest that disrupting GABA transmission from AVP or VIP-expressing neurons is not

sufficient to elicit arrhythmicity, and that a more complete disruption of local GABA transmission is necessary to provoke circadian arrhythmicity.

4.3 Cl^- regulation in SCN neurons

4.3.1 General conclusions

I used gramicidin perforated-patch electrophysiology and newly-developed Cl^- imaging techniques to study $[Cl^-]_i$ regulation in SCN neurons. Perforated-patch measurements of E_{GABA} were depolarizing, but Cl^- imaging results demonstrated inhibitory Cl^- influx in AVP+ and VIP+ neurons of the SCN at all times of day. Both electrophysiological and fluorometric techniques agree that $[Cl^-]_i$ is primarily determined by the KCC family of Cl^- transporters, and only minorly controlled by NKCC1.

4.3.2 Whole-cell recordings

My experiments demonstrate that whole-cell recording is not sufficient to study endogenous $[Cl^-]_i$ regulation in SCN neurons. Taking into account the mixed permeability of $GABA_A$ receptors and junction potential offsets, it became clear that E_{GABA} was primarily determined by the concentration of chloride in the patch pipette. Looking at developmental changes in E_{GABA} in SCN neurons, Chen et al. arrived at a similar conclusion, arguing for the necessity of perforated patch techniques (Chen et al. 1996; see also Wagner et al., 1997). As a workaround, Wagner et al. measured spontaneous activity in the first moments after rupture of the patch membrane, observing that both the amplitude and variance of the post-synaptic potentials

depended on the membrane potential. Using the standard deviation of membrane potential, they inferred that $[Cl^-]_i$ was generally higher than 15 mM during the day, and generally lower than 15 mM during the night (Wagner et al., 1997). In a follow-up study, Wagner et al. continued with elaborate whole-cell recording techniques to measure Cl^- regulation in SCN neurons, concluding that two Cl^- transport mechanisms operate in SCN, and that the uptake mechanism is reduced during the animal's night (Wagner et al., 2001). Therefore, although whole-cell recording may be informative, it does not adequately reflect cell physiology.

Originally, I measured E_{GABA} by pairing a voltage-step protocol with micro-application of 1 mM GABA (Figures 3.1 A & B). However, it soon became clear that the amplitude of GABA-evoked currents will not only depend on the driving force of the $GABA_A$ receptor, but also on $GABA_A$ receptor availability. For this reason, voltage ramp protocols were the preferred method of E_{GABA} assessment, as they are not susceptible to errors related to desensitization.

4.3.3 Gramicidin perforated-patch recordings

4.3.3.1 Methodological considerations

Gramicidin perforated-patch recordings afford the ability to study the native $[Cl^-]_i$. Indeed, it was reassuring to find that the measured $[Cl^-]_i$ differed from that of the pipette solution, and presumably reflected endogenous the $[Cl^-]_i$. Unfortunately, this advantage in accuracy comes at a considerable experimental cost. The gramicidin ionophore interferes with pipette seal formation with the cell membrane. Further, a significant amount of time is required for gramicidin molecules to diffuse to and insert into the

patch membrane. Naturally, this temporal limitation decreases the sampling potential of the technique.

Compared to whole-cell recordings, perforated-patch recordings yield higher series resistances, reducing the ability of the researcher to voltage clamp the neuron. High series resistance will reduce space clamp, and can introduce substantial offsets into measures of E_{GABA}. I restricted my recordings to cells that had series resistances lower than 100 MΩ. Occasionally, I observed sudden increases in series resistance after successful perforation. I attribute these increases to be related to pipette drift, which I consider to be more of a problem with perforated patch recording than with whole-cell recording.

From a methodological perspective, accidental rupture of the patch membrane may be the most challenging problem with gramicidin perforated-patch recording. After waiting up to 45 minutes for perforation, I was confounded to observe spontaneous rupture of the patch membrane. I often found it difficult to get through my complete experimental protocol before going whole-cell: control measures of E_{GABA}, chloride challenge and recovery, an allowance for drug perfusion and agency, and subsequent measures in test conditions. Anecdotally, I suspect that large voltage steps encourage disruption of the perforated patch membrane. To shorten my experimental protocol and thereby decrease the chance of patch rupture, I pre-incubated slices in bumetanide in one data set (results not shown). Although this experimental design shortened the experimental protocol, it came at a sacrifice to statistical resolution: paired statistical measures could no longer be used.

Tracking series resistance is one way to monitor the perforated membrane—R_s *should* noticeably decrease if the patch goes whole-cell. Another trick is to use a pipette solution with high concentration of chloride—Cl^- mediated currents should shift after accidental rupture, and reverse near 0 mV. Adding a fluorescent dye to the pipette can also be useful—the dye should be excluded from the cell if the perforation is intact. When possible, rupturing the patch at the end of experiment offers additional confidence in the prior integrity of the patch.

The aforementioned issues make each perforated patch recording highly precious. This problem is compounded when the investment includes targeted neurons. The AVP-eGFP rat line offered front-end selection of identified neurons as opposed to post-hoc histological analysis of experimental tissue (to look for co-labeling between neurobiotin and the neuropeptide antigen). However, this advantage comes with considerable trade-offs. The electrophysiologist contends with continuous bleaching of the fluorophore when attempting to identify fluorescent neurons. Further, the experimenter will need to switch between fluorescent and differential interference contrast optics in order to gain a successful seal with the cell membrane. My experimental design involved targeting green-fluorescent neurons with a red-fluorescent pipette solution. This technique required switching between filter cubes in the epi-illuminator turret which risked jostling the pipette and losing the perforated patch.

The technical limitations of gramicidin perforated patch recording made it difficult for me to resolve potential differences in $[Cl^-]_i$ regulation across my independent variables: dorsomedial (or AVP+) neurons in the day and night, ventrolateral neurons in the day and night, and drug effects for both bumetanide and VU across these

conditions. It became a daunting task. During this time, a group in Mexico published an extensive perforated-patch study addressing some of my very own specific aims (Alamilla et al., 2014). Meanwhile, we were in the process of getting Cl^- Sensor fluorometric techniques up and running. Cl^- Imaging presented a new and exciting approach to an old problem. Eventually, I abandoned gramicidin perforated patch techniques and switched my efforts to Cl^- imaging.

4.3.3.2 Measurements of E_{GABA}

Using gramicidin perforated patch recording, I measured E_{GABA} to be −37.9 mV in dorsomedial neurons during the night, −39.0 mV in dorsomedial neurons during the day, and −52.7 mV during ventrolateral neurons during the day. The difference between these populations of neurons is in agreement with a recent study by Alamilla et al. They concluded that during the day, most dorsal SCN neurons have an E_{GABA} close to −30 mV, but most ventral neurons have an E_{GABA} close to −60 mV (Alamilla et al., 2014). In a separate set of recordings from AVP+ neurons, E_{GABA} was −30.4 mV during the day and −32.3 mV during the night. (Although AVP+ neurons are generally localized to the dorsomedial SCN, it is difficult to relate values from AVP+ neurons to those from dorsomedial neurons, as AVP+ neurons were recorded with a HEPES-buffered solution while the regionally-selected neurons were recorded with a bicarbonate-buffered external solution.) Based on measured values of E_{GABA}, it is possible to estimate values of $[Cl^-]_i$. Assuming a 20% permeability for the $GABA_A$ receptor and an E_{HCO3} of −20 mV, $[Cl^-]_i$ was calculated to be between 8 and 27 mM. At a V_m of −55 mV, Cl^- would be passively distributed at an $[Cl^-]_i$ of 15 mM. Therefore, the measured values of E_{GABA}

indicate the presence of both active Cl^- uptake and active Cl^- extrusion in SCN neurons.

In general, I observed rather depolarized values of E_{GABA}. Although I did not measure membrane potential directly, V_m is generally reported to be around –55 mV in SCN neurons (Colwell, 2011). Therefore, E_{GABA} was close to V_m, but depolarizing. All extracellular solutions used in this study were adjusted to have $[Cl^-]_o$ near physiologically-relevant concentrations (~123 mM; Schrock and Kuschinsky, 1989). Compared to commonly-used aCSF ($[Cl^-]_o$ usually closer to 150 mM), this chloride concentration will favor depolarized values of E_{GABA}. An electrophysiologist's cell selection preferences can also bias measures of E_{GABA}. Because intracellular chloride is linked to cell volume regulation, visual preferences for neuronal shape and membrane turgor under DIC optics can introduce bias into measures of E_{GABA} (Delpire and Staley, 2014). Recordings from swollen neurons will favor depolarized values of E_{GABA}. Further, recordings are generally restricted to the top 50-100 µm of the brain slice surface. In 2012, Dzala et al. demonstrated that brain slice preparation elicits neuronal trauma that can severely affect $[Cl^-]_i$ (Dzhala et al., 2012). They observed elevated $[Cl^-]_i$ in the top 100 µm of a hippocampal slice that was dependent on neuron depth. Further, this chloride accumulation was found to correlate with neuronal damage and apoptosis. Therefore, it is possible that experimental artifacts may have contributed to the observed depolarizing values of E_{GABA}. I restricted my recordings to cells with holding currents greater than −30 pA. Therefore, this criteria should have helped to remove dead or “leaky” neurons from the data set.

Notably, I obtained measures of E_{GABA} remarkably close to those reported for V_m. Ultimately, whether GABA is excitatory or inhibitory depends not only on the driving force of GABA currents (E_{GABA} relative to V_m), but also on the ability of $GABA_A$ receptor activation to shunt the membrane. A depolarizing post-synaptic potential can still be inhibitory, especially when E_{GABA} is close to V_m. Therefore, the observed proximity between E_{GABA} and V_m in SCN neurons may explain the nuanced history of GABA's effect on SCN neurons.

I observed substantial variability in the GABAergic reversal potential. Resting E_{GABA} ranged from −80 to −15 mV, but was generally between −50 to −30 mV. This degree of variability is in agreement with prior reports of E_{GABA} in the SCN, including previous measurements from our own lab. In culture, Shimura et al. reported a range from −64 to −36 mV (Shimura et al. 2002). De Jeu et al. observed a range of −84 to −49 mV during the day and −82 to −38 mV during the night, concluding that, on average, E_{GABA} is depolarized during the night (de Jeu et al. 2002). Similarly, Choi et al. reported that GABAergic post-synaptic potentials reversed in the range of −72 to −32 mV, but that GABA-mediated EPSPs were more common in the dorsal neurons during the night. Finally, Alamilla reported a wide range of E_{GABA} in SCN neurons, varying from −87 to −9 mV (Alamilla et al., 2014). The observed variability in $[Cl^-]_i$ observed in SCN neurons parallels that found in other regions of the brain (Ebihara 1995; Kuner and Augustine, 2000; Dzhala et al. 2005; Berglund et al 2006; Glykys et al 2009). The degree of variability may be attributed to various artifacts related to the gramicidin perforated patch technique (as discussed previously), or it may be physiologically-relevant. One possibility is that SCN neurons use E_{GABA} to encode phase information. Therefore

variability in E_{GABA} may represent variability in phase. Indeed, SCN neurons are known to exhibit a variety of phases even within the intact SCN slice (Rohling et al., 2006; Farajnia et al., 2014). Further, membrane potential is known to be a major point of regulation for controlling the phase of SCN neurons, whereby excitation elicits *Per* induction and phase-advance (Shibata et al., 1994; Lundkvist et al., 2005; Colwell, 2011). Therefore, it could be that GABAergic excitation elicits phase-advances in SCN neurons, while GABAergic inhibition induces phase-delays, or alternatively, blocks phase shifts (Alamilla et al., 2014). Accordingly, the observed variability of E_{GABA} might represent the unique ability of SCN neurons to adjust their phase bidirectionally. Ultimately, the high degree of variability I observed in E_{GABA} made it difficult to distinguish potential regional and circadian differences in $[Cl^-]_i$ regulation and contributed to my decision to ultimately abandon perforated-patch recordings.

4.3.3.3 $[Cl^-]_i$ manipulation and recovery

Using voltage-clamp protocols, I was able to manipulate $[Cl^-]_i$ and monitor the subsequent recovery to resting levels. To manipulate $[Cl^-]_i$, GABA was applied to activate $GABA_A$ receptors, and V_m was clamped to either drive Cl^- into or out of the cell. It is well established that E_{GABA} can undergo both short-term and long-term changes. Short-term changes in E_{GABA} are considered to be due to collapse of the Cl^- gradient. Several studies have shown that intense activation of $GABA_A$ receptors can result in transient shifts in E_{GABA} (Alger and Nicoll, 1979; Andersen et al., 1980; Thompson and Gahwiler, 1989). Interestingly, in hippocampal interneurons, physiologically-relevant firing patterns were able to switch GABAergic input from inhibitory to excitatory,

suggesting that ionic plasticity may be a strategy interneurons use to promote sustained network activity (Lamsa and Taira, 2003). A similar finding was observed in hippocampal pyramidal neurons (Fiumelli et al., 2005).

After Cl^- depletion, I measured a rate of recovery with an average time constant of 28.2 seconds, meaning that $[Cl^-]_i$ would take about 45 seconds to return to baseline levels. After Cl^- loading, I measured a rate of recovery with an average time constant of 55.2 seconds, meaning that $[Cl^-]_i$ would take about 88 seconds to return to baseline levels. These measures are within the range of values that have been reported in other neurons (Staley and Proctor, 1999; Lamsa and Taira, 2003; Achilles et al., 2007; Raimondo et al., 2012). On average, recovery after Cl^- depletion took less time than recovery after Cl^- loading. This difference suggests that Cl^- loading mechanisms may be more influential than Cl^- extruding mechanisms in SCN neurons, which may explain why I observed $[Cl^-]_i$ to be higher than expected by a passive distribution. However, whether or not the rate of Cl^- transport is relevant to resting $[Cl^-]_i$ and will require further analysis.

The rates of recovery exhibited substantial variability between cells and sometimes even between trials. This variability can be partly attributed to variability in the net Cl^- flux elicited during the Cl^- challenge protocol. I found it difficult to control for this variable; net charge flux ranged from 1 to 4 nC between experiments. Measuring the instantaneous rate of Cl^- transport at the point of passive Cl^- distribution may have provided a more stable measure of Cl^- transport, as this value is not expected to be sensitive to differences in the amount of charge transfer (Achilles et al., 2007). Alternatively, the observed variation in recovery may represent physiological differences

between cells. Indeed, the cell surface expression and kinetic regulation of CCCs are known to be important determinants of $[Cl^-]_i$ (Kahle et al., 2013). Further experimentation will be necessary to address kinetic regulation of Cl^- transport in SCN neurons.

4.3.3.4 Effects of the NKCC1 antagonist bumetanide

At low concentrations, bumetanide specifically inhibits Cl^- uptake mediated by NKCC1 (Russell, 2000). I found little effect of bumetanide in dorsomedial SCN neurons during the day or night. Bumetanide did not significantly alter either resting E_{GABA} or the rate of Cl^- uptake after Cl^- loading. This result suggests that other Cl^- uptake mechanisms set $[Cl^-]_i$ in SCN neurons. In other parts of the brain, bumetanide did not have an effect despite $[Cl^-]_i$ concentrations greater than those expected by a passive Cl^- distribution (Balakrishnan et al., 2003; Price and Trussell, 2006; Zhang et al., 2007). Alternatively, the activity of NKCC1 may have been masked by other Cl^- uptake mechanisms, such as Cl/HCO_3 transport mediated by the anion exchangers (AE3, etc). Interestingly, I did observe a small effect of bumetanide in AVP+ neurons of the AVP-eGFP rat line. This effect could be due to differences in $[Cl^-]_i$ regulation between neuron types. Indeed, NKCC1 expression was found to be most dense in the dorsomedial SCN (Belenky et al., 2010). AVP+ neurons were recorded in HEPES-buffered ACSF. Therefore, removing HCO_3 and thereby reducing Cl/HCO_3 transport may have been sufficient to reveal an activity of NKCC1 in $[Cl^-]_i$ regulation. Accordingly, this mechanism may be able to explain why in Cl^- imaging experiments bumetanide resulted in a decrease in R_{Cl} in AVP+ neurons in HEPES-buffered

solutions, but a small increase in bicarbonate-buffered solutions. Alternatively, the efficacy of bumetanide on E_{GABA} observed in AVP+ neurons may be explained by the higher concentration of bumetanide used in these experiments (40 μM) compared to earlier experiments (10 μM). However, this explanation is probably not sufficient to explain the difference between the data sets, as the IC_{50} for bumetanide has been reported to be 0.1 μM in other preparations (Payne et al., 2003).

4.3.3.5 Effects of the KCC antagonist VU0240551

I found that blocking the KCCs with 20 μM VU decreased E_{GABA} and slowed the rate of recovery following Cl^- depletion. These results indicate that KCC2 is critically involved in setting resting $[Cl^-]_i$ in SCN neurons. Interestingly, although VU dramatically slowed the rate of recovery, it did not remove Cl^- extrusion completely, suggesting that other Cl^- extrusion mechanisms are present in SCN neurons. This Cl^- extrusion could be mediated by the sodium-dependent anion exchanger (NDAE) or ClC-2 (Rinke et al., 2010; Ratte and Prescott, 2011), although there is only minor evidence for the expression of these proteins in SCN neurons (see Allen Brain Atlas).

4.3.3.6 Future directions

Gramicidin perforated patch allows estimation of E_{GABA} without disrupting intracellular chloride. Tyzio et al. developed an alternative electrophysiological method for the determination of E_{GABA} (Tyzio et al., 2006; Tyzio et al., 2008). Using dual cell-attached recording of single-channel $GABA_A$ and NMDA receptor-mediated currents, Tyzio et al. were able to measure E_{GABA} noninvasively. One pipette allows calculation

of the driving force for $GABA_A$, while the second pipette is used to estimate V_m. This method offers a novel approach for the calculation of E_{GABA} in SCN neurons.

4.4 Cl^- imaging

4.4.1 Methodological considerations: advantages

Cl^- imaging offers the unique ability to monitor $[Cl^-]_i$ without disturbing the cell's membrane potential. Cl^- imaging allows direct calculation of $[Cl^-]_i$, while perforated-patch recording usually estimates $[Cl^-]_i$ from E_{GABA} or $E_{glycine}$. However, it is no small consideration that determining $[Cl^-]_i$ using Cl^- imaging relies on a calibration curve. Certainly, the calibration curve can be a major source of error in calculations of $[Cl^-]_i$.

After persevering through perforated-patch recording, the most striking advantage of Cl^- imaging was the ability to monitor multiple cells simultaneously. Cl^- imaging dramatically increased my experimental yield. Because the SCN is small, it is usually only possible to obtain one or two slices per mouse. Therefore, increased sampling was particularly beneficial when testing the effects of hydrophobic drugs, which would not be expected to washout from a brain slice.

When I arrived in the lab, Cl^- imaging experiments were planned for cultured SCN neurons. Cultures were to be transfected with Cl^- Sensor and imaged at different circadian phases with respect to PER2:LUC bioluminescence. Although feasible, this experimental design invites uncertainty about the phase and amplitude of the rhythmicity in the culture. Expressing Cl^- Sensor in live animals eliminated this uncertainty—the mice could be taken directly out of their LD cycle. Initial forays into Cl^- imaging involved stereotaxic injection of viral vectors into the SCN. Although an

improvement, this approach required a delay to allow the mouse to recover from surgery and to generate adequate Cl^- Sensor expression. Still, fluorescent signal was frequently absent from SCN slices. The advent of the ROSA26::Cl^- Sensor mouse guaranteed Cl^- Sensor expression. Further, genetic techniques present the opportunity to study Cl^- regulation in genetically-defined populations of neurons. As we predicted higher $[Cl^-]_i$ in AVP+ neurons, the use of the AVP-Cre, ROSA26 Cl^- Sensor mouse was the ideal model for our hypotheses.

Finally, Cl^- Sensor expression allowed me to monitor $[Cl^-]_i$ in cultured SCN neurons over several days. This feat would not be possible without genetically-encoded fluorescent reporters, and would not be possible with gramicidin perforated-patch recording.

4.4.2 Methodological considerations: disadvantages

Compared to perforated-patch recording, perhaps the greatest limitation of Cl^- imaging is its reduced temporal resolution. Perforated-patch recording is able to detect events with millisecond resolution—a timescale much more relevant to neurophysiology. For Cl^- imaging experiments, I sampled every two or five seconds. Due to the temporal requirements for excitation, emission, and mechanical delays, a one second increment approached the lower-limit of sampling. Therefore, it is possible that fast Cl^- fluxes were missed by my Cl^- imaging techniques.

I found Cl^- Sensor to also be limited in sensitivity. I measured a K_d of 82 mM, significantly higher than the range of $[Cl^-]_i$ that I observed in SCN neurons. Therefore, most of my values of R_{Cl} fell on the lower shoulder of the calibration curve, where small

changes in R_{Cl} give large changes in $[Cl^-]_i$, which may misrepresent the data. For this reason, I opted to present the results from these experiments in terms of R_{Cl}.

Whether $GABA_A$ receptor activation is hyperpolarizing or depolarizing depends on the driving force for chloride, which depends on the relationship between E_{GABA} and V_m. Just as membrane potential is unperturbed in Cl^- imaging, it is also not measured. Instead, I used the direction of $[Cl^-]_i$ change in response to $GABA_A$ agonists to infer whether GABA transmission was hyperpolarizing or depolarizing in SCN neurons. Therefore, the polarity of these $GABA_A$ receptor-mediated Cl^- transients can be used to infer the driving force for chloride. Although this information is useful to relate E_{GABA} to V_m, it of course does not provide an absolute measure of V_m.

Cl^- Sensor is composed of a cyan fluorescent protein fused to a chloride-sensitive yellow fluorescent protein, YFP_{Cl}. Due to the intrinsic sensitivity of YFP_{Cl} to H^+, Cl^- Sensor is sensitive to pH in addition to $[Cl^-]$. At a Cl^- concentration of 10 mM, Cl^- Sensor has a p*K*α of 7.3, signifying a high degree of sensitivity within a physiologically relevant pH range (Markova et al., 2008). The pH sensitivity of Cl^- Sensor was problematic throughout my experiments. Certainly, using a reporter with dual sensitivity can make interpretation difficult. I occasionally observed changes in R_{Cl} after brief bath applications of control ACSF. I attribute this artifact to be caused by degassing of stagnant solution in the perfusion system. In bicarbonate-buffered solutions, pH is maintained by an equilibrium between HCO_3^- and CO_2. In the perfusion system, CO_2 is absent, resulting in an increase of pH. To avoid alkalization of ungassed solution, I switched to a HEPES-buffered solution in a series of experiments. Although HEPES solution helped to reduce pH artifacts, it is less physiologically

relevant, as bicarbonate is the endogenous buffer in acid-base homeostasis, and is cotransported with Cl^- by a family of bicarbonate/chloride exchangers (Chesler, 2003; Alka and Casey, 2014). Furthermore, the permeability of the $GABA_A$ receptor to HCO_3^- complicates the interpretation of results in HEPES-buffered solutions.

My experiments demonstrate remarkably different rates of inactivation for Cl^- Sensor's YFP and CFP moieties. This property gives R_{Cl} a high degree of instability, and leaves Cl^- Sensor imperfectly ratiometric. I corrected for the instability of R_{Cl} by fitting the data with exponential functions. Usually, exponential functions fit the data very accurately. Corrected data was stable with respect to time. In order to correct for imperfections in R_{Cl}, I attempted whenever possible to measure R_{Cl} at steady-state values.

4.4.3 Estimation of $[Cl^-]_i$ in SCN neurons

Using Cl^- imaging, I obtained estimates of $[Cl^-]_i$ to be approximately 20 mM in SCN neurons. I observed no differences between AVP+ and VIP+ neurons, or between day and night neurons, despite the observed rhythmicity in R_{Cl} in AVP+ neurons. This discrepancy may be attributed to the small amplitude of the rhythm, or the high degree of variability in R_{Cl} across acute slice experiments. I observed baseline R_{Cl} values between 0.8 and 1.15, which correspond to values for $[Cl^-]_i$ between 0 and 60 mM. A significant limitation of Cl^- imaging is the dependence on a calibration curve for ratiometric estimates of $[Cl^-]_i$. Most of my measured values for R_{Cl} fall on the lower shoulder of the calibration curve, which give big changes in $[Cl^-]_i$ for small changes in R_{Cl}. Using gramicidin perforated patch recording, I observed values for $[Cl^-]_i$ between 8

and 27 mM, with a median value near 18 mM. Therefore, average estimates of $[Cl^-]_i$ were fairly close despite large variability with both techniques. Furthermore, these estimates are similar to those previously reported in the SCN (Chen et al., 1996; Wagner et al., 1997; De Jeu and Pennartz, 2002; Shimura et al., 2002; Choi et al., 2008; Alamilla et al., 2014; Farajnia et al., 2014)

4.4.4 Cl^- influx upon $GABA_A$ receptor activation

Upon puff application of the $GABA_A$ agonist isoguvacine, I observed an increase in R_{Cl}, indicating an increase in $[Cl^-]_i$ upon $GABA_A$ receptor activation. These Cl^- transients are known to be downstream of $GABA_A$ receptor activation, as they required isoguvacine, and were absent in picrotoxin. This Cl^- influx would be expected to hyperpolarize V_m. This finding is at odds with the GABAergic reversal potentials measured using gramicidin perforated-patch recording, which would predict Cl^- efflux through $GABA_A$ receptors. It is possible that these Cl^- transients represent neuronal acidification. Acidification has been shown to occur after neuronal depolarization, or would be expected following HCO_3^- efflux through the $GABA_A$ receptor (Chesler, 2003). However, I observed a much larger effect of VU relative to bumetanide, suggesting that the KCCs keep $[Cl^-]_i$ low in SCN neurons, in agreement with an inhibitory action of GABA. Also, increasing $[Cl^-]_i$ with VU was able to reverse the direction of Cl^- transients in several experiments (data not shown). Nevertheless, further experimentation will be necessary to eliminate the possibility that these transients represent intracellular acidification.

I observed Cl^- efflux in HEPES-buffered solution, but Cl^- influx in bicarbonate-buffered solutions. This result suggests that E_{GABA} was depolarizing in HEPES-buffered solutions, and that $[Cl^-]_i$ may be differentially regulated in HEPES solutions. However, changes in R_{Cl} after blocking KCC2 and NKCC1 were similar to those observed in bicarbonate-buffered solutions. Generally, blocking NKCC1 had a minor effect on R_{Cl} while blocking KCC2 caused a major increase in R_{Cl}. The sodium-dependent anion-exchanger (NDAE) offers one possible explanation for the observed Cl^- efflux in HEPES-buffered solutions. NDAE transports Na^+ and HCO_3^- into neurons in exchange for H^+ and Cl^-. Therefore, removing extracellular HCO_3^- will result in Cl^- accumulation, which would be expected to depolarize the GABAergic reversal potential.

4.4.5 Effects of the NKCC1 antagonist bumetanide

In both perforated-patch and Cl^- imaging experiments, only minor effects of bumetanide were observed, suggesting that NKCC1 is not a major regulator of $[Cl^-]_i$ in SCN neurons. It is possible that $[Cl^-]_i$ is higher in other populations of SCN neurons. Alternatively, a somatodendritic Cl^- gradient could explain why previous groups have reported greater bumetanide effects (see Discussion, Chapter 3). Although NKCC1 may not be a major contributor to $[Cl^-]_i$ in SCN neurons, my estimates of $[Cl^-]_i$ across techniques suggest the presence of active Cl^- uptake mechanisms in SCN neurons. Further research will be necessary to identify these Cl^- transport pathways.

4.4.6 Effects of the KCC antagonist VU0240551

I observed significant increases in $[Cl^-]_i$ after applying the KCC antagonist VU0240551. VU is a newly-developed drug; until recently, it has been difficult to reveal KCC activity. Our results are the first to demonstrate KCC regulation of $[Cl^-]_i$ in SCN neurons. VU resulted in ~20 mM increases in $[Cl^-]_i$. These results were similar with those measured in HEPES-buffered solutions, and are in agreement with the increase in the GABAergic reversal potential observed with perforated patch recording. With Cl^- imaging, I observed different changes in $[Cl^-]_i$ between AVP+ and VIP+ neurons, with VIP+ neurons having a larger change in R_{Cl} after VU. This finding is in agreement with Belenky et al. who demonstrated dense expression of KCC2 in the ventrolateral SCN, but weak expression in the dorsomedial SCN. KCC2 reaches thermodynamic equilibrium when $[Cl^-]_i$ equals 3 mM. My results indicate that, although KCC2 contributes to $[Cl^-]_i$, other pathways are involved in setting resting intracellular chloride.

A previous study demonstrated differential expression of the KCCs throughout the SCN. KCC2 expression was dense in the ventrolateral SCN but deficient in the dorsomedial SCN, while KCC3 and KCC4 were prominent in dorsomedial SCN (Belenky et al., 2008). However, preliminary in situ hybridization results from our lab showed KCC2 expression throughout the SCN. Further, although billed as a KCC2-selective drug, VU is likely to inhibit KCC1, KCC3 and KCC4 with similar efficacy (Delpire et al., 2009). Therefore the SCN-wide effectiveness of VU observed in my study can be explained by either the non-specificity of VU for the KCCs, or KCC2 expression throughout the SCN.

4.4.7 Future directions

4.4.7.1 Calibration of Cl^- Sensor

Ratiometric imaging relies on calibration curves in order to relate ratio values to the substrate of interest. In order to better interpret my Cl^- imaging results, I plan to produce a more dependable calibration curve for Cl^- Sensor under my imaging conditions. My preliminary calibration curve gave a K_d of 81.6 mM. Previously reported K_d values for Cl^- Sensor are significantly lower, between 40 and 60 mM. Because K_d should represent an intrinsic biochemical property of the protein, my measured K_d suggests that some parameter is obscuring Cl^- Sensor's sensitivity. Other reports have used high K^+ HEPES-buffered solutions during calibration, but I was not able to obtain an interpretable range of values with these solutions (baseline was lower than that obtained in zero chloride). Therefore, the observed differences in K_d may reflect a difference imposed by the non-chloride species within the different calibration solutions.

I plan to add more points to the calibration curve. Additional data may improve the accuracy of $[Cl^-]_i$ calibration. Alternatively, manipulating $[Cl^-]_i$ with whole-cell pipette solution may give a more accurate calibration curve, allowing measurement of single-cell R_{Cl}, with minimal influence from a changing background signal.

4.4.7.2 Cl^- imaging in other subpopulations of SCN neurons

The direction of Cl^- flux after $GABA_A$ receptor activation indicates that GABA is inhibitory in both AVP+ and VIP+ SCN neurons. AVP+ and VIP+ neurons only constitute approximately 13% and 9% of SCN neurons, respectively (Welsh et al., 2010; Lee et al., 2015). Therefore, it is possible that depolarizing GABA transmission is

present in other populations of SCN neurons that were not addressed in this study. Therefore, I would like to cross the Rosa26::Cl Sensor mouse with other Cre driver lines to perform Cl^- imaging in other populations of SCN neurons. *Drd1a*-Cre mice would be expected to yield Cl^- Sensor expression in up to 90% of SCN neurons, in multiple subtypes of SCN neurons (Jones et al., 2015). Besides AVP and VIP, several other Cre lines for SCN-expressed neuropeptides are available including neuromedin S, GRP, somatostatin, neurotensin, enkephalin, and cholecystokinin (Ohtsuki et al., 1993; Leinninger et al., 2011; Taniguchi et al., 2011; Muller et al., 2012; Gerfen et al., 2013; Lee et al., 2015). These genetic tools open up exciting new avenues for dissection of the heterogeneous SCN.

4.4.7.3 Potential improvements for Cl^- imaging methodology

As discussed, both the poor photostability and intrinsic pH sensitivity of Cl^- Sensor's YFP_{Cl} moiety presented me with formidable experimental challenges. Recently, a YFP with improved photostability, increased Cl^- sensitivity, and reduced pH interference has been described (Zhong et al., 2014). The YFP derivative has a K_d of 14 mM and a pK_a of 5.9, significantly shifted outside of the physiological range. Photostability is approximately 15-fold greater than Cl^- Sensor. Further, this group and others have added membrane targeting domains to genetically-encoded reporters which have facilitated sensitivity and stability (Watts et al., 2012; Zhong et al., 2014). I hope to see these improvements added to ratiometric Cl^- indicators. They would be of great assistance to physiological measures of $[Cl^-]_i$ and Cl^- fluxes.

Instead of leaving pH an unknown variable, Arosio et al. designed a reporter named ClopHensor that is able to monitor both Cl^- and pH simultaneously (Arosio et al., 2010). This group made use of E^2GFP which is sensitive to both chloride concentration and pH, but possesses a pH isobestic point at 458 nm. By exciting at three wavelengths (488 nm for the pH-dependent E^2GFP signal, 458 nm for the pH-independent E^2GFP signal, and 543 nm for the Cl^- and pH-independent DsRed signal), Arosio et al. were able to obtain ratiometric measures of both $[Cl^-]_i$ and pH simultaneously. A follow-up study optimized ClopHensor for neurons, replacing DsRed with TdTomato, producing ClopHensorN (Raimondo et al., 2013). The use of ClopHensorN would allow simultaneous measurement of both $[Cl^-]_i$ and pH in SCN neurons, and therefore remove the ambiguity when interpreting Cl^- Sensor fluorescent signal.

4.4.7.4 Two-photon imaging

Isoguvacine application increased R_{Cl} indicating Cl^- influx. Regions of interest were defined around neuronal soma; neurites were not able to be resolved. Therefore, it is possible that somatodendritic or somato-axonal Cl^- gradients exist within SCN neurons that were missed with my techniques. Indeed, subcellular gradients have been described in several other neuron types (Wright et al., 2011). Compared to epifluorescence microscopy, both confocal and two-photon excitation microscopy provide improved spatial resolution. I would like to use two-photon excitation microscopy to measure $[Cl^-]_i$ in dendritic processes of SCN neurons to look for

subcellular Cl^- gradients. Alternatively, preparing dispersed cultures of SCN neurons may facilitate imaging of dendritic profiles.

4.5 General Conclusions

I have used new genetic techniques to address the physiological and functional roles of GABA in the SCN. I have described a role for GABA in coordinating the synchrony of SCN neurons, and thereby regulating the output of the mammalian circadian clock. Further, newly-developed Cl^- imaging techniques have allowed me to address the physiological mechanisms regulating GABA's action in SCN neurons. Membrane potential and calcium influx have been linked to the phase and period of circadian rhythms within SCN neurons. Therefore, these two studies of SCN GABA may be related—GABA's effects on membrane potential may coordinate the synchrony of SCN neurons.

REFERENCES

Abe M, Herzog ED, Yamazaki S, Straume M, Tei H, Sakaki Y, Menaker M, Block GD (2002) Circadian rhythms in isolated brain regions. J Neurosci 22:350-356.

Abraham U, Granada AE, Westermark PO, Heine M, Kramer A, Herzel H (2010) Coupling governs entrainment range of circadian clocks. Mol Syst Biol 6:438.

Abrahamson EE, Moore RY (2001) Suprachiasmatic nucleus in the mouse: retinal innervation, intrinsic organization and efferent projections. Brain Res 916:172-191.

Abrahamson EE, Leak RK, Moore RY (2001) The suprachiasmatic nucleus projects to posterior hypothalamic arousal systems. Neuroreport 12:435-440.

Achilles K, Okabe A, Ikeda M, Shimizu-Okabe C, Yamada J, Fukuda A, Luhmann HJ, Kilb W (2007) Kinetic properties of Cl uptake mediated by Na+-dependent K+-2Cl cotransport in immature rat neocortical neurons. J Neurosci 27:8616-8627.

Aguilar-Roblero R, Verduzco-Carbajal L, Rodríguez C, Mendez-Franco J, Morán J, Perez de la Mora M (1993) Circadian rhythmicity in the GABAergic system in the suprachiasmatic nuclei of the rat. Neuroscience letters 157:199-202.

Alamilla J, Perez-Burgos A, Quinto D, Aguilar-Roblero R (2014) Circadian modulation of the cl(-) equilibrium potential in the rat suprachiasmatic nuclei. BioMed research international 2014:424982.

Albus H, Vansteensel MJ, Michel S, Block GD, Meijer JH (2005) A GABAergic mechanism is necessary for coupling dissociable ventral and dorsal regional oscillators within the circadian clock. Curr Biol 15:886-893.

Alger BE, Nicoll RA (1979) GABA-mediated biphasic inhibitory responses in hippocampus. Nature 281:315-317.

Alka K, Casey JR (2014) Bicarbonate transport in health and disease. IUBMB Life 66:596-615.

Andersen P, Dingledine R, Gjerstad L, Langmoen IA, Mosfeldt Laursen A (1980) Two different responses of hippocampal pyramidal cells to application of gamma-amino butyric acid. The Journal of physiology (london) 305:279-296.

Arosio D, Ricci F, Marchetti L, Gualdani R, Albertazzi L, Beltram F (2010) Simultaneous intracellular chloride and pH measurements using a GFP-based sensor. Nature methods 7:516-518.

Aton SJ, Herzog ED (2005) Come together, right...now: synchronization of rhythms in a mammalian circadian clock. Neuron 48:531-534.

Aton SJ, Huettner JE, Straume M, Herzog ED (2006) GABA and Gi/o differentially control circadian rhythms and synchrony in clock neurons. Proceedings of the National Academy of Sciences of the United States of America 103:19188-19193.

Aton SJ, Colwell CS, Harmar AJ, Waschek J, Herzog ED (2005) Vasoactive intestinal polypeptide mediates circadian rhythmicity and synchrony in mammalian clock neurons. Nature neuroscience 8:476-483.

Bae K, Jin X, Maywood ES, Hastings MH, Reppert SM, Weaver DR (2001) Differential Functions of mPer1, mPer2, and mPer3 in the SCN Circadian Clock. Neuron 30:525-536.
Balakrishnan V, Becker M, Lohrke S, Nothwang HG, Guresir E, Friauf E (2003) Expression and function of chloride transporters during development of inhibitory neurotransmission in the auditory brainstem. J Neurosci 23:4134-4145.
Barberis A, Petrini EM, Cherubini E (2004) Presynaptic source of quantal size variability at GABAergic synapses in rat hippocampal neurons in culture. The European journal of neuroscience 20:1803-1810.
Barberis A, Petrini EM, Mozrzymas JW (2011) Impact of synaptic neurotransmitter concentration time course on the kinetics and pharmacological modulation of inhibitory synaptic currents. Frontiers in cellular neuroscience 5:6.
Batschelet E (1981) Circular statistics in biology. London: Academic Press.
Batti L, Mukhtarov M, Audero E, Ivanov A, Paolicelli O, Zurborg S, Gross C, Bregestovski P, Heppenstall PA (2013) Transgenic mouse lines for non-invasive ratiometric monitoring of intracellular chloride. Front Mol Neurosci 6:11.
Belenky M, Wagner S, Yarom Y, Matzner H, Cohen S, Castel M (1996) The suprachiasmatic nucleus in stationary organotypic culture. Neuroscience 70:127-143.
Belenky MA, Yarom Y, Pickard GE (2008) Heterogeneous expression of gamma-aminobutyric acid and gamma-aminobutyric acid-associated receptors and transporters in the rat suprachiasmatic nucleus. The Journal of comparative neurology 506:708-732.
Belenky MA, Sagiv N, Fritschy J, Yarom Y (2003) Presynaptic and postsynaptic GABA(A) receptors in rat suprachiasmatic nucleus. Neuroscience 118:909-923.
Belenky MA, Sollars PJ, Mount DB, Alper SL, Yarom Y, Pickard GE (2010) Cell-type specific distribution of chloride transporters in the rat suprachiasmatic nucleus. Neuroscience 165:1519-1537.
Ben-Ari Y, Woodin MA, Sernagor E, Cancedda L, Vinay L, Rivera C, Legendre P, Luhmann HJ, Bordey A, Wenner P, Fukuda A, van den Pol AN, Gaiarsa JL, Cherubini E (2012) Refuting the challenges of the developmental shift of polarity of GABA actions: GABA more exciting than ever! Frontiers in cellular neuroscience 6:35.
Blaesse P, Airaksinen MS, Rivera C, Kaila K (2009) Cation-chloride cotransporters and neuronal function. Neuron 61:820-838.
Bos NPA, Mirmiran M (1993) Effects of excitatory and inhibitory amino acids on neuronal discharges in the cultured suprachiasmatic nucleus. Brain research bulletin 31:67-72.
Brancaccio M, Maywood ES, Chesham JE, Loudon AS, Hastings MH (2013) A Gq-Ca2+ axis controls circuit-level encoding of circadian time in the suprachiasmatic nucleus. Neuron 78:714-728.
Brown TM, Colwell CS, Waschek JA, Piggins HD (2007) Disrupted neuronal activity rhythms in the suprachiasmatic nuclei of vasoactive intestinal polypeptide-deficient mice. Journal of neurophysiology 97:2553-2558.
Buhr ED, Takahashi JS (2013) Molecular components of the Mammalian circadian clock. Handb Exp Pharmacol 217:3-27.

Buhr ED, Yoo SH, Takahashi JS (2010) Temperature as a universal resetting cue for mammalian circadian oscillators. Science 330:379-385.
Cagampang FRA, Rattray M, Powell JF, Campbell IC, Coen CW (1996) Circadian changes of glutamate decarboxylase 65 and 67 mRNA in the rat suprachiasmatic nuclei. Neuroreport 7:1925-1928.
Card JP, Moore RY (1982) Ventral lateral geniculate nucleus efferents to the rat suprachiasmatic nucleus exhibit avian pancreatic polypeptide-like immunoreactivity. The Journal of comparative neurology 206:390-396.
Card JP, Moore RY (1984) The suprachiasmatic nucleus of the golden hamster: immunohistochemical analysis of cell and fiber distribution. Neuroscience 13:415-431.
Card JP, Moore RY (1989) Organization of lateral geniculate-hypothalamic connections in the rat. The Journal of comparative neurology 284:135-147.
Castel M, Morris JF (2000) Morphological heterogeneity of the GABAergic network in the suprachiasmatic nucleus, the brain's circadian pacemaker. J Anat 196:1-13.
Chen G, Trombley P, Van den Pol AN (1996) Excitatory actions of GABA in developing rat hypothalamic neurones. The Journal of physiology (london) 494:451-464.
Cheng HY, Alvarez-Saavedra M, Dziema H, Choi YS, Li A, Obrietan K (2009) Segregation of expression of mPeriod gene homologs in neurons and glia: Possible divergent roles of mPeriod1 and mPeriod2 in the brain. Human molecular genetics 18:3110-3124.
Chesler M (2003) Regulation and modulation of pH in the brain. Physiological reviews 83:1183-1221.
Chiang PH, Wu PY, Kuo TW, Liu YC, Chan CF, Chien TC, Cheng JK, Huang YY, Chiu CD, Lien CC (2012) GABA Is Depolarizing in Hippocampal Dentate Granule Cells of the Adolescent and Adult Rats. J Neurosci 32:62-67.
Choi HJ, Lee CJ, Schroeder A, Kim YS, Jung SH, Kim JS, Kim do Y, Son EJ, Han HC, Hong SK, Colwell CS, Kim YI (2008) Excitatory Actions of GABA in the Suprachiasmatic Nucleus. J Neurosci 28:5450-5459.
Clayton GH, Owens GC, Wolff JS, Smith RL (1998) Ontogeny of cation-Cl- cotransporter expression in rat neocortex. Brain Res Dev Brain Res 109:281-292.
Colwell CS (2011) Linking neural activity and molecular oscillations in the SCN. Nature reviews 12:553-569.
Colwell CS, Michel S, Itri J, Rodriguez W, Tam J, Lelievre V, Hu Z, Liu X, Waschek JA (2003) Disrupted circadian rhythms in VIP- and PHI-deficient mice. Am J Physiol Regul Integr Comp Physiol 285:R939-949.
De Jeu M, Pennartz CMA (2002) Circadian modulation of GABA function in the rat suprachiasmatic nucleus: excitatory effects during the night phase. Journal of neurophysiology 87:834-844.
Delpire E, Staley KJ (2014) Novel determinants of the neuronal Cl- concentration. The Journal of physiology.
Delpire E, Days E, Lewis LM, Mi D, Kim K, Lindsley CW, Weaver CD (2009) Small-molecule screen identifies inhibitors of the neuronal K-Cl cotransporter KCC2. Proceedings of the National Academy of Sciences of the United States of America 106:5383-5388.

Duebel J, Haverkamp S, Schleich W, Feng G, Augustine GJ, Kuner T, Euler T (2006) Two-photon imaging reveals somatodendritic chloride gradient in retinal ON-type bipolar cells expressing the biosensor Clomeleon. Neuron 49:81-94.
Dzhala V, Valeeva G, Glykys J, Khazipov R, Staley K (2012) Traumatic alterations in GABA signaling disrupt hippocampal network activity in the developing brain. J Neurosci 32:4017-4031.
Dzhala VI, Kuchibhotla KV, Glykys JC, Kahle KT, Swiercz WB, Feng G, Kuner T, Augustine GJ, Bacskai BJ, Staley KJ (2010) Progressive NKCC1-Dependent Neuronal Chloride Accumulation during Neonatal Seizures. J Neurosci 30:11745-11761.
Ebihara S, Shirato K, Harata N, Akaike N (1995) Gramicidin-perforated patch recording: GABA response in mammalian neurones with intact intracellular chloride. The Journal of physiology (london) 484:77-86.
Ehlen JC, Paul KN (2009) Regulation of light's action in the mammalian circadian clock: role of the extrasynaptic GABAA receptor. Am J Physiol Regul Integr Comp Physiol 296:R1606-1612.
Ehlen JC, Novak CM, Karom MC, Gamble KL, Albers HE (2008) Interactions of GABA A receptor activation and light on period mRNA expression in the suprachiasmatic nucleus. Journal of biological rhythms 23:16-25.
Evans JA, Leise TL, Castanon-Cervantes O, Davidson AJ (2013) Dynamic interactions mediated by nonredundant signaling mechanisms couple circadian clock neurons. Neuron 80:973-983.
Fan J, Zeng H, Olson DP, Huber KM, Gibson JR, Takahashi JS (2015) Vasoactive intestinal polypeptide (VIP)-expressing neurons in the suprachiasmatic nucleus provide sparse GABAergic outputs to local neurons with circadian regulation occurring distal to the opening of postsynaptic GABAA ionotropic receptors. J Neurosci 35:1905-1920.
Farajnia S, van Westering TL, Meijer JH, Michel S (2014) Seasonal induction of GABAergic excitation in the central mammalian clock. Proceedings of the National Academy of Sciences of the United States of America 111:9627-9632.
Fiumelli H, Cancedda L, Poo MM (2005) Modulation of GABAergic transmission by activity via postsynaptic Ca2+-dependent regulation of KCC2 function. Neuron 48:773-786.
Freeman GM, Jr., Krock RM, Aton SJ, Thaben P, Herzog ED (2013) GABA Networks Destabilize Genetic Oscillations in the Circadian Pacemaker. Neuron 78:799-806.
Friedel P, Bregestovski P, Medina I (2013) Improved method for efficient imaging of intracellular Cl(-) with Cl-Sensor using conventional fluorescence setup. Front Mol Neurosci 6:7.
Gamba G (2005) Molecular physiology and pathophysiology of electroneutral cation-chloride cotransporters. Physiological reviews 85:423-493.
Gao B, Fritschy JM, Moore RY (1995) GABAA-receptor subunit composition in the circadian timing system. Brain Res 700:142-156.
Gerfen CR, Paletzki R, Heintz N (2013) GENSAT BAC cre-recombinase driver lines to study the functional organization of cerebral cortical and basal ganglia circuits. Neuron 80:1368-1383.

Gillespie CF, Huhman KL, Babagbemi TO, Albers HE (1996) Bicuculline increases and muscimol reduces the phase-delaying effects of light and VIP/PHI/GRP in the suprachiasmatic region. Journal of biological rhythms 11:137-144.
Gillespie CF, Mintz EM, Marvel CL, Huhman KL, Albers HE (1997) GABAA and GABAB agonists and antagonists alter the phase-shifting effects of light when microinjected into the suprachiasmatic region. Brain Res 759:181-189.
Glykys J, Dzhala VI, Kuchibhotla KV, Feng G, Kuner T, Augustine G, Bacskai BJ, Staley KJ (2009) Differences in cortical versus subcortical GABAergic signaling: a candidate mechanism of electroclinical uncoupling of neonatal seizures. Neuron 63:657-672.
Glykys J, Dzhala V, Egawa K, Balena T, Saponjian Y, Kuchibhotla KV, Bacskai BJ, Kahle KT, Zeuthen T, Staley KJ (2014) Local impermeant anions establish the neuronal chloride concentration. Science 343:670-675.
Gompf HS, Allen CN (2004) GABAergic synapses of the suprachiasmatic nucleus exhibit a diurnal rhythm of short-term synaptic plasticity. European Journal of Neuroscience 19:2791-2798.
Gompf HS, Irwin RP, Allen CN (2006) Retrograde suppression of GABAergic currents in a subset of SCN neurons. The European journal of neuroscience 23:3209-3216.
Gonzalez-Islas C, Chub N, Wenner P (2009) NKCC1 and AE3 appear to accumulate chloride in embryonic motoneurons. Journal of neurophysiology 101:507-518.
Gribkoff VK, Pieschl RL, Wisialowski TA, Park WK, Strecker GJ, de Jeu MT, Pennartz CMA, Dudek FE (1999) A reexamination of the role of GABA in the mammalian suprachiasmatic nucleus. Journal of biological rhythms 14:126-130.
Haam J, Popescu IR, Morton LA, Halmos KC, Teruyama R, Ueta Y, Tasker JG (2012) GABA Is Excitatory in Adult Vasopressinergic Neuroendocrine Cells. J Neurosci 32:572-582.
Harris JA, Hirokawa KE, Sorensen SA, Gu H, Mills M, Ng LL, Bohn P, Mortrud M, Ouellette B, Kidney J, Smith KA, Dang C, Sunkin S, Bernard A, Oh SW, Madisen L, Zeng H (2014) Anatomical characterization of Cre driver mice for neural circuit mapping and manipulation. Frontiers in neural circuits 8:76.
Hastings MH, Reddy AB, Maywood ES (2003) A clockwork web: circadian timing in brain and periphery, in health and disease. Nature reviews 4:649-661.
Herzog ED, Kiss IZ, Mazuski C (2015) Measuring synchrony in the mammalian central circadian circuit. Methods in enzymology 552:3-22.
Herzog ED, Aton SJ, Numano R, Sakaki Y, Tei H (2004) Temporal precision in the mammalian circadian system: a reliable clock from less reliable neurons. Journal of biological rhythms 19:35-46.
Honma S, Shirakawa T, Nakamura W, Honma K (2000) Synaptic communication of cellular oscillations in the rat suprachiasmatic neurons. Neuroscience letters 294:113-116.
Hsu CC, Thomas C, Chen W, Davis KM, Foos T, Chen JL, Wu E, Floor E, Schloss JV, Wu JY (1999) Role of synaptic vesicle proton gradient and protein phosphorylation on ATP-mediated activation of membrane-associated brain glutamate decarboxylase. The Journal of biological chemistry 274:24366-24371.
Hubner CA, Lorke DE, Hermans-Borgmeyer I (2001) Expression of the Na-K-2Cl-cotransporter NKCC1 during mouse development. Mech Dev 102:267-269.

Hughes AT, Guilding C, Lennox L, Samuels RE, McMahon DG, Piggins HD (2008) Live imaging of altered period1 expression in the suprachiasmatic nuclei of Vipr2-/- mice. Journal of neurochemistry 106:1646-1657.
Hughes ME, Hogenesch JB, Kornacker K (2010) JTK_CYCLE: an efficient nonparametric algorithm for detecting rhythmic components in genome-scale data sets. Journal of biological rhythms 25:372-380.
Huhman KL, Hennessey AC, Albers HE (1996) Rhythms of glutamic acid decarboxylase mRNA in the suprachiasmatic nucleus. Journal of biological rhythms 11:311-316.
Huhman KL, Jasnow AM, Sisitsky AK, Albers HE (1999) Glutamic acid decarboxylase mRNA in the suprachiasmatic nucleus of rats housed in constant darkness. Brain research 851:266-269.
Irwin RP, Allen CN (2009) GABAergic signaling induces divergent neuronal Ca(2+) responses in the suprachiasmatic nucleus network. The European journal of neuroscience 30:1462-1475.
Itri J, Colwell CS (2003) Regulation of Inhibitory Synaptic Transmission by Vasoactive Intestinal Peptide (VIP) in the Mouse Suprachiasmatic Nucleus. Journal of neurophysiology 90:1589-1597.
Itri J, Michel S, Waschek JA, Colwell CS (2004) Circadian rhythm in inhibitory synaptic transmission in the mouse suprachiasmatic nucleus. Journal of neurophysiology 92:311-319.
Jammalamadaka SRaS, A. (2001) Topics in Circular Statistics, Section 2.2.4. Singapore: World Scientific Press.
Jiang Z-G, Allen CN, North RA (1995) Presynaptic inhibition by baclofen of retinohypothalamic excitatory synaptic transmission in rat suprachiasmatic nucleus. Neuroscience 64:813-819.
Jiang Z-G, Yang Y-Q, Liu Z-P, Allen CN (1997) Membrane properties and synaptic inputs of suprachiasmatic nucleus neurons in rat brain slices. The Journal of physiology (london) 499:141-159.
Jin H, Wu H, Osterhaus G, Wei J, Davis K, Sha D, Floor E, Hsu CC, Kopke RD, Wu JY (2003) Demonstration of functional coupling between gamma -aminobutyric acid (GABA) synthesis and vesicular GABA transport into synaptic vesicles. Proceedings of the National Academy of Sciences of the United States of America 100:4293-4298.
Jobst EE, Robinson DW, Allen CN (2004) Potential pathways for intercellular communication within the calbindin subnucleus of the hamster suprachiasmatic nucleus. Neuroscience 123:87-99.
Jonas P, Bischofberger J, Sandkuhler J (1998) Corelease of two fast neurotransmitters at a central synapse. Science 281:419-424.
Jones JR, Tackenberg MC, McMahon DG (2015) Manipulating circadian clock neuron firing rate resets molecular circadian rhythms and behavior. Nature neuroscience 18:373-375.
Kahle KT, Rinehart J, Lifton RP (2010) Phosphoregulation of the Na-K-2Cl and K-Cl cotransporters by the WNK kinases. Biochimica et biophysica acta.
Kahle KT, Staley KJ, Nahed BV, Gamba G, Hebert SC, Lifton RP, Mount DB (2008) Roles of the cation-chloride cotransporters in neurological disease. Nat Clin Pract Neurol 4:490-503.

Kahle KT, Deeb TZ, Puskarjov M, Silayeva L, Liang B, Kaila K, Moss SJ (2013) Modulation of neuronal activity by phosphorylation of the K-Cl cotransporter KCC2. Trends in neurosciences 36:726-737.
Kaila K (1994) Ionic basis of GABAA receptor channel function in the nervous system. Progress in neurobiology 42:489-537.
Kalsbeek A, Teclemariam-Mesbah R, Pévet P (1993) Efferent projections of the suprachiasmatic nucleus in the golden hamster (Mesocricetus auratus). The Journal of comparative neurology 332:293-314.
Kanaka C, Ohno K, Okabe A, Kuriyama K, Itoh T, Fukuda A, Sato K (2001) The differential expression patterns of messenger RNAs encoding K-Cl cotransporters (KCC1,2) and Na-K-2Cl cotransporter (NKCC1) in the rat nervous system. Neuroscience 104:933-946.
Khawaled R, Bruening-Wright A, Adelman JP, Maylie J (1999) Bicuculline block of small-conductance calcium-activated potassium channels. Pflugers Archiv European Journal of Physiology 438:314-321.
Kim YI, Dudek FE (1992) Intracellular electrophysiological study of suprachiasmatic nucleus neurons in rodents: Inhibitory synaptic mechanisms. The Journal of physiology (london) 458:247-260.
Ko CH, Yamada YR, Welsh DK, Buhr ED, Liu AC, Zhang EE, Ralph MR, Kay SA, Forger DB, Takahashi JS (2010) Emergence of noise-induced oscillations in the central circadian pacemaker. PLoS Biol 8:e1000513.
Kononenko NI, Dudek FE (2004) Mechanism of irregular firing of suprachiasmatic nucleus neurons in rat hypothalamic slices. Journal of neurophysiology 91:267-273.
Krout KE, Kawano J, Mettenleiter TC, Loewy AD (2002) CNS inputs to the suprachiasmatic nucleus of the rat. Neuroscience 110:73-92.
Lamsa K, Taira T (2003) Use-dependent shift from inhibitory to excitatory GABAA receptor action in SP-O interneurons in the rat hippocampal CA3 area. Journal of neurophysiology 90:1983-1995.
Lee IT, Chang AS, Manandhar M, Shan Y, Fan J, Izumo M, Ikeda Y, Motoike T, Dixon S, Seinfeld JE, Takahashi JS, Yanagisawa M (2015) Neuromedin s-producing neurons act as essential pacemakers in the suprachiasmatic nucleus to couple clock neurons and dictate circadian rhythms. Neuron 85:1086-1102.
Leinninger GM, Opland DM, Jo YH, Faouzi M, Christensen L, Cappellucci LA, Rhodes CJ, Gnegy ME, Becker JB, Pothos EN, Seasholtz AF, Thompson RC, Myers MG, Jr. (2011) Leptin action via neurotensin neurons controls orexin, the mesolimbic dopamine system and energy balance. Cell metabolism 14:313-323.
LeSauter J, Kriegsfeld LJ, Hon J, Silver R (2002) Calbindin-D(28K) cells selectively contact intra-SCN neurons. Neuroscience 111:575-585.
Li JD, Burton KJ, Zhang C, Hu SB, Zhou QY (2009a) Vasopressin receptor V1a regulates circadian rhythms of locomotor activity and expression of clock-controlled genes in the suprachiasmatic nuclei. Am J Physiol Regul Integr Comp Physiol 296:R824-830.
Li Y, Liu Z, Zhang J, Wang R, Chen L (2009b) Synchronisation mechanisms of circadian rhythms in the suprachiasmatic nucleus. IET systems biology 3:100-112.

Liou SY, Albers HE (1990) Single unit response of neurons within the hamster suprachiasmatic nucleus to GABA and low chloride perfusate during the day and night. Brain research bulletin 25:93-98.
Liu AC, Welsh DK, Ko CH, Tran HG, Zhang EE, Priest AA, Buhr ED, Singer O, Meeker K, Verma IM, Doyle FJ, 3rd, Takahashi JS, Kay SA (2007) Intercellular coupling confers robustness against mutations in the SCN circadian clock network. Cell 129:605-616.
Liu C, Reppert SM (2000) GABA synchronizes clock cells within the suprachiasmatic circadian clock. Neuron 25:123-128.
Lowrey PL, Takahashi JS (2011) Genetics of circadian rhythms in Mammalian model organisms. Adv Genet 74:175-230.
Lundkvist GB, Kwak Y, Davis EK, Tei H, Block GD (2005) A calcium flux is required for circadian rhythm generation in mammalian pacemaker neurons. J Neurosci 25:7682-7686.
Markova O, Mukhtarov M, Real E, Jacob Y, Bregestovski P (2008) Genetically encoded chloride indicator with improved sensitivity. Journal of neuroscience methods 170:67-76.
Martina M, Royer S, Pare D (2001) Cell-type-specific GABA responses and chloride homeostasis in the cortex and amygdala. Journal of neurophysiology 86:2887-2895.
Mason R, Biello SM, Harrington ME (1991) The effects of GABA and benzodiazepines on neurones in the suprachiasmatic nucleus (SCN) of Syrian hamsters. Brain Res 552:53-57.
Maywood ES, Chesham JE, O'Brien JA, Hastings MH (2011) A diversity of paracrine signals sustains molecular circadian cycling in suprachiasmatic nucleus circuits. Proceedings of the National Academy of Sciences of the United States of America 108:14306-14311.
Maywood ES, Reddy AB, Wong GK, O'Neill JS, O'Brien JA, McMahon DG, Harmar AJ, Okamura H, Hastings MH (2006) Synchronization and maintenance of timekeeping in suprachiasmatic circadian clock cells by neuropeptidergic signaling. Curr Biol 16:599-605.
McDearmon EL, Patel KN, Ko CH, Walisser JA, Schook AC, Chong JL, Wilsbacher LD, Song EJ, Hong HK, Bradfield CA, Takahashi JS (2006) Dissecting the functions of the mammalian clock protein BMAL1 by tissue-specific rescue in mice. Science 314:1304-1308.
McElroy B, Zakaria A, Glass JD, Prosser RA (2009) Ethanol modulates mammalian circadian clock phase resetting through extrasynaptic gaba receptor activation. Neuroscience 164:842-848.
Mieda M, Ono D, Hasegawa E, Okamoto H, Honma K, Honma S, Sakurai T (2015) Cellular Clocks in AVP Neurons of the SCN Are Critical for Interneuronal Coupling Regulating Circadian Behavior Rhythm. Neuron 85:1103-1116.
Mikawa S, Wang C, Shu F, Wang T, Fukuda A, Sato K (2002) Developmental changes in KCC1, KCC2 and NKCC1 mRNAs in the rat cerebellum. Brain Res Dev Brain Res 136:93-100.
Mohawk JA, Takahashi JS (2011) Cell autonomy and synchrony of suprachiasmatic nucleus circadian oscillators. Trends in neurosciences.

Moldavan MG, Allen CN (2013) GABAB receptor-mediated frequency-dependent and circadian changes in synaptic plasticity modulate retinal input to the suprachiasmatic nucleus. The Journal of physiology 591:2475-2490.
Moldavan MG, Irwin RP, Allen CN (2006) Presynaptic $GABA_B$ receptors Regulate Retinohypothalamic Tract Synaptic Transmission by inhibiting Voltage-Gated Ca^{2+} Channels. Journal of neurophysiology 95:3727-3741.
Moore RY, Eichler VB (1972) Loss of circadian adrenal corticosterone rhythm following suprachiasmatic nucleus lesions in the rat. Brain research 42:201-206.
Moore RY, Lenn NJ (1972) A retinohypothalamic projection in the rat. The Journal of comparative neurology 146:1-14.
Moore RY, Speh JC (1993) GABA is the principal neurotransmitter of the circadian system. Neuroscience letters 150:112-116.
Moore RY, Card JP (1994) Intergeniculate leaflet: An anatomically and functionally distinct subdivision of the lateral geniculate complex. The Journal of comparative neurology 344:403-430.
Morin LP (1994) The circadian visual system. Brain research reviews 19:102-127.
Morin LP (2007) SCN organization reconsidered. Journal of biological rhythms 22:3-13.
Morin LP (2013) Neuroanatomy of the extended circadian rhythm system. Experimental neurology 243:4-20.
Mortensen M, Patel B, Smart TG (2012) GABA Potency at GABA(A) Receptors Found in Synaptic and Extrasynaptic Zones. Frontiers in cellular neuroscience 6:1.
Mozrzymas JW, Zarnowska ED, Pytel M, Mercik K (2003) Modulation of GABA(A) receptors by hydrogen ions reveals synaptic GABA transient and a crucial role of the desensitization process. J Neurosci 23:7981-7992.
Muller M, Triaca V, Besusso D, Costanzi M, Horn JM, Koudelka J, Geibel M, Cestari V, Minichiello L (2012) Loss of NGF-TrkA signaling from the CNS is not sufficient to induce cognitive impairments in young adult or intermediate-aged mice. J Neurosci 32:14885-14898.
Naum OG, Fernanda Rubio M, Golombek DA (2001) Rhythmic variation in gamma-aminobutyric acid(A)-receptor subunit composition in the circadian system and median eminence of Syrian hamsters. Neuroscience letters 310:178-182.
Novak CM, Albers HE (2004) Novel phase-shifting effects of GABAA receptor activation in the suprachiasmatic nucleus of a diurnal rodent. Am J Physiol Regul Integr Comp Physiol 286:R820-825.
O'Hara BF, Andretic R, Heller HC, Carter DB, Kilduff TS (1995) GABAA, GABAC, and NMDA receptor subunit expression in the suprachiasmatic nucleus and other brain regions. Mol Brain Res 28:239-250.
Ohtsuki T, Matsumoto M, Suzuki K, Taniguchi N, Kamada T (1993) Effect of transient forebrain ischemia on superoxide dismutases in gerbil hippocampus. Brain Res 620:305-309.
Okamura H, Berod A, Julien J-F, Geffard M, Kitahama K, Mallet J, Bobillier P (1989) Demonstration of GABAergic cell bodies in the suprachiasmatic nucleus: in situ hybridization of glutamic acid decarboxylase (GAD) mRNA and immunochemistry of GAD and GABA. Neuroscience letters 102:131-136.

Panda S, Antoch MP, Miller BH, Su AI, Schook AB, Straume M, Schultz PG, Kay SA, Takahashi JS, Hogenesch JB (2002) Coordinated transcription of key pathways in the mouse by the circadian clock. Cell 109:307-320.
Payne JA, Rivera C, Voipio J, Kaila K (2003) Cation-chloride co-transporters in neuronal communication, development and trauma. Trends in neurosciences 26:199-206.
Price GD, Trussell LO (2006) Estimate of the chloride concentration in a central glutamatergic terminal: a gramicidin perforated-patch study on the calyx of Held. J Neurosci 26:11432-11436.
Raimondo JV, Kay L, Ellender TJ, Akerman CJ (2012) Optogenetic silencing strategies differ in their effects on inhibitory synaptic transmission. Nature neuroscience.
Raimondo JV, Joyce B, Kay L, Schlagheck T, Newey SE, Srinivas S, Akerman CJ (2013) A genetically-encoded chloride and pH sensor for dissociating ion dynamics in the nervous system. Frontiers in cellular neuroscience 7:202.
Ralph MR, Foster RC, Davis FC, Menaker M (1990) Transplanted suprachiasmatic nucleus determines circadian period. Science 247:975-978.
Ratte S, Prescott SA (2011) ClC-2 Channels Regulate Neuronal Excitability, Not Intracellular Chloride Levels. J Neurosci 31:15838-15843.
Riazanski V, Deriy LV, Shevchenko PD, Le B, Gomez EA, Nelson DJ (2011) Presynaptic CLC-3 determines quantal size of inhibitory transmission in the hippocampus. Nature neuroscience 14:487-494.
Rinke I, Artmann J, Stein V (2010) ClC-2 voltage-gated channels constitute part of the background conductance and assist chloride extrusion. J Neurosci 30:4776-4786.
Roenneberg T, Daan S, Merrow M (2003) The art of entrainment. Journal of biological rhythms 18:183-194.
Rohling J, Meijer JH, VanderLeest HT, Admiraal J (2006) Phase differences between SCN neurons and their role in photoperiodic encoding; a simulation of ensemble patterns using recorded single unit electrical activity patterns. Journal of physiology, Paris 100:261-270.
Romijn HJ, Sluiter AA, Pool CW, Wortel J, Buijs RM (1997) Evidence from confocal fluorescence microscopy for a dense, reciprocal innervation between AVP-, somatostatin-, VIP/PHI-, GRP- and VIP/PHI/GRP-immunoreactive neurons in the rat suprachiasmatic nucleus. European Journal of Neuroscience 9:2613-2623.
Russell JM (2000) Sodium-potassium-chloride cotransport. Physiological reviews 80:211-276.
Schone C, Burdakov D (2012) Glutamate and GABA as rapid effectors of hypothalamic "peptidergic" neurons. Front Behav Neurosci 6:81.
Schrock H, Kuschinsky W (1989) Cerebrospinal fluid ionic regulation, cerebral blood flow, and glucose use during chronic metabolic alkalosis. The American journal of physiology 257:H1220-1227.
Shibata S, Liou SY, Ueki S (1986) Influence of excitatory amino acid receptor antagonists and of baclofen on synaptic transmission in the optic nerve to the suprachiasmatic nucleus in slices of rat hypothalamus. Neuropharmacology 25:403-409.
Shibata S, Watanabe A, Hamada T, Ono M, Watanabe S (1994) N-methyl-D-aspartate induces phase shifts in circadian rhythm of neuronal activity of rat SCN in vitro.

American Journal of Physiology: Regulatory,Integrative and Comparative Physiology 267:R360-R364.
Shimura M, Akaike N, Harata N (2002) Circadian rhythm in intracellular Cl(-) activity of acutely dissociated neurons of suprachiasmatic nucleus. Am J Physiol Cell Physiol 282:C366-373.
Shirakawa T, Honma S, Katsuno Y, Oguchi H, Honma K (2000) Synchronization of circadian firing rhythms in cultured rat suprachiasmatic neurons. European Journal of Neuroscience 12:2833-2838.
Silver R, LeSauter J, Tresco PA, Lehman MN (1996) A diffusible coupling signal from the transplanted suprachiasmatic nucleus controlling circadian locomotor rhythms. Nature 382:810-813.
Smith MB, Karatekin E, Gohlke A, Mizuno H, Watanabe N, Vavylonis D (2011) Interactive, computer-assisted tracking of speckle trajectories in fluorescence microscopy: application to actin polymerization and membrane fusion. Biophysical journal 101:1794-1804.
Smith MR, Eastman CI (2012) Shift work: health, performance and safety problems, traditional countermeasures, and innovative management strategies to reduce circadian misalignment. Nat Sci Sleep 4:111-132.
Smith RD, Inouye S, Turek FW (1989) Central administration of muscimol phase-shifts the mammalian circadian clock. Journal of comparative physiology 164:805-814.
Sokolove PG, Bushell WN (1978) The chi square periodogram: its utility for analysis of circadian rhythms. Journal of theoretical biology 72:131-160.
Staley KJ, Proctor WR (1999) Modulation of mammalian dendritic GABA(A) receptor function by the kinetics of Cl- and HCO3- transport. The Journal of physiology 519:693-712.
Stephan FK, Zucker I (1972) Circadian rhythms in drinking behavior and locomotor activity of rats are eliminated by hypothalamic lesions. Proc Natl Acad Sci USA 69:1583-1586.
Strecker GJ, Wuarin JP, Dudek FE (1997) GABAA-mediated local synaptic pathways connect neurons in the rat suprachiasmatic nucleus. Journal of neurophysiology 78:2217-2220.
Taniguchi H, He M, Wu P, Kim S, Paik R, Sugino K, Kvitsani D, Fu Y, Lu J, Lin Y, Miyoshi G, Shima Y, Fishell G, Nelson SB, Huang ZJ (2011) A resource of cre driver lines for genetic targeting of GABAergic neurons in cerebral cortex. Neuron 71:995-1013.
Teshima K, Kim SH, Allen CN (2003) Characterization of an apamin-sensitive potassium current in suprachiasmatic nucleus neurons. Neuroscience 120:65-73.
Thompson SM, Gahwiler BH (1989) Activity-dependent disinhibtion. II. Effects of extracellular potassium, furosemide and membrane potential on ECl- in hippocampal CA3 neurons. Journal of neurophysiology 61:512-523.
Tong Q, Ye CP, Jones JE, Elmquist JK, Lowell BB (2008) Synaptic release of GABA by AgRP neurons is required for normal regulation of energy balance. Nature neuroscience 11:998-1000.
Tyzio R, Cossart R, Khalilov I, Minlebaev M, Hubner CA, Represa A, Ben-Ari Y, Khazipov R (2006) Maternal oxytocin triggers a transient inhibitory switch in GABA signaling in the fetal brain during delivery. Science 314:1788-1792.

Tyzio R, Minlebaev M, Rheims S, Ivanov A, Jorquera I, Holmes GL, Zilberter Y, Ben-Ari Y, Khazipov R (2008) Postnatal changes in somatic gamma-aminobutyric acid signalling in the rat hippocampus. The European journal of neuroscience 27:2515-2528.

Ueta Y, Fujihara H, Serino R, Dayanithi G, Ozawa H, Matsuda K, Kawata M, Yamada J, Ueno S, Fukuda A, Murphy D (2005) Transgenic expression of enhanced green fluorescent protein enables direct visualization for physiological studies of vasopressin neurons and isolated nerve terminals of the rat. Endocrinology 146:406-413.

Van den Pol AN (1980) The hypothalamic suprachiasmatic nucleus of rat: Intrinsic anatomy. Journal of Comparative Neurology 191:661-702.

Van den Pol AN (1986) Gamma-aminobutyrate, gastrin releasing peptide, serotonin, somatostatin, and vasopressin: ultrastructural immunocytochemical localization in presynaptic axons in the suprachiasmatic nucleus. Neuroscience 17:643-659.

Van den Pol AN, Gorcs T (1986) Synaptic relationships between neurons containing vasopressin, gastrin-releasing peptide, vasoactive intestinal polypeptide, and glutamate decarboxylase immunoreactivity in the suprachiasmatic nucleus: dual ultrastructural immunocytochemistry with gold-substituted silver peroxidase. Journal of Comparative Neurology 252:507-521.

Vogelbaum MA, Menaker M (1992) Temporal chimeras produced by hypothalamic transplants. J Neurosci 12:3619-3627.

Wagner S, Sagiv N, Yarom Y (2001) GABA-induced current and circadian regulation of chloride in neurones of the rat suprachiasmatic nucleus. The Journal of physiology 537:853-869.

Wagner S, Castel M, Gainer H, Yarom Y (1997) GABA in the mammalian suprachiasmatic nucleus and its role in diurnal rhythmicity. Nature 387:598-603.

Wang C, Shimizu-Okabe C, Watanabe K, Okabe A, Matsuzaki H, Ogawa T, Mori N, Fukuda A, Sato K (2002) Developmental changes in KCC1, KCC2, and NKCC1 mRNA expressions in the rat brain. Brain Res Dev Brain Res 139:59-66.

Waseem T, Mukhtarov M, Buldakova S, Medina I, Bregestovski P (2010) Genetically encoded Cl-Sensor as a tool for monitoring of Cl-dependent processes in small neuronal compartments. Journal of neuroscience methods.

Watts AG, Swanson LW (1987) Efferent projections of the suprachiasmatic nucleus II. Studies using retrograde transport of fluorescent dyes and simultaneous peptide immunohistochemistry in the rat. The Journal of comparative neurology 258:230-252.

Watts SD, Suchland KL, Amara SG, Ingram SL (2012) A sensitive membrane-targeted biosensor for monitoring changes in intracellular chloride in neuronal processes. PLoS ONE 7:e35373.

Webb AB, Angelo N, Huettner JE, Herzog ED (2009) Intrinsic, nondeterministic circadian rhythm generation in identified mammalian neurons. Proceedings of the National Academy of Sciences of the United States of America 106:16493-16998.

Welsh DK, Takahashi JS, Kay SA (2010) Suprachiasmatic nucleus: cell autonomy and network properties. Annual review of physiology 72:551-577.

Welsh DK, Logothetis DE, Meister M, Reppert SM (1995) Individual neurons dissociated from rat suprachiasmatic nucleus express independently phased circadian firing rhythms. Neuron 14:697-706.
Wojcik SM, Katsurabayashi S, Guillemin I, Friauf E, Rosenmund C, Brose N, Rhee JS (2006) A shared vesicular carrier allows synaptic corelease of GABA and glycine. Neuron 50:575-587.
Wright R, Raimondo JV, Akerman CJ (2011) Spatial and temporal dynamics in the ionic driving force for GABA(A) receptors. Neural Plast 2011:728395.
Yamada J, Okabe A, Toyoda H, Kilb W, Luhmann HJ, Fukuda A (2004) Cl- uptake promoting depolarizing GABA actions in immature rat neocortical neurones is mediated by NKCC1. The Journal of physiology 557:829-841.
Yamaguchi S, Isejima H, Matsuo T, Okura R, Yagita K, Kobayashi M, Okamura H (2003) Synchronization of cellular clocks in the suprachiasmatic nucleus. Science 302:1408-1412.
Yamazaki S, Numano R, Abe M, Hida A, Takahashi R, Ueda M, Block GD, Sakaki Y, Menaker M, Tei H (2000) Resetting central and peripheral circadian oscillators in transgenic rats. Science 288:682-685.
Yan L, Silver R (2002) Differential induction and localization of mPer1 and mPer2 during advancing and delaying phase shifts. The European journal of neuroscience 16:1531-1540.
Yan Y, Dempsey RJ, Sun D (2001) Expression of Na(+)-K(+)-Cl(-) cotransporter in rat brain during development and its localization in mature astrocytes. Brain Res 911:43-55.
Yoo SH, Yamazaki S, Lowrey PL, Shimomura K, Ko CH, Buhr ED, Siepka SM, Hong HK, Oh WJ, Yoo OJ, Menaker M, Takahashi JS (2004) PERIOD2::LUCIFERASE real-time reporting of circadian dynamics reveals persistent circadian oscillations in mouse peripheral tissues. Proceedings of the National Academy of Sciences of the United States of America 101:5339-5346.
Zeger SL, Liang KY (1986) Longitudinal data analysis for discrete and continuous outcomes. Biometrics 42:121-130.
Zhang LL, Delpire E, Vardi N (2007) NKCC1 does not accumulate chloride in developing retinal neurons. Journal of neurophysiology 98:266-277.
Zheng B, Albrecht U, Kaasik K, Sage M, Lu W, Vaishnav S, Li Q, Sun ZS, Eichele G, Bradley A, Lee CC (2001) Nonredundant roles of the mPer1 and mPer2 genes in the mammalian circadian clock. Cell 105:683-694.
Zhong S, Navaratnam D, Santos-Sacchi J (2014) A genetically-encoded YFP sensor with enhanced chloride sensitivity, photostability and reduced ph interference demonstrates augmented transmembrane chloride movement by gerbil prestin (SLC26a5). PLoS ONE 9:e99095.